EUROPEAN ORGANIZATION FOR NUCLEAR RESEARCH
Technology Department
Magnets Superconductors and Cryostat - Group

POLITECNICO DI MILANO
Facoltà di Ingegneria dei Processi Industriali
Dipartimento di Energia

Master Thesis in Material Engineering

Tesi di Laurea Specialistica in Ingegneria dei Materiali

Irradiation Effects in Superconductors for the Large Hadron Collider Upgrade: Overview and Experiment Design

CERN Supervisor: Dr. Luca Bottura
University Supervisor: Prof. Marco Beghi

Candidate:
Filippo Liberati
Matricule nº 682386

Academic Year 2009-2010

In Memory of My Father

Introduction

Nb_3Sn strands are of interest for Nuclear Fusion Devices (Superconducting Magnets for the Plasma Confinement) and High Energy Physics (Superconducting Magnets for the Guide of Nuclear Particle Beams) applications, due to their high critical current density J_c at the highest applied magnetic fields. On the other side, the critical parameters of this material are very sensitive to intense nuclear radiation fields, so that a deep characterization and study of their radiation damage is crucial for their development and correct manufacturing.

Goal of present work has been the conceptual design and preliminary testing of an experiment for the study of the radiation resistance of Nb_3Sn superconducting wires, in view of CERN's "Large Hadron Collider - LHC - Phase II" upgrade project of 2016. This experiment has been called "Nb_3Sn - Superconductor's Irradiation Tests" (from now on, it will always be cited as "SIT - Nb_3Sn" Project).

The work has been performed at CERN, where I have done, from March 2009 to September 2010 a training period as Technical Student at the Accelerator Technology Department, and represents the *starting point* for the organization of the whole irradiation experiments. It is consequently structured as follows:

Part 1 Experimental and Management Part

1. Identification of the LHC's sectors where the nuclear radiation fields are expected to be the most intense one, and selection of the most significant nuclear particle energies and fluxes for the experiment.

2. Search and selection, at CERN and worldwide, of irradiation facilities capable to host irradiation experiments with the same kind of beams.

3. Conceptual Design of the test stations that will simultaneously host the *irradiation* and *critical current measurement* on the *irradiated* superconducting samples.

4. Design, test and validation of the central component of the whole test station: *the sample holder.*

Part 2 Theoretical Part

1. Review and summary of the literature data on the irradiation studies of Nb_3Sn's *wires* and *thin films*.

2. Estimations of the material degradation under LHC's characteristics radiation fields.

Starting from this organization of the work, the present thesis is structured as follows

Chapter 1 Superconductivity and Nb_3Sn

Chapter 2 Superconductors in Radiation Environment

Chapter 3 First Engineering Activities of the "SIT - Nb_3Sn Project"

Chapter 4 First Experimental Activities of the SIT - Nb_3Sn Project

Conclusion

Future Work

References

Acknowledgements

Index

Chapter 1

Superconductivity and the Nb_3Sn

1.1 Introduction

1911 the dutch physicist Onnes discovered that, if liquid mercury is cooled below a certain critical temperature T_C, the metal completely loses its electrical resistivity ρ. Figure 1 shows the classic behavior ρ against T for a superconductor.
Starting from that date, the superconductive phenomenon has widely been studied and characterized. Aim of the next sections is to give a brief overview of the general macroscopic properties of a superconductor, highlighting those that have been of greater interests for the present thesis work. The manufacturing methods of Nb_3Sn wires will then be presented.

1.2 Definition of Superconductivity

Bardeen, Cooper and Schrieffer's "BCS - Theory" is today the most accepted physical theory on superconductivity. According to this theory, the superconductive phenomenon is due to the creation of electron pairs, via an interaction which is mediated by a lattice phonon. These pairs are called "Cooper Pairs". Under the application of an electric field $\vec{E}$ these pairs can propagate into the lattice, undergoing no scattering. In this way, the electrical resistivity drops to zero and a "super-current" is created.

Three are the most important parameters for the definition of the thermodynamic state of a superconductor: the temperature, the electric current and the applied magnetic field. There are three critical values of these parameters, above which the superconducting state is destroyed and the material behaves as a normal conductor. These are:

- The critical temperature T_C
- The critical current density J_C
- The critical magnetic field B_C

Each of the critical parameters is defined at the critical value when the other two are set to zero. So, we have T_{C0}, J_{C0} and B_{C0}.

The *normal state resistivity* ρ_0, defined as the resistivity value just above the critical temperature, is separately treated as a critical parameter.

In its engineering applications, a superconductor works with a mixed combination of temperature, critical current and applied field. For this reason, a *critical surface* is defined in a three dimensional (T, J, B) space as the boundary of the region in which the material is in its superconducting state. According to the shape of the critical surface, a classification of the superconductors has been proposed. This will be presented in the next section.

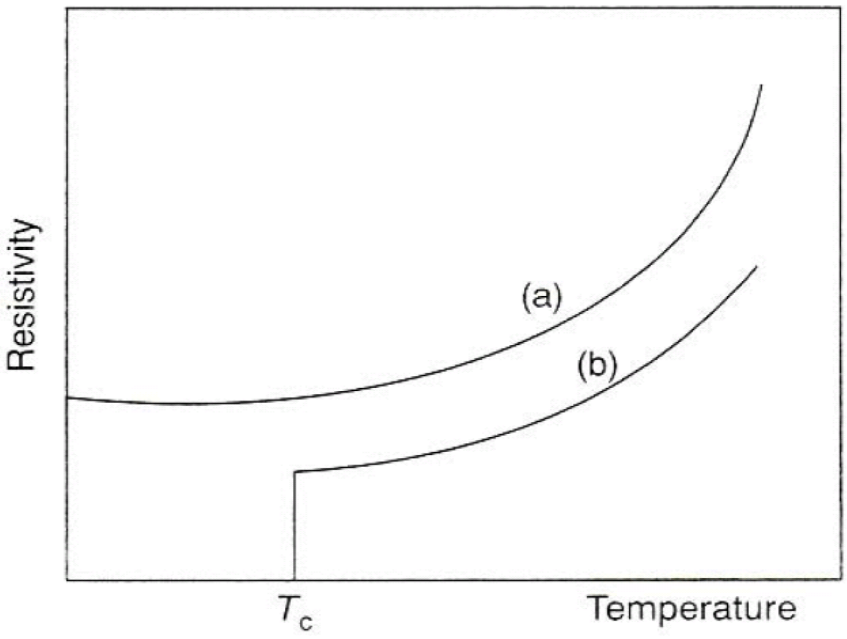

Figure 1. An schematic example of the dependence of the electrical resistivity against the temperature for a normal conductor (a) and a superconductor (b). Normal state resistivity is the resitivity value just above the superconductor's curve.

1.3 Classification of the superconductors

The first family of superconductors is the "Type I" one. These materials are characterized by the existence of a critical temperature T_{C0}, a critical current density J_{C0}, and, most importantly, a critical magnetic field B_{C0}.

The attention has been put on the magnetic field due to one of the most important properties of the Type I superconductors. That is, when the material is placed into an external field *B*, it completely expulses the force line of the field. This behavior is called "perfect diamagnetism", and figure 2 illustrates this behavior.

Concerning the magnetic behavior, there is a second family of superconductors, the "Type II" one. These materials exhibit a "mixed state", which is delimited by an upper critical field B_{C20} and a lower critical field B_{C0}. In this state, the magnetic flux lines can penetrate the material, but they do it in a "vortex shape". These vortexes are distributed in a regular pattern on the outer surface of the material, as shown in Figure 3. The centers where each vortex is *fixed* or *pinned* are called *pinning centers*. When the applied magnetic field is lower than B_{C0}, the material behaves as a Type I superconductor. Over B_{C20} the superconducting state is completely destroyed.

Among the Type I family there are almost all pure metals, and their T_{C0} values are lower than 10 K. Conversely, Type II family is composed by the alloy superconductors, such as Nb_3Sn, NbTi and MgB_2. These materials are today's most promising superconductors from the research's point of view, having T_{C0} of several tents of K.

Specifically, Nb_3Sn belongs to the so called "A15 superconductors", together with all the V- and Nb- based alloys of the stoichiometric form A_3B.

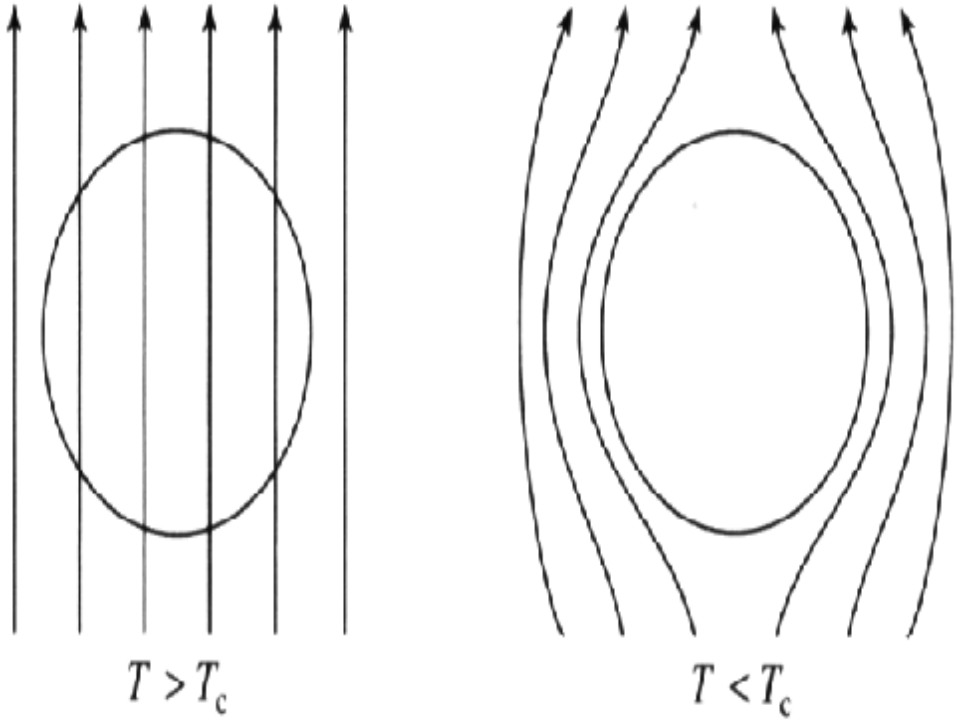

Figure 2. Meissner Effect in a Type I Material

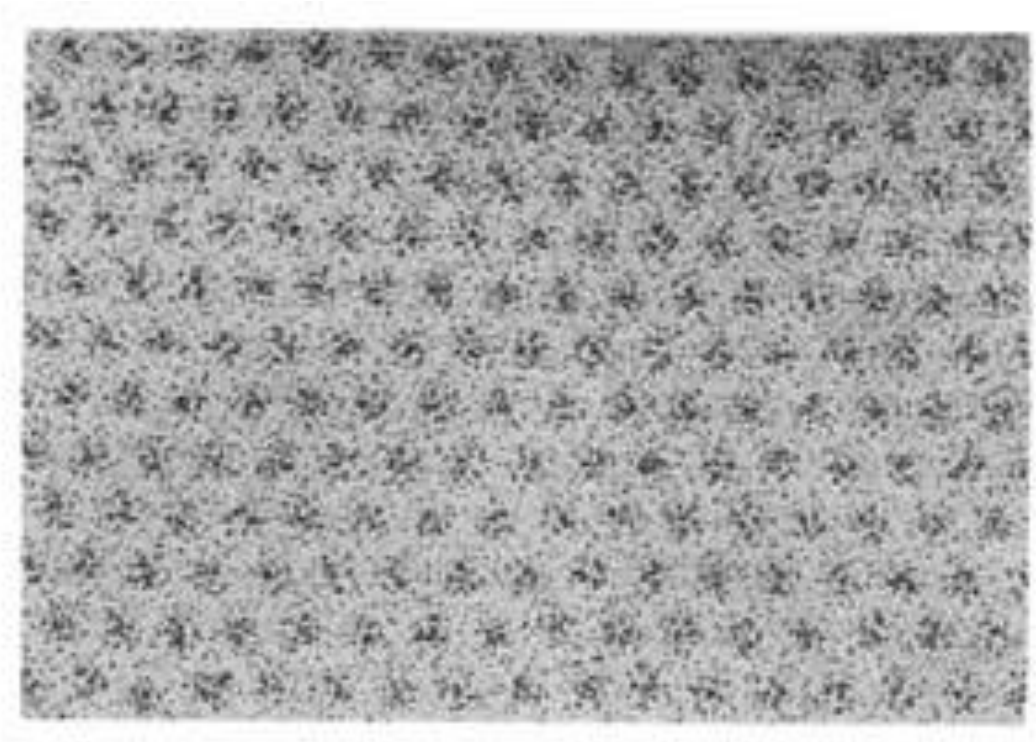

Figure 3. TEM images of the vortex array in a Type II Material

1.4 Properties and Manufacturing Methods of Nb_3Sn wires

This work is focused on Nb_3Sn to be exploited in LHC's future upgrade. The scientific and technological interest of this material lies into his high critical current density at the magnetic fields of interest. Aim of this section is to introduce the reader to the general aspects of this material that have been of greatest importance for this work.

1.4.1 Internal Structure

For its engineering applications, Nb_3Sn is usually manufactured under the form of wires, whose diameter generally ranges between 0.5 and 1 mm. On the wire cross section, the superconducting phase assumes the shapes of "islands" and, according to the *specific fabrication process*, these islands can be grouped into arrays of various shapes: circular, disc etc.

At the same time, the islands are formed by filaments of superconducting phase. The shape of these filaments varies from *columnar* to *equiaxial*, and its *diameter* is of usually of the order of some tents of micrometers. Figure 4 shows a micrograph of a Nb_3Sn wire cross section.

Cu usually constitutes the rest of the cross section of the wire. This metal posses a finite but low electrical resistance at the temperatures at which Nb_3Sn is in the superconducting state. Consequently, it acts as electrical shunt for stability. The ratio between the Cu and the Superconducting Phase is indicated in the literature as "Cu/Sc ratio"; it's one of the most important properties of the wire; it depends from the specific manufacturing process.

The superconducting phase is separated by the stabilizing phase by a Sn diffusion barrier, that avoids the contamination of Cu with some of the superconducting phase elements. Lastly, *Ti* and *Ta* are added as doping elements, to improve specific critical properties of the material.

1.4.2 Manufacturing Methods

The superconducting phase is produced imposing the *non - reacted* wires to a isothermal heat treatment at 600 °C to 700 °C for 50 to 200 hrs, and this rule is valid for all the manufacturing processes.

The variation of the heat treatment parameters, which is one of today's most important R&D aspects on Nb_3Sn, allows to control: the superconducting filament's *diameter* and *shape*, as well as the *Sn concentration gradient* on the filament's thickness.

In the *Bronze Route* process, *Nb* filaments are embedded in *Bronze* wires, and the superconducting phase is produced via diffusion of the *Nb* in the Bronze and its chemical reaction with *Sn*.

The starting material for the *Internal Tin* technique is constituted by *Nb* filaments and *Sn* rods, that are first embedded in *Cu* wires. The *Restacked Roll Process* or *RRP technique* is a modification of the *Internal Tin* one, and it's one of today's most advanced technique to control the filament's size and shape.

Figure 5 shows the structure of the non - reacted wire for the Internal Tin technique.

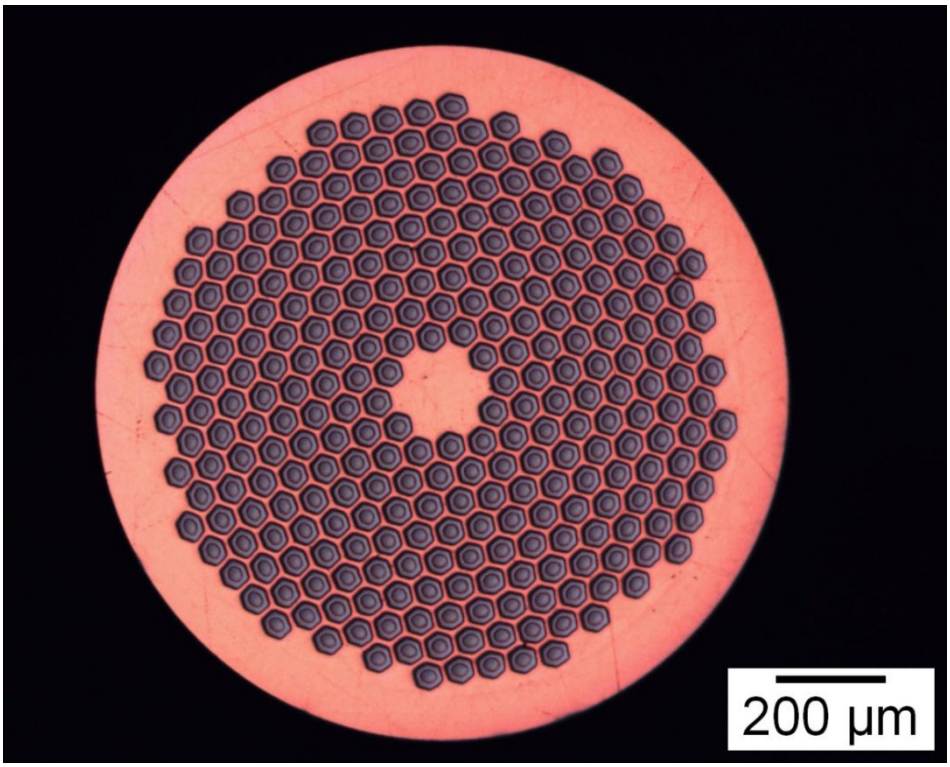

Figure 4. A Nb_3Sn wire's cross section produced via the *Bronze Route* process.

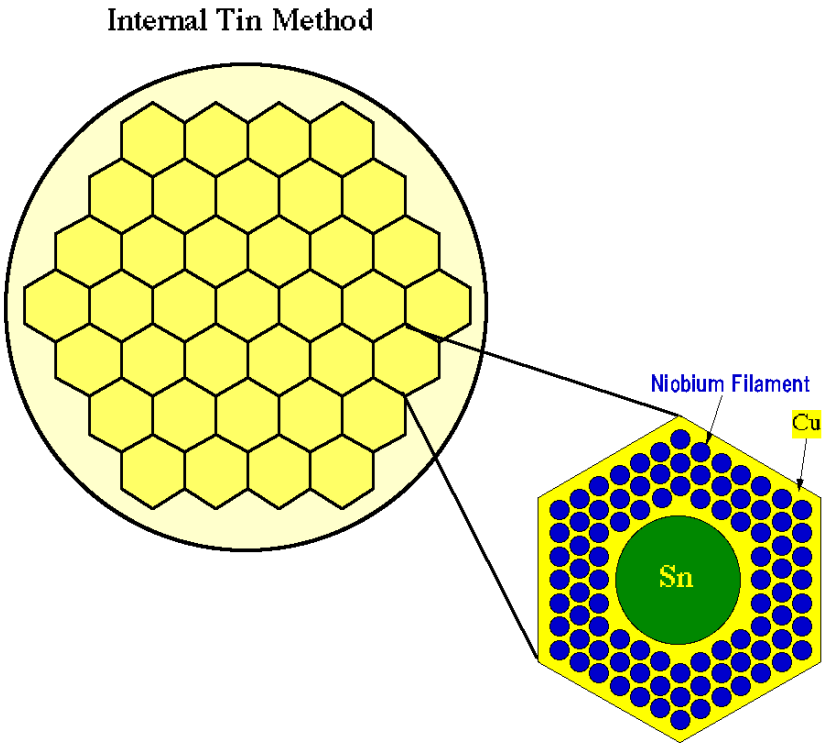

Figure 5. Internal Structure of a non reacted wire before its *Internal Tin* treatment

1.4.3 Physico - Metallurgical Properties of Nb_3Sn wires

The normal *Sn* content in *binary* Nb_3Sn varies between 18 at% and 25.5 at%, that is, in a composition interval that is very proxy to the exact stoichiometric one. The addition of *Ti* and *Ta* as doping elements leads then to a *ternary* system. In Figure 6, the ternary phase diagrams are separately shown for the addition of the two doping elements.

The critical parameters of the material depend on its electronic structure near the Fermi Level, and thus, on the degree of atomic order. For *binary* Nb_3Sn, this can be quantified by the value of the *Bragg - Williams* order parameter *S* [1, 2]:

$$S(P,F) = \frac{P-F}{1-F} \quad (1)$$

which value ranges between two extreme situations: 0 (complete disorder) and 1 (perfect order). From eq. (1), S can be separately written for *Nb* and *Sn* atoms. For example, it is a function of the fraction $\boldsymbol{P_{Nb}}$ of crystallographic sites that are *effectively* occupied by *Nb* atoms and of the fraction $\boldsymbol{F_{Nb}}$ of *Nb* atoms in the alloy. Figure 7 shows the crystalline structure of Nb_3Sn. S can be measured by X - rays diffraction on Nb_3Sn sample [1, 2].

Some of the material's critical parameters will be now briefly discussed for the case of binary systems as a function of the *Sn* content in the material; the additives effect will be then presented.

- *The Critical Temperature* T_{C0} linearly scales with the *Sn*, up to 19 K for %Sn = 24 at%, as shown in Figure 8 [2]. This parameter is *directly* related to the electronic structure of the superconductor, and thus, to its degree of atomic order.

- The *Normal State Resistivity* ρ_0 is plotted as a function of various alloying elements in Figure 9 [2]. It shows a rapid decrease, and reaches 0 for Sn = 25 at% [2]. Available data refer to *quenched*, as well as *annealed* samples, having different values of *S*.

- The *Upper Critical Field* B_{C20} linearly scales with the Sn content, up to a maximum of 30 T placed at Sn = 25 at%, then decreasing [2]. The correspondent plot is shown in Figure 10 [2].

Specifically, the functional behavior of T_c ρ_0 and B_{C20} against the Tin concentration can be explained starting from the GLAG theory's result [2]

$$B_{C2} \propto T_C * \rho_0 * \gamma \quad (2)$$

where γ is the linear term in the functional behavior of the electronic specific heat against the temperature, that depends on the electronic density near the Fermi Level, and so, on the *Sn* concentration [2]. The available specific heat data [2] do refer to measurement that have been performed on binary Nb_3Sn samples, whose *Sn* content lied between 20 at% and 25 at%.

The major contribution of the *Ti* and *Ta* addition is to give a maximum to T_{C0} and to B_{C0}. Both maxima are placed at a concentration of *Ti* - *Ta* varying between 2 at% and 4 at%, as shown in Figure 11 [2]. Eq. (1) and (2) can be still used to comment this behavior.

The irradiation of Nb_3Sn with nuclear particles can, in principle, vary the *S* value, and thus, the material's critical parameter that can be related to *S*. This aspect will be discussed in Chapter 2.

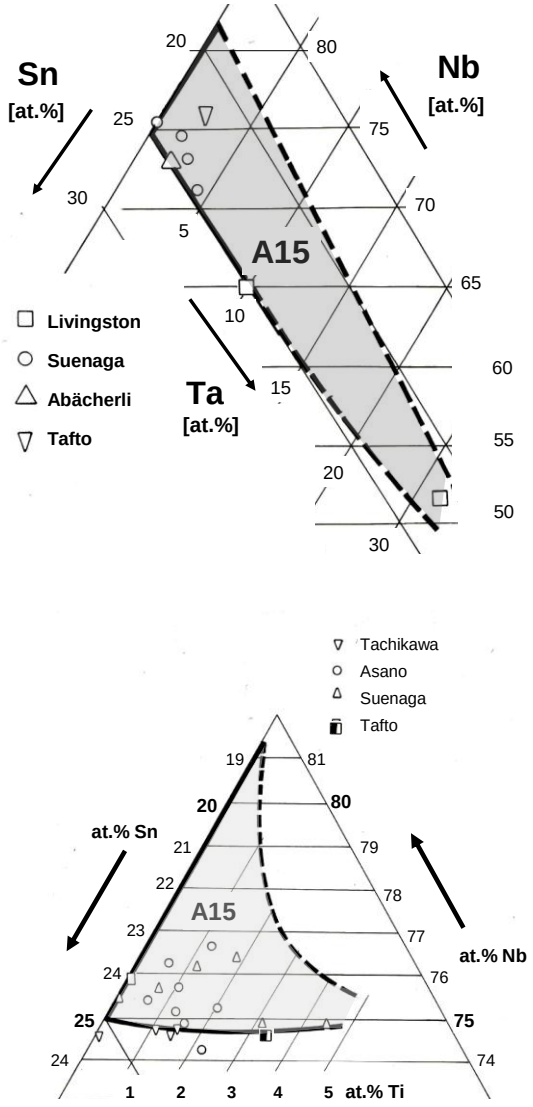

Figure 6. Ternary Phase Diagrams for Alloyed Nb_3Sn. Ref [2].

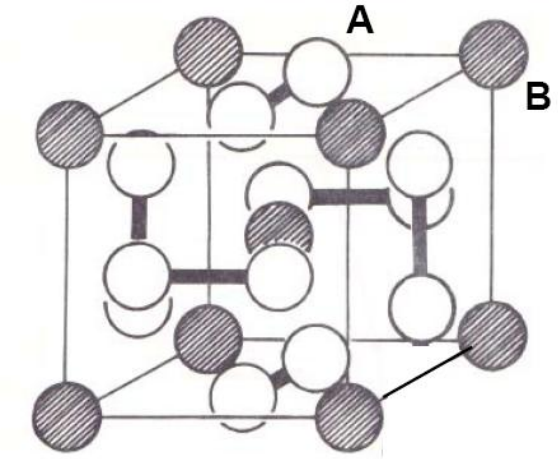

Figure 7. The crystalline structure of *binary/stochiometric* Nb_3Sn. "A" are Nb atoms, while Sn atoms are the "B". Ref [2].

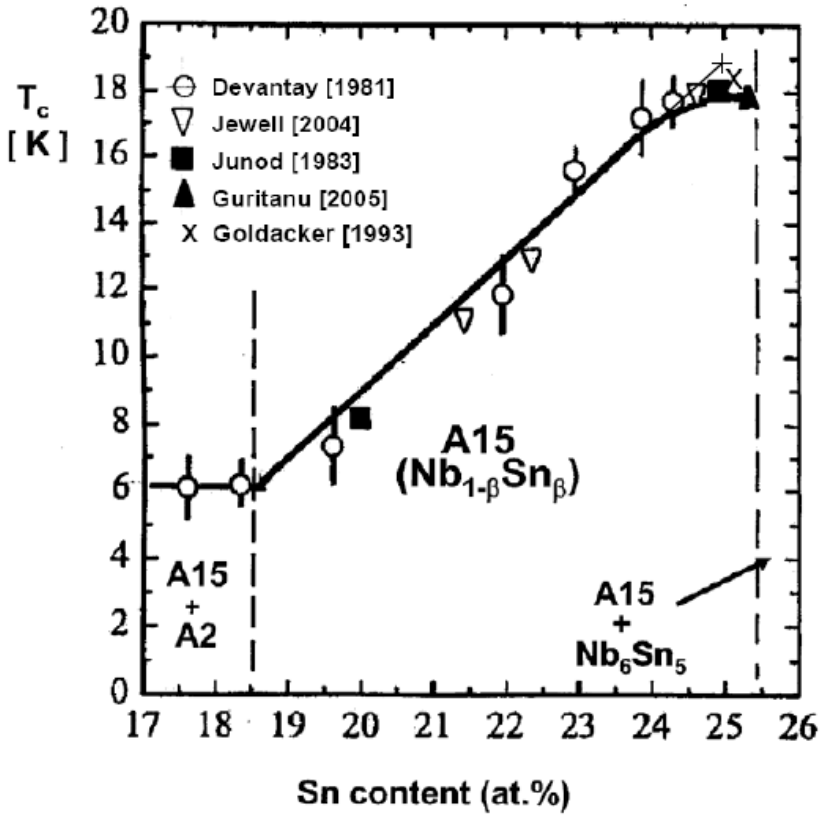

Figure 8. T_{C0} against the *Sn* concentration for *binary* Nb_3Sn. The maximum in critical temperature is reached at %Sn = 25.5 at%, and it's equal to 19.4 K. Ref. [2].

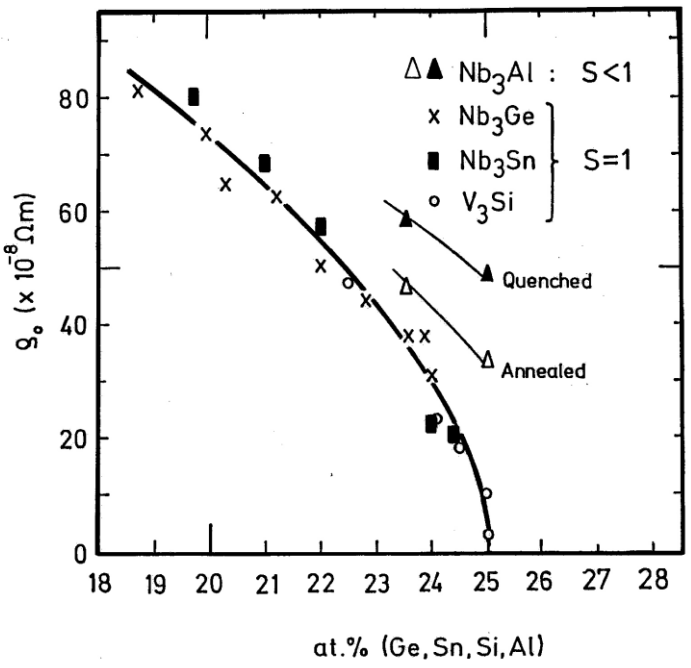

Figure 9. Normal State Resistivity against the *B* at% for A_3B superconducting samples, having different values of *S*. Ref. [2].

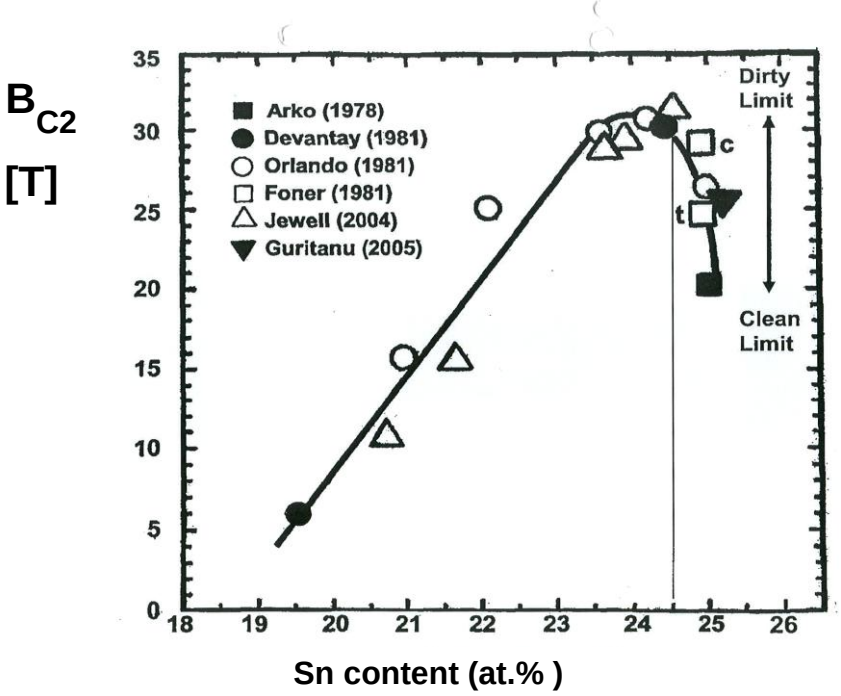

Figure 10. Upper Critical Field against the Sn concentration for binary Nb_3Sn. Ref. [2].

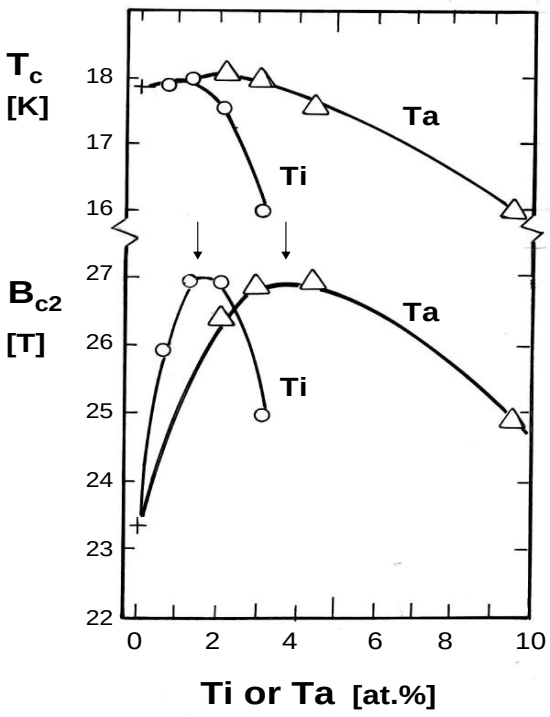

Figure 11. Zero Field Critical Temperature and Upper Critical Field for Ti and/or Ta alloyed Nb_3Sn. Ref. [2].

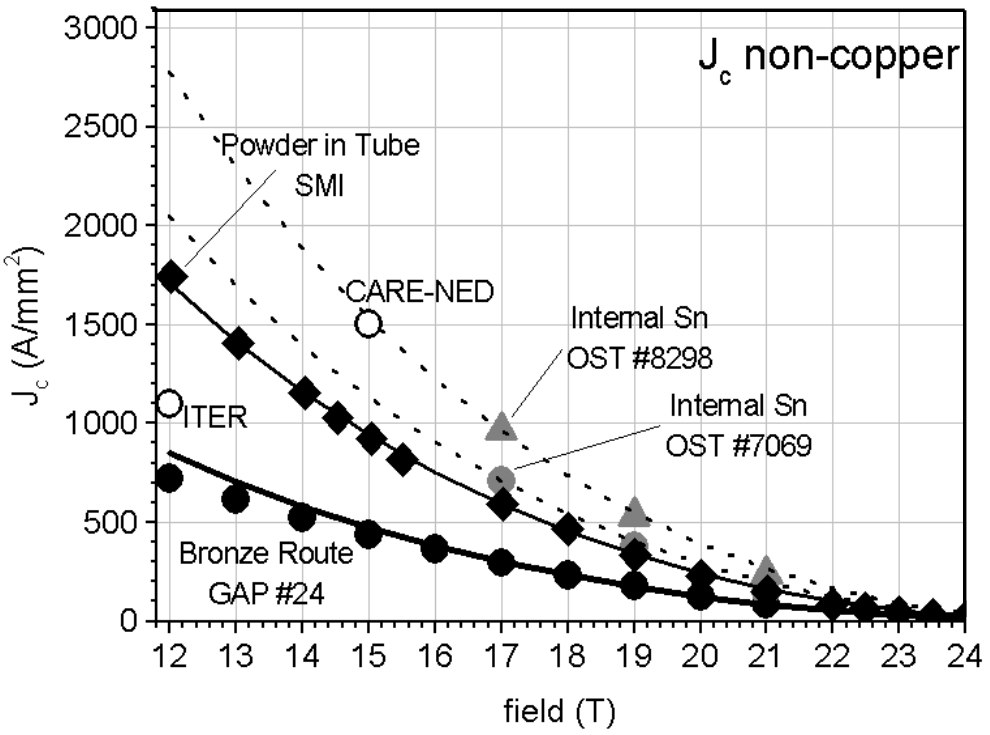

Figure 12. *Non - Cu* critical current density for Nb_3Sn samples produced using different manufacturing methods. Ref [2].

The critical current density is generally a decreasing function of the applied magnetic field, as shown in Figure 12 [2]. Also, it is experimentally defined in two ways:

- The *engineering* J_C , that is, as a first approximation, given by the wire's critical current divided per the wire's total cross section. This definition takes into account current sharing phenomena between the electrical shunt and the superconducting filaments.

- The *Non - Cu* J_C, that is defined as the effective current density flowing through the superconducting phase of the composite wire.

For the goals of this work, the engineering critical current density has been always considered, where necessary.

The enhancements of the critical current density can be related to the density of pinning centers in the material, as for example the *grain boundaries* in the superconducting phase. Thus, a reduced diameter of the superconducting filaments can increase the critical current density. The highest values of J_C range between 1500 and 3000 A*mm^{-2} at $B = 12\ T$, and depending on the specific manufacturing process.

Radiation induced crystalline defects in the superconducting phase of the material can increase the critical current density value.

1.5 The present and future superconductors of the Large Hadron Collider magnets

NbTi and Nb_3Sn superconducting wires are winded together to produce a Rutherford Cable at the end of their fabrication process. The number of wires in the cable and the specific internal structure of the wire depend on the specific cable's properties. A *winding machine*, and the internal structure of a NbTi cable are shown, respectively, in Figure 13, 14 and 15, as *general examples* of the Rutherford Cable's technology.

When the wire winding is finished, the cables are first covered with a metallic thin film, and then electrically insulated, applying different technological solution, that generally consist either in the *wrapping* of a polymeric tape around the cable, either in the cable *impregnation* in a resin bath. The cable is ready for its final use at the end of the insulation process.

Superconducting Rutherford Cables are of interest for *High Field Magnet* technology. Thanks to the diamagnetic properties of the superconductor, these devices are able to generate magnetic fields, whose intensity tipically ranges between 1 and 15 T, when kept under the critical temperature of the material. The cooling is usually achieved by a bath or forced flow of liquid or superfluid Helium, at temperatures less than 5 K and at atmospheric pressure.

In the past 40 years, the *superconducting coils* of High Field Magnets have been constructed using NbTi Rutherford Cables. The Large Hadron Collider dipoles, whose cross section is shown in Figure 16, have been realized in this way.

More recently, CERN has focused his attention on Nb_3Sn for the LHC's "2016 Phase II - Upgrade", because of the higher J_C at the highest applied magnetic field. Nb_3Sn Cables will be installed in magnets that will undergo to an intense nuclear radiation fields, in a way that will be illustrated in the next chapter. The material's critical parameters are known to be *very sensitive* to these radiation fields.

Various R&D programs have been recently started to investigate the irradiation effects in Nb_3Sn. Following this trend, CERN has started in March 2009 its own research project from the available literature data. The research project has been called "Nb_3Sn - Superconductor's Irradiation Test".

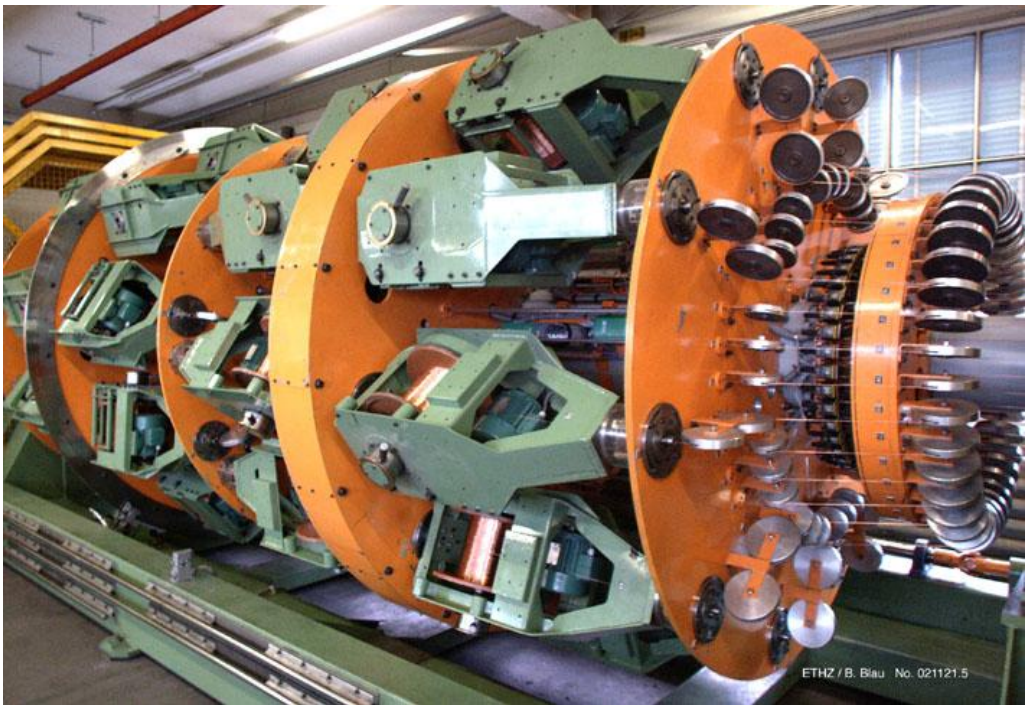

Figure 13. An example of a machine for the winding of superconducting wires. Acknowledgements: Christian Scheuerlein (CERN - TE - MSC group).

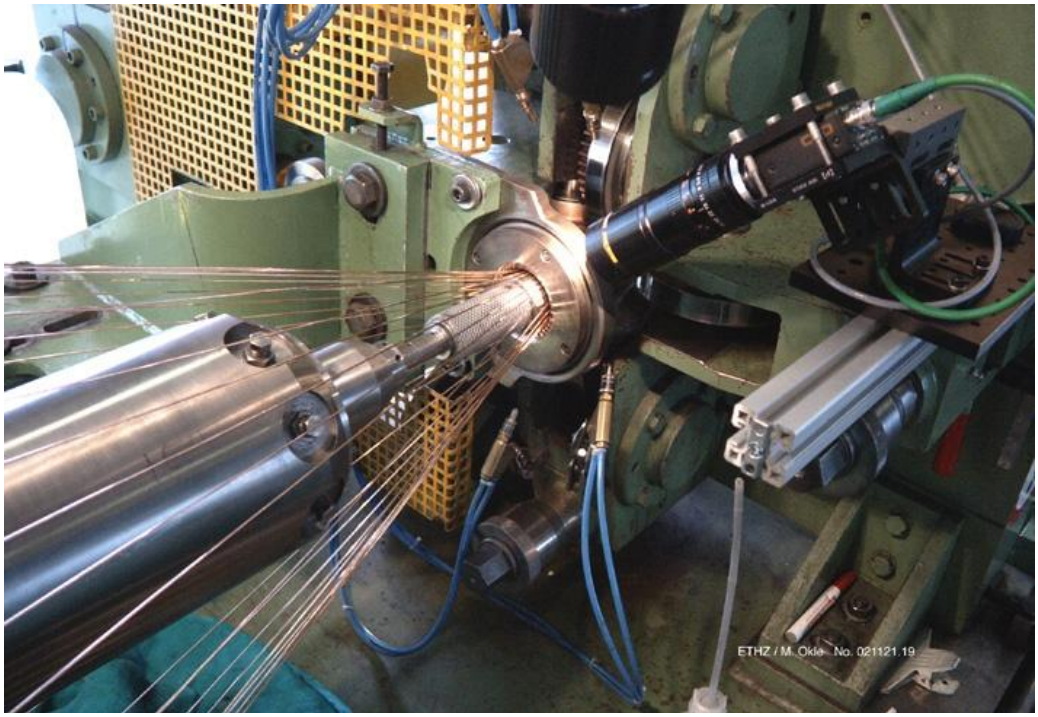

Figure 14. View of the wire's entrance in the winding machine of the precedent figure. Acknowledgements: Christian Scheuerlein (CERN - TE - MSC group).

Figure 15. Internal structure of a Rutherford Cable, that has been built with NbTi wires. NbTi filaments come out of the three wires, that have been "isolated" on the cable. Acknowledgements: Christian Scheuerlein (CERN - TE - MSC group).

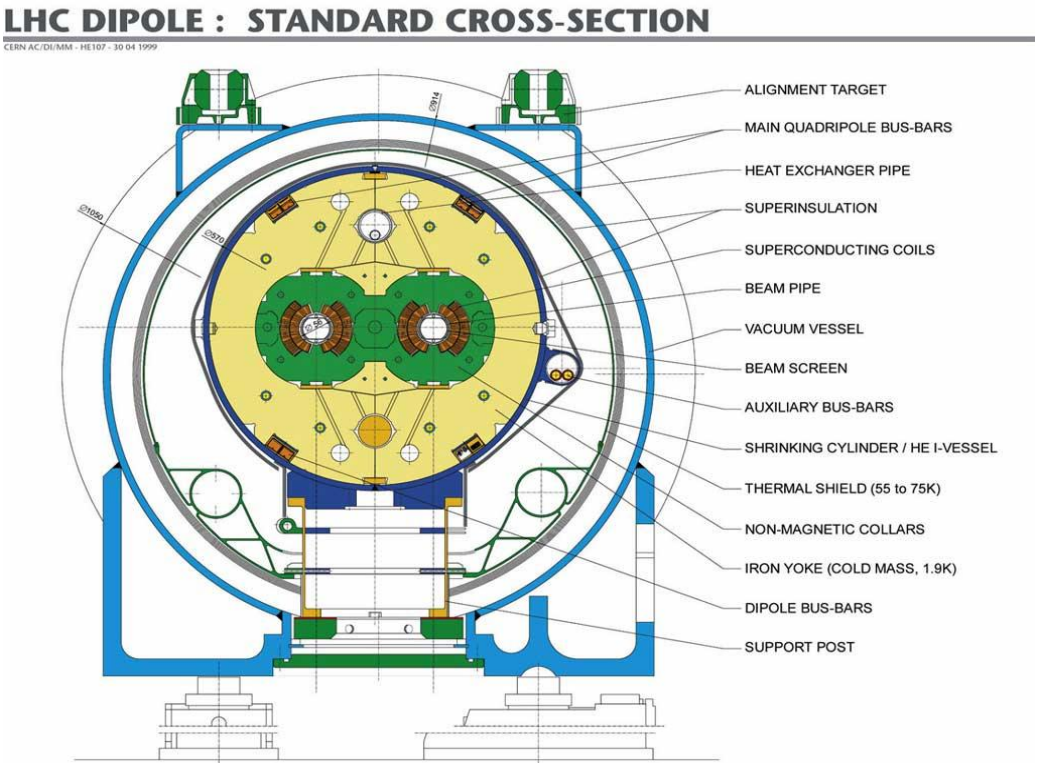

Figure 16. The cross section of a LHC dipole.

Chapter 2

Superconductors in Radiation Environments

2.1 Introduction

In the last 50 years several irradiation tests have been performed on Nb_3Sn *thin films* and *wires*, using different kind of radiations. For the present work, only those who are of interest for the LHC upgrade have been considered.

The results of the simulation of the expected radiation environment in the LHC sectors will be first presented. Starting from these data, the main results on Nb_3Sn's radiation damage studies will be illustrated, in link with the radiation-induced modifications of the material micro- and crystalline structure.

After the conclusions of the data summary, the motivations for the SIT project will be presented.

2.2 Expected Radiation Environments in the LHC Magnets

A simulation campaign of the expected radiation environment in the LHC's structures has been done by Cerutti *et. al.* [3, 4], considering a 10 year operating time of the particle accelerator. More precisely, it has been determined:

- The expected radiation types
- The energies of the incident radiations $E_{Particle}$, given in [eV]
- The radiation fluence φ , expressed as [particles*cm^{-2}]

The LHC's sectors where the radiation field will be the most intense are the magnets most proxy to the 4 detectors (ALICE, ATLAS, LHCb and CMS). These groups of quadrupoles constitute the so called "*HLI - High Luminosity Insertions"*. Figure 17 illustrates the general layout of the LHC and the approximate location of the HLIs near one of the detectors; Figure 18 the inner layout of the HLI quadrupoles.

The radiation that will hit the superconducting coils of these magnets will be produced from the collision debris of the 4 experiments and will have already interact with the detector's structure, the concrete shielding walls and the outer structures of the quadrupoles.

More precisely, the superconducting coils that will receive the most intense radiation load will be located at 23 meters from the interaction point, that is, the center of the 4 detectors where the 14 TeV center of mass proton-proton collisions will take place.

In these zones, it has been determined that the radiation hitting HLI's inner superconducting coils will be mainly composed by *neutrons, protons, photons, electron, positrons and (+,-) pions*.

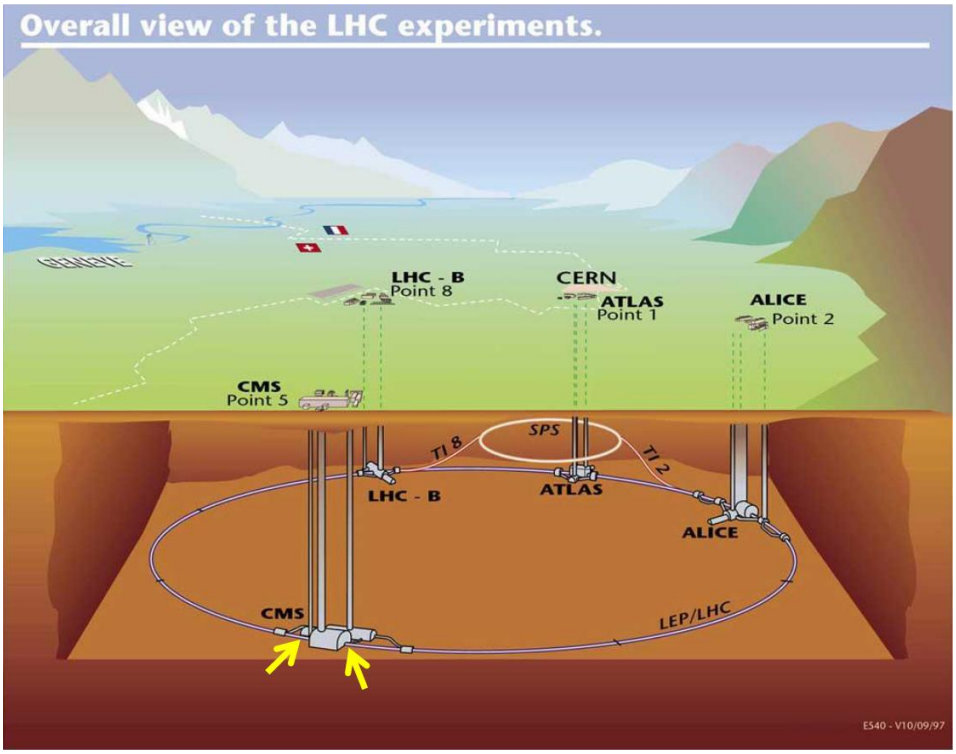

Figure 17. Sketch of the Large Hadron Collider with its 4 detectors (CMS, ALICE, LHCb and ATLAS). The approximate position of the High Luminosity Insertions is indicated with two yellow arrows on the figure, for the case on the HLIs near the CMS detector.

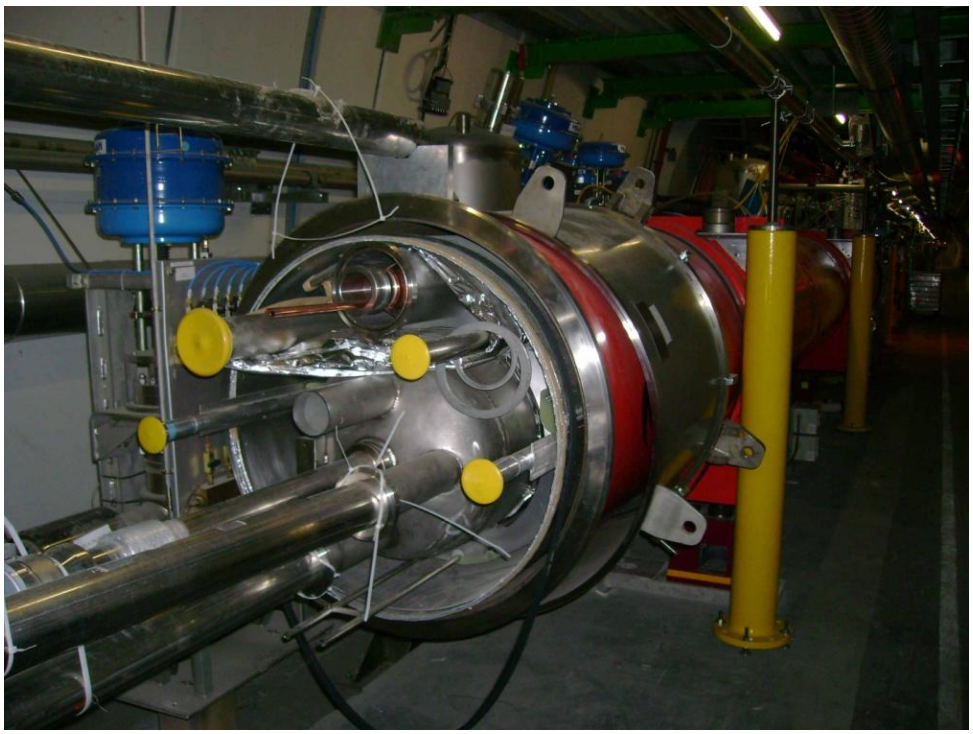

Figure 18. Inner view of the High Luminosity Insertion magnets, placed in the LHC tunnel just before the caverns that host one of the 4 detectors.

The radiation that will hit the HLI, will be composed of these particles in the following percentages [3, 4]:

- Neutrons 6 %
- Protons 0.15 %
- Photons 87 %
- Electrons 3.5 %
- Positrons 2.5 %
- Pions (+, -) 0.4 %

Photons [3, 4, 5] are the most damaging for the properties of the Nb_3Sn polymeric insulator, but will go through the whole coil [3, 4, 5]. *Electrons* and *Positrons* will give a negligible interaction with Nb_3Sn [3, 4, 5].

While the effect of *Pions* on Nb_3Sn *is still under investigation*, the attention has been initially focused on *Neutrons* and *Protons* for the organization of the SIT project, respectively due to the *mass* and *mass + electric charge's* effects of these particles on Nb_3Sn wires.

The *highest value* of the deposited is expected in the points of the HLI that are placed at distance of 23 m from the *interaction point* of the detectors [3, 4]. Figure 20 and 21 show the expected *neutron* and *proton* energy spectra [4] in the *superconducting coils* of these magnets.

The ordinate of these particle spectra are given in [Particles*Energy^{-1*}Area^{-1}]*[Particle Energy]*[Collision Event^{-1}] and have been calculated for a proton-proton collision of 14 TeV energy in the center of mass. Converting it in [particles*cm^{-2}], and considering that this conversion is based on an estimation[1] on the future exploiting of the LHC, it has been noticed that:

- Neutrons exhibit a pronounced peak at roughly 1 MeV energy. The correspondent integrated flux has been calculated to be roughly between 5*^{16} and *10^{17} neutrons*cm^{-2}.
- The proton energy distributions spreads over a *wider* energy interval respect to the neutron's distribution. In this case, the maximum is located at c.a. 100 MeV at a fluence of c.a. 6*10^{15} protons*cm^{-2}.

These values have been the starting point for the organization of the SIT project, as well for a first literature review on the irradiation studies that have been done Nb_3Sn from 1950 to present time.

2.3 1950 – 2010 Nb_3Sn Irradiation Tests Literature Review

The physical laws that describe the interaction between a nuclear particle incident crystalline material are so complex, and strongly radiation dependent, that a simple theoretical treatment is not possible. Aim of this section is to give a brief description of the mechanisms that allow neutrons and protons to change Nb_3Sn internal structure, and, on the macroscopic scale, his critical parameters.

[1] 10 years of operation, including 2 shut down periods of the LHC for its maintenance.

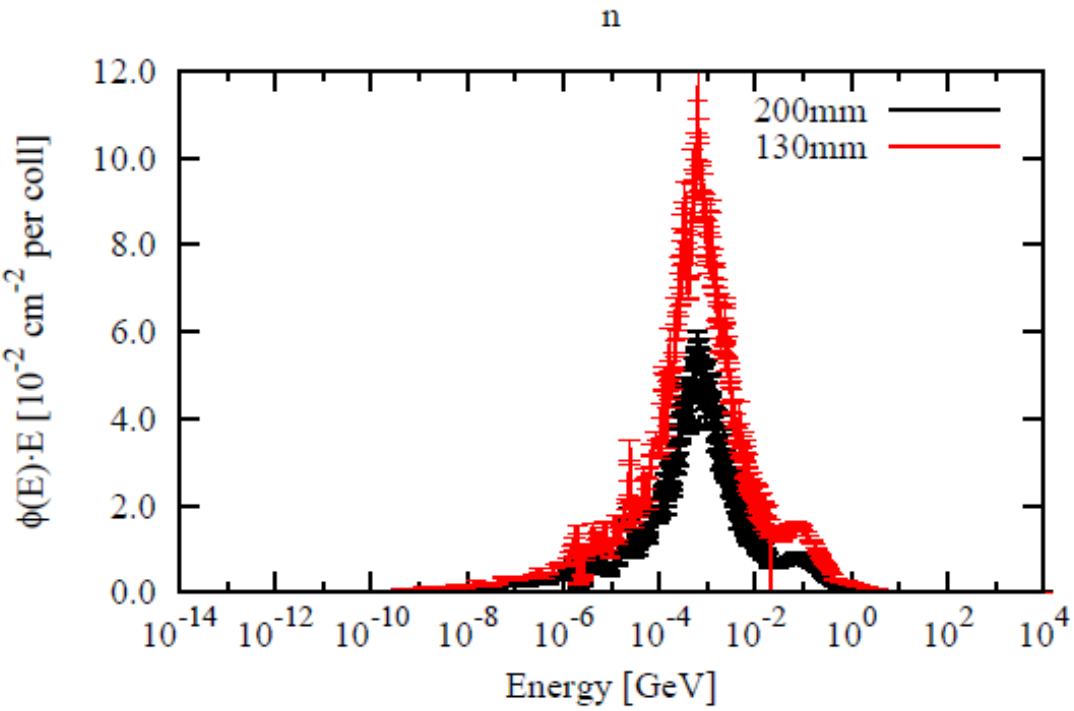

Figure 19. Expected neutron's energy distribution at 23 m from the Interaction Points in the HLI's superconducting coils. The spectrum has been calculated for two possible values of the coil aperture. Ref. [4].

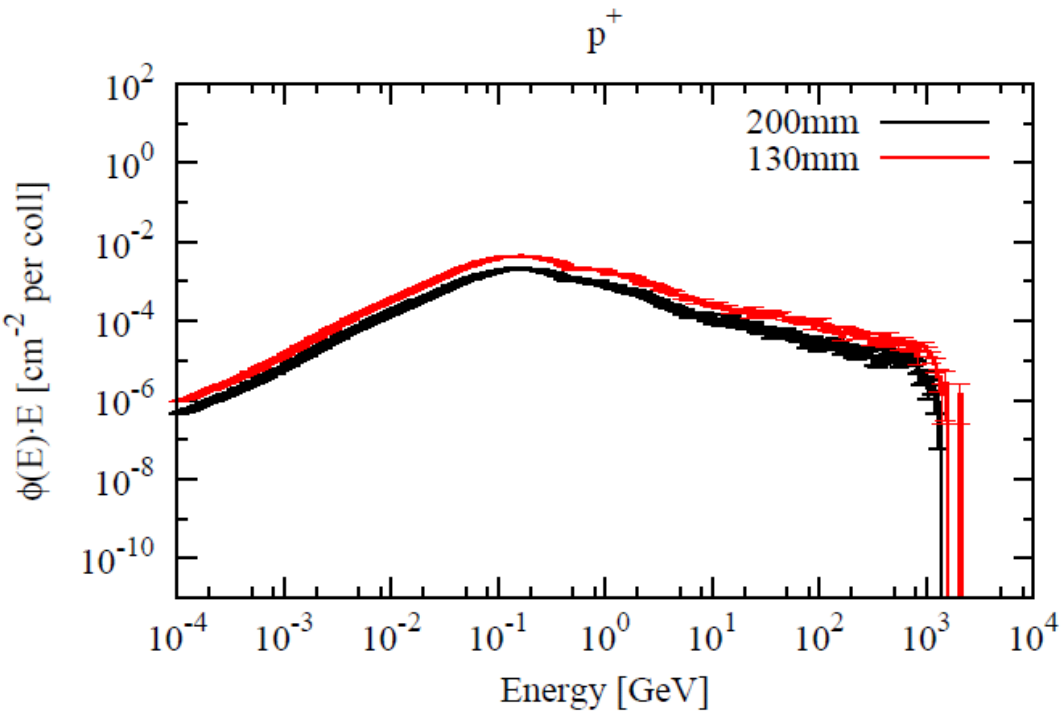

Figure 20. Expected protons energy distribution at 23 m from the Interaction Points in the HLI's superconducting coils. The spectrum has been calculated for two possible values of the coil aperture. Ref. [4]. It's also interesting to note that this energy distribution spreads up to an energy of the orders of the TeV, and that presumably some of the protons that will hit the HLI won't have interacted at the center of the LHC detectors.

2.3.1 Plots of the Experimental Data

The parameters of the energy distributions that have been chosen to analyze the calculated radiation spectra in the LHC magnets, are exactly those that have been frequently used in the past irradiation experiments of Nb_3Sn and on other A15's samples.

Fixing the particle type and energy used in the irradiation tests on superconducting *thin films* and *wires*, it has been more precisely plotted the ratio between a certain critical parameter P_C , measured on a sample that had been irradiated with a given value of φ, and the critical parameter in the material's non-irradiated state P, against φ. This kind of plotting procedure will be used in the rest of the section.

For completeness, it's worthwhile to note that some testing norms [6, 7], prescribe another kind of plot, that will be introduced now.

When a nuclear particle strikes against a material's crystalline lattice, it displaces atoms. These displacements are responsible for the variation of the physical properties of the material after irradiation, and manifest themselves into *displacement cascades*, that is, a succession of atomic displacement caused by the first atom - the *Primary Knocked out Atom* or *PKA* - that is hit by the incident particle.

Depending on the temperature, the displaced atoms are able to wander in the lattice and reorganize themselves into different forms (but frequently *clusters*) and, neglecting the exact shape of the *final* defect, the norms suggest to calculate the damage energy E_d for a *pure metal*, as follows [6]:

$$E_d = \langle \sigma * T \rangle * \Psi * t \tag{3}$$

where $\langle \sigma * T \rangle$ is the mean value of total energy transferred to each struck atom. More precisely, the damage energy is usually given in [keV*barns], and it's a function of:

- $\sigma(E)$, the particle's scattering cross section, function of the energy E of the particle
- $T(E)$, the primary recoil energy distribution, that is, the energy distribution of the first atoms undergoing recoil events after the collision with the incident particle
- Ψ, the particle flux, that is used in the irradiation tests, given in [particles*cm^{-2}*sec^{-1}]
- t, the exposure time of the sample to the particle field, given in [sec]

The damage energy is not only a function of the particle's fluence, but also of the energy spectrum of the irradiation source that is used in the irradiation tests. In fact, $\langle \sigma * T \rangle$ is calculated as [6]:

$$\langle \sigma * T \rangle = \frac{\int \left[\sigma(E) * T(E) * \left(\frac{d\Psi_t}{dE} \right) \right] dE}{\int \left(\frac{d\Psi_t}{dE} \right) dE} \tag{4}$$

integrating over the whole energy spectrum $\frac{d\Psi_t}{dE}$ of the radiation source.

For *alloys*, eq. (3) still holds, but the mean value of the transferred energy is written as [6]:

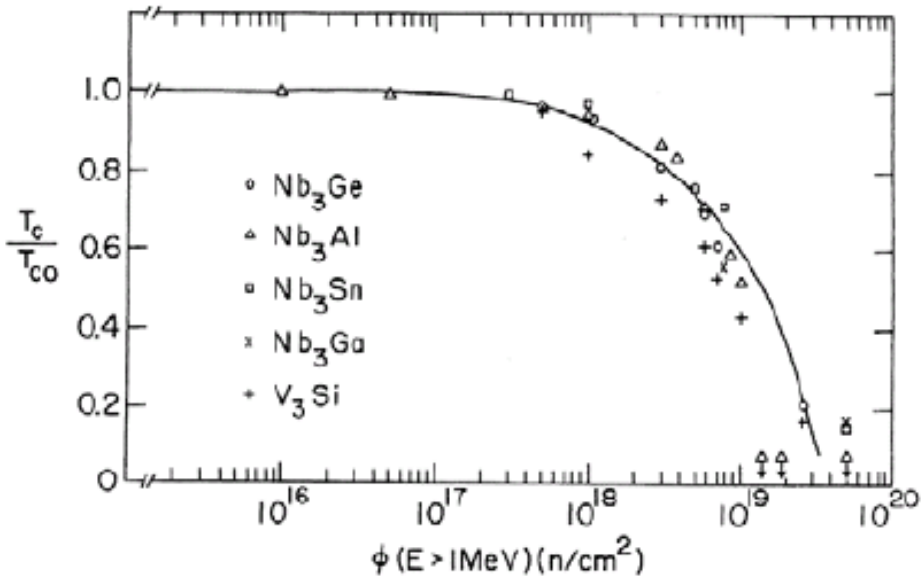

Figure 21. The Reduced Critical Temperature against the Fast Neutron total dose for several A15 materials. The fitting curve has been obtained from the *Aronin Model*. Ref. [1, 5].

$$\langle \sigma * T \rangle_{Alloy} = \sum_i C_i * \langle \sigma_i * T_i \rangle \quad (5)$$

and is a function of the at% C_i of the *i-th* element and of its specific transferred energy $\langle \sigma_i * T_i \rangle$.

Various measurements are performed on specimens, and after the irradiation, the specific material's property is measured in well defined experimental conditions. The results are then plotted as a function of the increasing damage energy, as it will be done in the future by the SIT research team at CERN.

2.3.2 Critical Temperature Variation

Fast Neutron (E > 1 MeV) irradiation tests performed on several A15's *thin films* and *wires* have shown a common behavior of the reduced critical temperature $\frac{T_C}{T_{C0}}$ against φ [5]. Figure 21 shows this trend, where $\frac{T_C}{T_{C0}}$ stays constant for a fluence value up to 10^{17} neutrons*cm^{-2}, then rapidly decreasing to zero for $\varphi t > 10^{19}$ neutrons*cm^{-2}.

When an A15 superconductor is placed in the non - irradiated state, their atoms are arranged in a simple cubic crystal, in which Nb form three dimensional chains. In these chains, the strong overlapping of the *d - orbitals* forms routes where the cooper pairs can propagate.

A general interruption of the Nb chains can have, in principle, an influence on the superconductive properties of the material. Starting from this observation, Sweedler *et. al.* [1, 5] have shown that the neutron irradiation produce *focused displacement collision sequences* in the [102] direction with the creation of *anti - site* defects, that is, site exchanges between *Nb* and *Sn* atoms. Among all the crystalline defects that fast neutrons can induce in the A15 lattice, *anti - site* defects are supposed to be the principal cause for the interruption of the *Nb* chains [5].

Figure 22 illustrates this phenomenon.

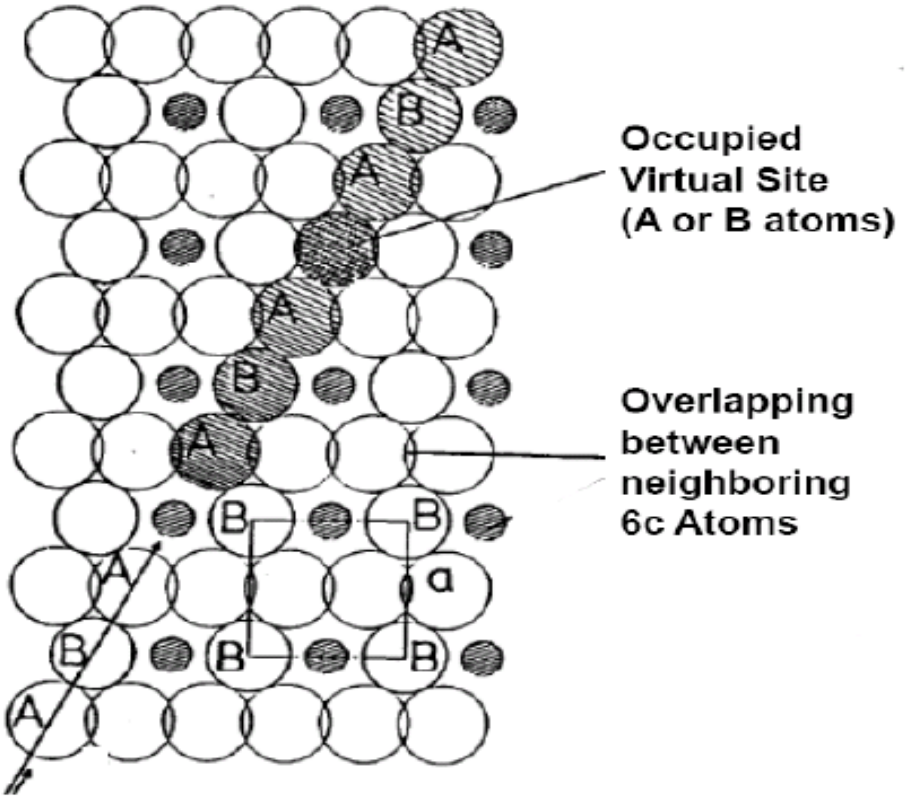

Figure 22. The fast neutron induced focusing displacement collision sequence in the Nb_3Sn lattice. Ref. [5].

The variation of the reduced critical temperature has been well described by Sweedler *et. al.* [1] thanks to the measurement of the *S* value via X - Rays measurements performed on the irradiated Nb_3Sn samples.

According to Aronin [1], the Bragg Williams order parameter scales with the neutron fluence as:

$$S = S_0 * \exp(-k\varphi) \tag{6}$$

where S_0 is the value of the superconducting sample's order parameter value before the irradiation tests and *k* a material's dependent constant ($k = 10^{-20}$ cm^2 for Nb_3Sn [11]). At the same time $\frac{T_C}{T_{C0}}$ scales with *S* as [1]:

$$\frac{T_c}{T_{co}} = \exp\left(-5 * \left(1 - \frac{S(\varphi)}{S_0}\right)\right) \tag{7}$$

and substituting eq. (6) into eq. (7), the final expression for $\frac{T_C}{T_{C0}}$ against φ can be obtained:

$$\frac{T_c}{T_{co}} = \exp\left(-5 * \left(1 - exp(-(10^{-20}) * \varphi)\right)\right) \tag{8}$$

Specifically for Nb_3Sn, this formula can be assumed to be valid for binary *thin films* and *wires*. In fact, some authors [1, 5] do report that the *Cu* matrix of the wire, in which the superconducting phase is enclosed, is supposed to not have any *shielding* effect on energies of the incoming particles.

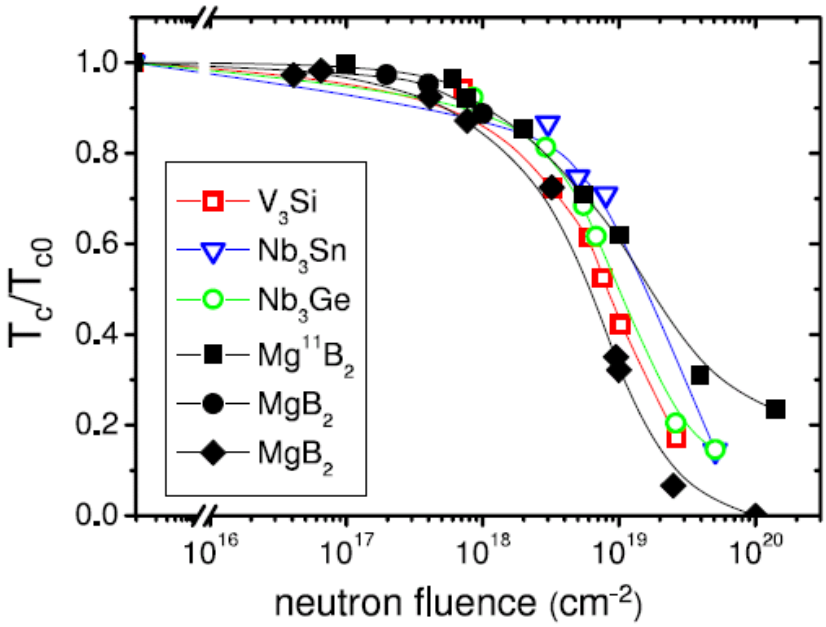

Figure 23. The reduced critical temperature against the fast neutron integrated flux for some of the A15's materials and MgB_2. Ref. [8].

It's interesting to note that, even though MgB_2 does not belong to the A15's family, its $\frac{T_C}{T_{C0}}$ against φ behavior is the same as the A15's one, as shown in Figure 23. In this case, the Mg^{11} isotope's (n, n) reaction cross section is big enough to produce, during the irradiation, new neutrons that contribute to the atom's displacements in the material [8].

Significant data of the variation of $\frac{T_C}{T_{C0}}$ with *protons*, as well with other particle's total dose have *not yet* been found.

2.3.3 Upper critical field and normal state resistivity variation

Flükiger *et. al.* [5] have irradiated binary and Ti- Alloyed Nb_3Sn *wires* with 14.8 MeV neutrons, and measured the changements of the reduced upper critical field. Figure 24 shows these results, where the upper critical field shows a maximum, that is placed at φ = 10^{18} neutrons*cm^{-2}. The alloying shifts the maximum in $\frac{B_{C2}}{B_{C20}}$ towards lower flux values by roughly one order of magnitude.

Fitting then the data obtained by Brown *et. al.* [9] for fluencies greater than 10^{17} neutrons*cm^{-2}, the following relationship for the variation of the normal state resistivity against the fast neutron fluence has been *precisely* determined:

$$\rho_0 = -7 * 10^{-37}(\varphi)^2 + 5 * 10^{-18}(\varphi) + 15{,}45\ [\mu\Omega * cm] \qquad (9)$$

where the fast neutron fluence φ is expressed in [neutrons*cm^{-2}]. Eq. (9) has been plotted, together with the experimental results [6], in Figure 25. It's interesting to note that, in the fast neutron flux interval [10^{18}, 10^{19}] *neutrons*cm^{-2}* (where the increase in ρ_0 have been observed) the reduced upper critical field and the normal state resistivity scale linearly with φ, because the experimental points of Figure 26 can be also be *linearly* with sense.

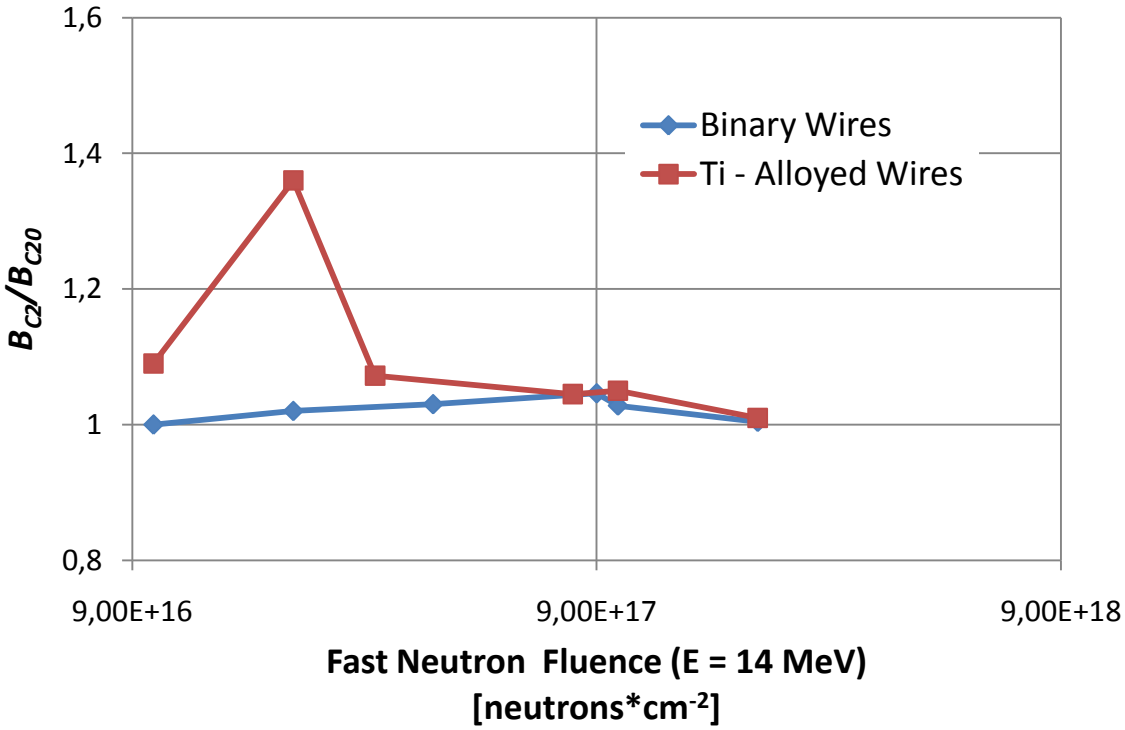

Figure 24. Reduced upper critical field against the *fast* neutron fluence (E = 14 MeV) for binary and Ti - Alloyed wires. Ref. [5].

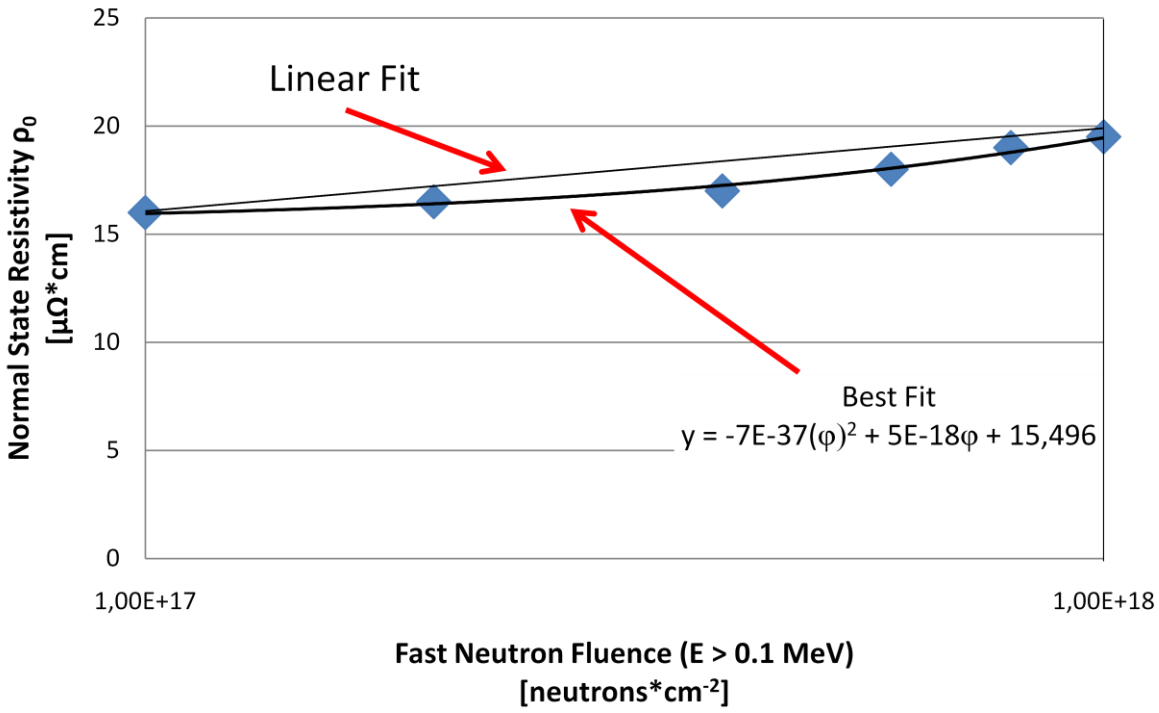

Figure 25. Normal state resistivity against the *fast* neutron fluence for binary Nb_3Sn. Considering the orders of magnitude of the resistivity, and supposing that the resistivity is proportional to the density of scattering centers (radiation induced defects), the best fit does not produce a substantial difference in the fitting procedure respect to the best fit. Ref. [9].

2.3.4 Critical Current Density Variation

In a similar way to the reduced critical temperature and upper critical field, the reduced critical current $\frac{J_C}{J_{C0}}$ can be defined. A big amount of data has been found for the irradiation of Nb_3Sn *thin films* and *wires*; less on the other Nb- and V- base superconducting compounds.

A *unique* plot of the available experimental data, has not been feasible because the energy spectra of the neutron irradiation souces, that have been used for the test, were sometimes not given in the literature. The results of the neutron and proton irradiation tests will be therefore separately presented. Also, the less amount of the experimental points has not allowed to find scaling relationship of $\frac{J_C}{J_{C0}}$ against the fluence and the applied magnetic field

Fast neutron irradiation studies (***E > 0.1 MeV***), performed on *binary*, as well as *alloyed* Nb_3Sn *thin films* and *wires* [10, 11] show a pronouced peak in $\frac{J_C}{J_{C0}}$ up to an applied field of 16 T, that is centered at roughly $\varphi = 10^{18}$ neutrons*cm^{-2}. The highest values of this maximum is roughly $\frac{J_C}{J_{C0}} = 2$ at the highest fields, as shown in Figure 27.

Separate attention has been given to the neutron irradiation studies (***E > 1 MeV***) performed by *Weber et. al.* on *binary* and *alloyed* Nb_3Sn wires [12]. These peak values in $\frac{J_C}{J_{C0}}$ are centered at a fluence value higher than the previous one, and the authors have related this results to the different energies *neutron energies intervals*, that they have used for the determination of *φ(E)*.

Figure 28 shows these results. In particular, Figure 28 shows that the effect of the Ti addition is to shift the values of the maximum towards lower fluences, respect to the case of the *binary* wires.

In a more recent work, Weber *et. al.* [13] have calculated the value of the damage energies, and plotted their $\frac{J_C}{J_{C0}}$ data as a function of E_d, as reported in Figure 29. Also, they have measured the reduced critical current density to applied fields up to 16 T, reaching a highest value of $\frac{J_C}{J_{C0}} = 4$.

Figure 28 shows the effects of the proton irradiation on *binary* Nb_3Sn wires and thin films [14, 15, 16]. 2.6 MeV, 2.83 MeV and 30 GeV ***monochromatic*** proton beams have been respectively used for these irradiation studies, and in this case, a ***unique*** plot of the experimental results has been possible. In this case, the proton irradiation produces a maximum in $\frac{J_C}{J_{C0}}$, which is now centered at φ = 8*10^{16} *protons*cm^{-2}*.

The major reason for the prensence of the maxima after neutron, as well after proton irradiation, may be the formation of *clusters*, created by the *diffusion* and *reorganization* of the Frenkel defects that the nuclear particles are able to produce in the superconductor's crystal lattice [5, 12, 13]. It is nowadays *not yet clear* if these clusters act as *pinning centers*, or if the the enhacement in the reduced critical current density may be principally related to the variation of the Bragg Williams order parameter [5]. This aspect will be further investigated by the SIT resarch team.

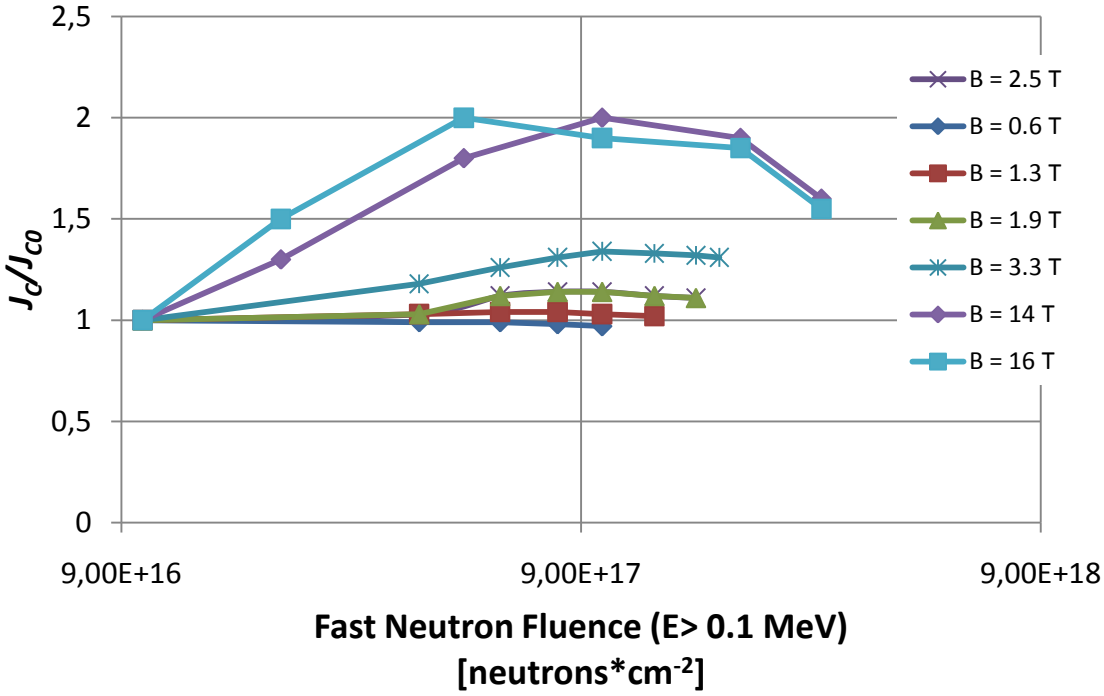

Figure 26. The reduced critical current density against the fast neutron (*E > 0.1 MeV*) fluence for binary Nb_3Sn wires. *B* is the value of the applied magnetic field used in the critical current measurements on the irradiated samples. Ref. [10, 11].

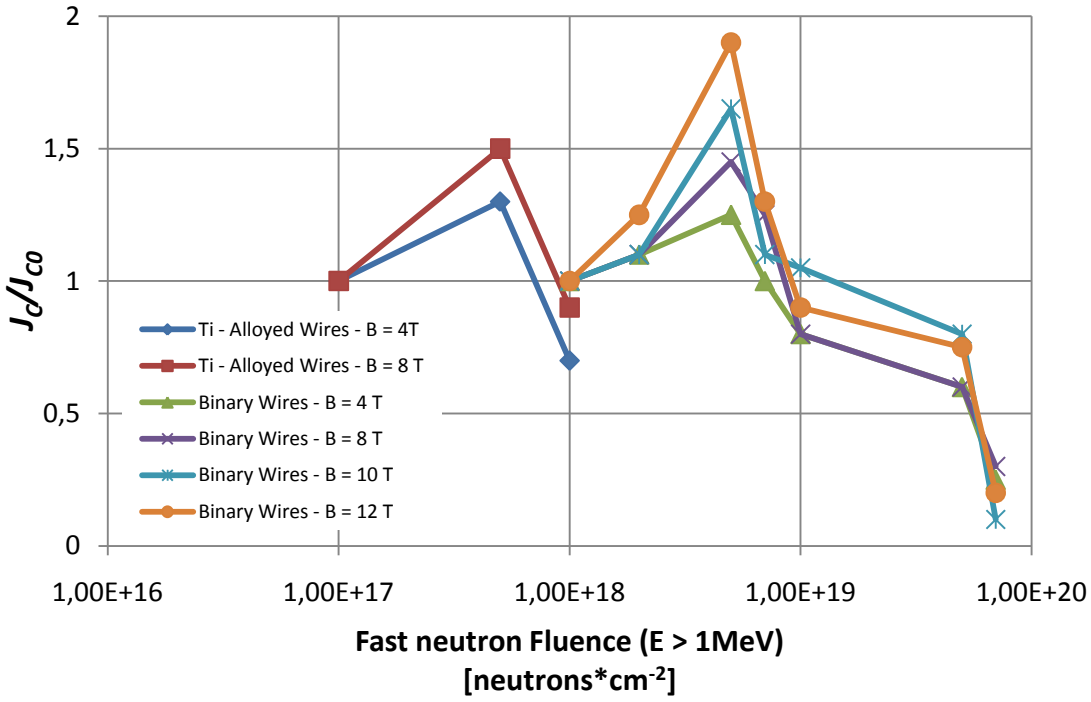

Figure 27. The reduced critical current density against the fast neutron (*E > 1 MeV*) fluence for binary and for Ti alloyed Nb_3Sn wires. *B* is the value of the applied magnetic field used in the critical current measurements on the irradiated samples. Ref. [12]

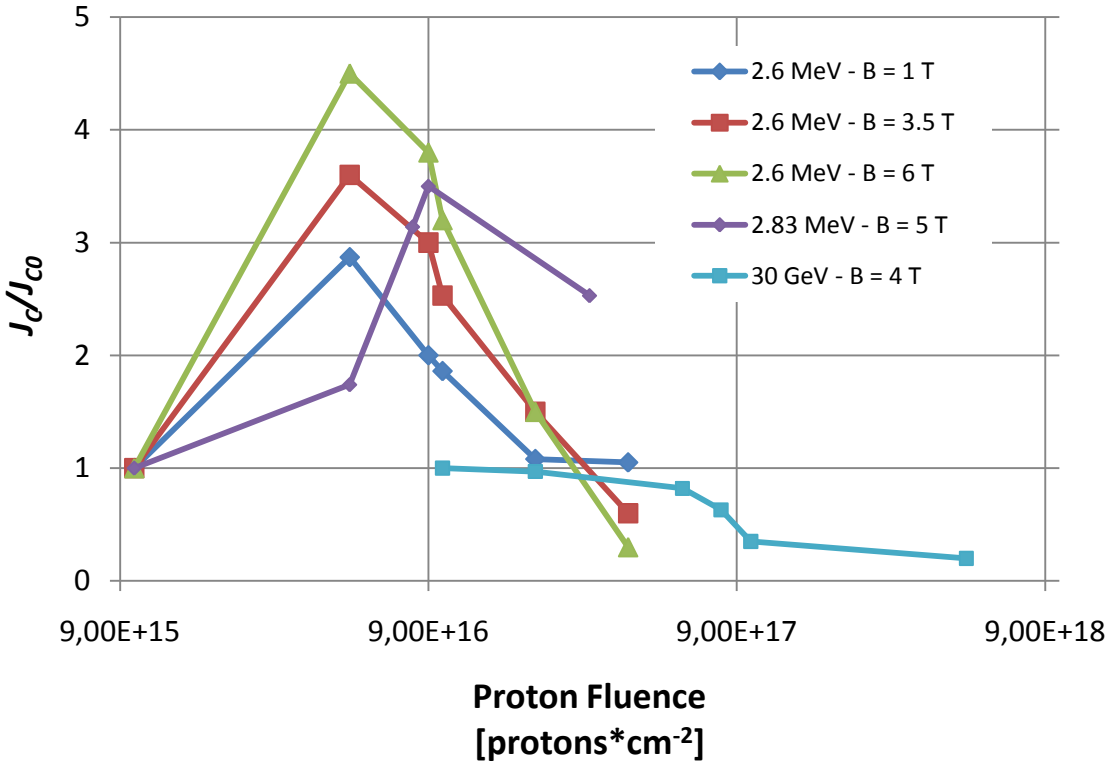

Figure 28. The reduced critical current density against the proton fluence. *B* is the applied magnetic field used in the critical current measurements on the irradiated Nb_3Sn samples. Data Ref.: 2.6 MeV - B from 1 to 6 T [14], 2.83 MeV - B = 5 T [15] and 30 GeV - B 4 T [16].

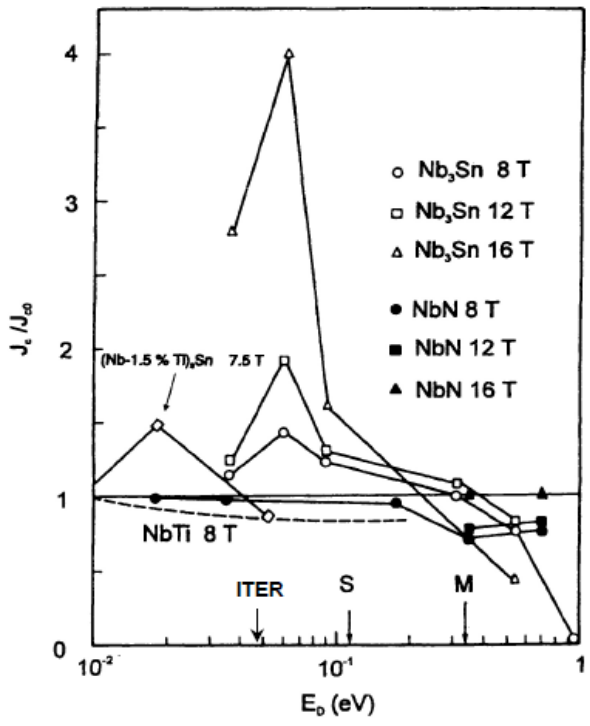

Figure 29. The reduced critical current density of binary and Ti alloyed Nb_3Sn and of NbTi wires against the fast neutron (*E > 1 MeV*) damage energy E_d. Ref. [13].

Nevertheless, a first *attempt* to compare the results of the neutron and of the proton irradiation studies performed on *binary* Nb_3Sn samples has been done, plotting the reduced critical current density values for the nearest values of applied magnetic fields. This plot is shown in Figure 30, and it is seen that:

- The proton irradiation produces a 2 times higher values of the maximum in $\frac{J_C}{J_{C0}}$
- This maximum is shifted towards lower fluxes in the case of proton irradiation, respect to the neutron irradiation case.

At the same time, the displacement cross sections $\sigma(E)$ have been *estimated* from the available experimental data [15] and compared in Table 1, under the hypothesis that the *Cu* matrix of the wires does not *shield* the superconducting phase under irradiation. It is seen that they differ by roughly 1 order of magnitude. Even tough the units are differents, a similar shift that is present in the neutron and proton irradiations plots of Figure 31.

According to Flükiger [5, 17], these data should confirm that the difference between the neutron and proton irradiation rely in the variation of the electronic density of state near the Fermi Level, that is caused by the variation of *S* after the irradiation. The formation of clusters, and the consequent enhancement of the density of the pinning center may be seen as a a connected, but not but not main reason.

2.3.5 Copper matrix resistivity variation

Starting from the available literature data [18, 19], estimations of the flux and energy distributions of the energy and flux distribution of fast neutrons (*E > 0.1 MeV*) and protons (*E c.a. 100 MeV*) on the cross section of a composite Nb_3Sn wire have been done, in relation with expected particle spectra and penetration lengths in the HLI's superconducting coils. Significant variations of the Cu matrix resistivity in the Nb_3Sn composite wires are thus not expected.

In order to complete on the irradiation studies of Nb_3Sn composite wires, the results of the literature review on the copper's resistivity variation will be only *summarized* now.

The copper resistivity increase is a function of the neutron's integrated flux and of the applied magnetic field. An a hypothesis, the Matthiessen rule can be applied, because the simultaneous effect of neutron and proton irradiation have not yet been clarified, and it can be written:

$$\rho_{Cu}\left(T, \varphi_n, \varphi_{p^+}\right) = \rho_{Cu}(T) + \Delta\rho(\varphi_n) + \Delta\rho(\varphi_{p^+}) \tag{10}$$

where $\Delta\rho(\varphi_n)$ and $\Delta\rho(\varphi_{p^+})$ are, respectively, the neutron's and protons contribution to the copper matrix resistivity, both function of the particle fluences.

Blewitt *et. al.* [18] have proposed the following model for $\Delta\rho(\varphi_n)$, fitting the data of different authors:

$$\Delta\rho(\varphi_n) = s * \left(1 - exp(-K * \varphi)\right) \tag{11}$$

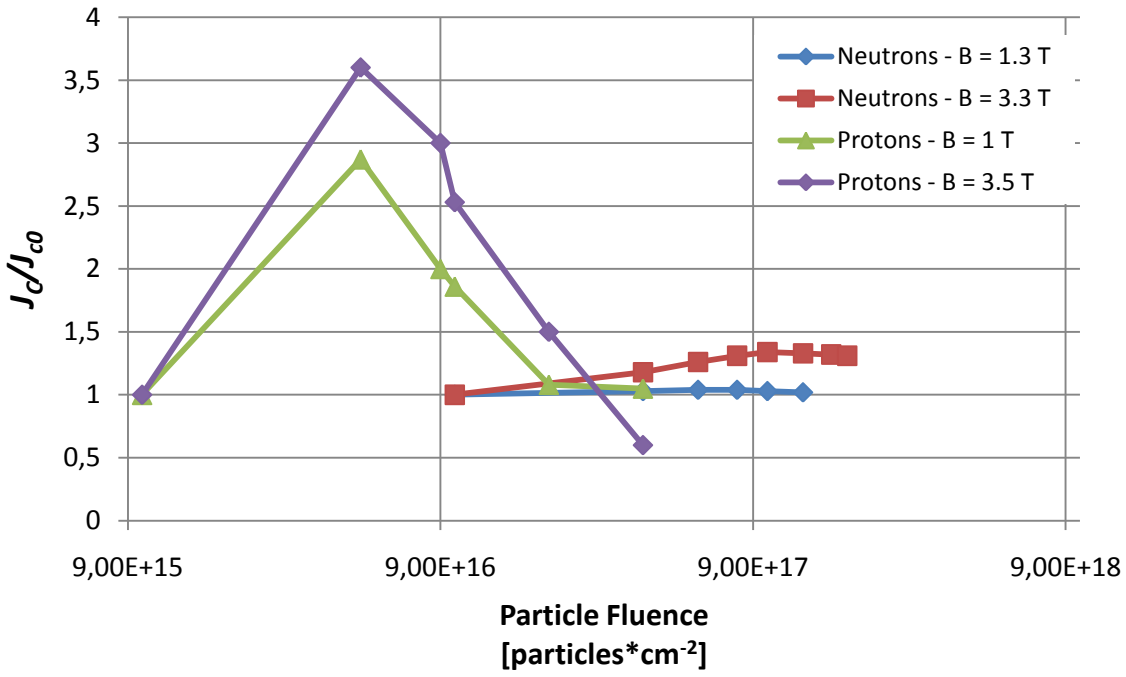

Figure 30. Comparison between the fast neutron (E > 0.1 MeV) and the 2.6 MeV proton irradiation studies on *binary* Nb_3Sn samples. *B* is the applied magnetic field used in the critical current measurements on the irradiated samples. Data Ref. [10, 14].

Particle	**Energy** **[MeV]**	σ_D **[barns]**
Neutrons	> 1 Mev	10^3
Protons	2.83 MeV	$1.6*10^4$

Table 1. The estimated neutron's and proton's displacement cross section values in Nb_3Sn. Ref. for the estimation [15].

where *K* is a constant, that has been found to depend from the energy of the incident particles, and *s* the saturation value of the normal state resistivity at high neutron fluences. For fast neutrons (*E > 0.1 MeV*) $K = 1.62*10^{-23}$ m^2 and $s = 4*10^{-9}$ Ω*m [20].

Omar [19] has irradiated *Cu* thin foils with 10 - 16 MeV proton beams, finding that the rate of increase of the resistivity against the flux, can be written as :

$$\frac{d\Delta\rho_{Cu}}{d\varphi_{p^+}} = 10^{-25} * \frac{k*E_d}{2*E_D} * \Delta\rho_{F.P.} \qquad (12)$$

and tells that the linear increase in the *Cu* resistivity is a function of the Frenkel Pair's resistivity $\Delta\rho_{F.P.}$ (given in [nΩ*m]), the damage energy E_D and of the energy threshold E_d (given in [eV]) for

the displacement of atoms in a *Cu* crystal. In the selected proton energy range, $\Delta\rho_{F.P.} = 1.3\text{n}\Omega * \text{m}$, while E_d = 25 eV. Values for E_D can be found in [19], as a function of the proton energy.
Considering then the applied field contribution [18]:

$$\Delta\rho(H) = \Delta\rho(\varphi_n) + 10^{\alpha} * H^{\beta} * \Delta\rho(\varphi_n)^{1-\beta} \quad (13)$$

where α and β are *fitting parameters*, and *adding* eq. (13) to eq. (10), the final expression for the variation of the copper resistivity can be given:

$$\rho_{Cu}(T, \varphi_n, \varphi_{p^+}, H) = \rho_{Cu}(T) + \Delta\rho(\varphi_n) + \Delta\rho(\varphi_{p^+}) + \Delta\rho(H) \quad (14)$$

where $\rho_{Cu}(T)$ is the temperature - dependent value of the Cu resistivity.

First estimations of the variation of the copper resistivity with *simultaneous* neutron and proton irradiation and *with the application* of the highest magnetic fields in the HLI, have shown that ρ_{Cu} will be enhanced by a max. factor of 10 respect to its low temperature value.

2.4 Data Summary Conclusions

The fast neutrons (E > 0.1 MeV) irradiation tests performed on *binary* Nb_3Sn wires and thin films from 1950 up to date have characterized the variation of the critical temperature, the upper critical field, the normal state resistivity and in an extensive way. Also the variation of the critical current density has been studied, up to the highest applied magnetic fields.

Data on proton irradiation studies have been found only for *binary* Nb_3Sn *samples*, *only* on the variation of the critical current density after irradiation with 2.6, 2.83 MeV and 30 GeV monochromatic beams. These data show that the proton irradiation also generates a peak in the reduced critical current density, and that this peak is centered at a lower fluence value respect to the neutron irradiation case.

The neutron and proton irradiation effects on *Ti - and Ta - alloyed* superconducting Nb_3Sn wires, have not yet been totally clarified, especially on the position of the maxima of the critical current density values respect to the expected neutron and proton fluences in the HLI.

2.5 Motivations for the "SIT - Nb_3Sn" Project

Alloyed Nb_3Sn superconducting wires are planned to be used in the LHC - Phase II upgrade, because of the better critical properties respect to the binary wires.

These materials will be installed in the HLI quadrupoles, that are close to the 4 detectors of the particle accelerator. The proton - proton collision events are going to produce debris, whose trajectories are principally contained by a cone that starts from the interaction points in the detector and invests the closest structure of the LHC. In Figure 32 this process has been sketched.

The collision debris will interact with the detector's outer structures (shielding, magnets etc.) and deposit energy along the HLI. Cerutti et. al. [3, 4] have shown that this energy deposition varies along the HLI system axis, having his maximum value in the superconducting coils of the HLI at 23 m from the interaction points; the particle energy distributions, of Figure 19 and 20 , are

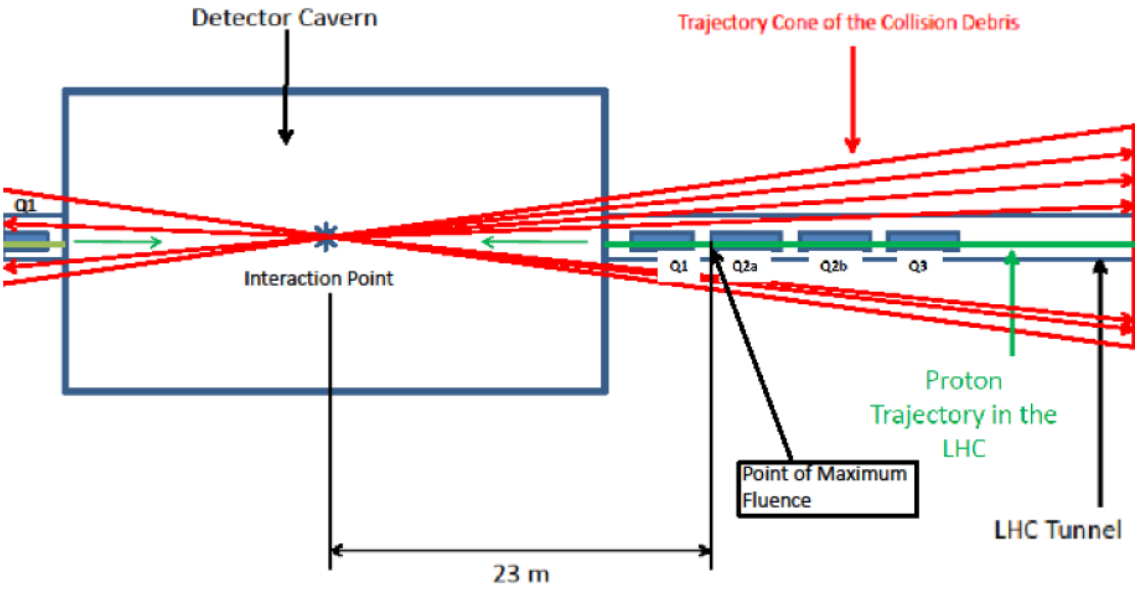

Figure 31. Sketch of the LHC structures, that are close the 4 detectors. When the collider works at highest power, a 7 TeV proton beam of the LHC is focalized into the detector thanks to the 4 HLI magnets Q1, Q2a, Q2b and Q3. A proton - proton collision will produce debris, whose trajectories are *principally* enclosed in a cone, that will outgo from the Interaction Point to the external structures of the collider, thereby depositing energy in the HLI, with a maximum at 23 m distance from the interaction point. To keep the sketch as simple as possible, the detector structure and the shielding walls have not been drawn.

referred to the superconducting coils of the HLI exactly in this point.

Neutron and proton are the particle that, in principle, can cause the highest variation of the critical current density of the alloyed superconducting material. Because experimental data on the radiation damage rate of these superconductors are missing, a new research activity has now to be started to allow the collider's power enhancement in 2016.

In addition, the available experimental data are not enough to extrapolate a reasonable model for J_C as a function of the other critical parameter of the alloyed superconductor in the irradiated state.

Under these motivations, CERN has started in March 2009 the "Nb3Sn - Superconductor Irradiation Test" project. The first organization and experimental activities of the SIT project, that have been done from March 2009 up to date, will be presented in the next chapters.

Chapter 3

The First Engineering Activities of the Superconductors Irradiation Test Project

3.1 Introduction

At the beginning of the SIT project, it was not yet clear if the irradiation experiments will have been performed into structure that had the necessary technical equipment (particle beam, cryogenic system, radiation confinement area etc.) to perform irradiations and following critical current measurements on samples of superconductors. The SIT project has thus started with the *a conceptual design* of the irradiation test, that has been based on the traditional layout of installation for radiation damage studies and CERN critical current measurements test stations.

Once the different stages of the SIT irradiation tests have been accurately defined, the search for the candidate irradiation facilities has been done. As it will be presented in the next sections, fast neutron irradiation tests have been assigned in May 2010, while proton irradiation tests not yet.

The *preliminary design* of the most important component of the SIT irradiation test equipment, the *sample holder*, has been done from the conceptual design of the SIT experiment and the first tests of this apparatus constitute the first SIT *experimental* activities.

These aspects will be presented in the next sections.

3.2 Basic Conceptual Design of the SIT Irradiation Test

A sketch of the SIT irradiation test conceptual design is shown in Figure 32. Starting from this layout, the design will be discussed now in detail.

The irradiation of superconducting Nb_3Sn samples is performed into an appositely built vessel. A beam will enter through a proton transparent window, that will be centered with the geometrical axis of a proton beam line, and strike the basis of an appositely built sample holder.

If the SIT research team would not have found a *nuclear reactor* for neutron irradiation of the superconducting samples, then the neutrons could have been obtained replacing the proton transparent window of the irradiation vessel with a material that allows (p, n) reactions.

Keeping the proton irradiation as a reference, the significant heat load that is deposited in the sample holder is be extracted thanks to a cooling system connected with the irradiation vessel. This cooing system is composed by a pipe line, a pumping system and a re-condensation system, and the coolant flows in this circuit under *forced flow*. A stationary level of the in the irradiation vessel can be thus thought during the irradiation, and the use of three possible coolants (He at 4.222K, N_2 at 77 K and H_20 at room temperature) is currently under investigation. More precisely, the irradiation in a He or N_2 bath has the advantage to:

- Reproduce at closest the working conditions of the material in the LHC magnets
- Avoid annealing effect of the sample during the irradiation

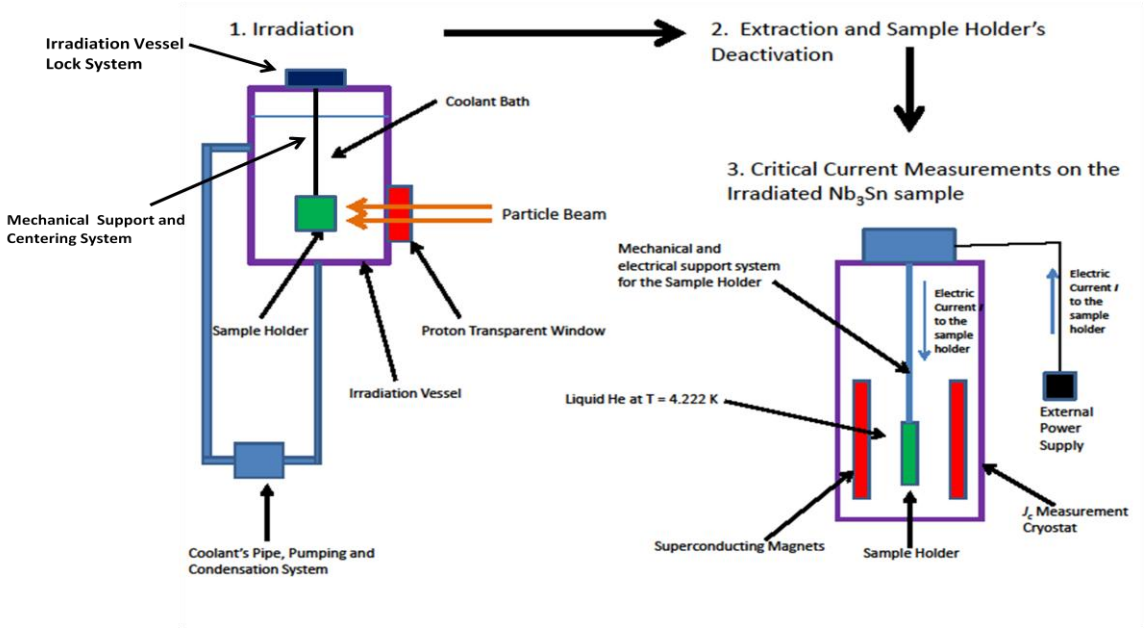

Figure 32. The basic conceptual design of the SIT irradiation tests

Conversely, the use of water as coolant does not allow to place the superconductors in the same environment as the one of the HLI magnets, but this fluid is frequently used for the cooling of particle accelerator electromechanical components. Also, the activation energy for the annealing of Nb_3Sn is very high compared to *kT* (where k is the Boltzmann constant) at T = 298 K [5], and annealing effect during the irradiation can be, in principle, ignored.

It's also worth to note that, if the institute that does the irradiation, is *a priori* not equipped to host the vessel and the attached cooling system in proximity to the beam line, the design and test of the irradiation station requires a new R&D activity, that is planned to last, in principle, some years. Also, the choice of the coolant determines the acceptable temperature distribution in the sample holder during the irradiation stage, and has to be consequently related to the best working conditions of the beam line. For these reasons this year's activity of the SIT project has been focalized on the design and test of the sample holder. A first attempt to study the working conditions of the sample holder has been done in an *ideal proton* irradiation environment has been done, and will be presented in the next sections.

Once the irradiation stage is finished, the sample holder is extracted from the irradiation vessel thanks to a crane and put into a confinement area, to wait to its *deactivation*. At the end of the deactivation period, the device is mounted on a mechanical and electrical support, to its insertion in the cryostat for the measurement of the critical current on the irradiated sample.
An external power supply is connected via current lead system to the sample thanks to this support system, and a steady DC current ramp rate $\frac{\Delta I}{\Delta t}$ is given to the irradiated sample until the superconducting transition is reached. Also, the support system centers the sample holder between superconducting magnets that impose the sample the applied field *B* during the critical current test, that is done in a Helium environment at a temperature of 4.222 K.

This procedure is repeated irradiating several samples with different radiation doses φ during an irradiation time τ, that is, in first approximation, given by:

$$\tau = \frac{\varphi}{\Psi} \tag{15}$$

where Ψ is the particle *flux* of the beam line. Ψ determines the deposited power on the sample holder, and has consequently to be related to the *future* design of the irradiation test stations, in strong connection with the *cost* for the use of the beam line. Measuring then the critical current for different applied fields *B*, on samples that have been irradiated with a given fluence φ, the plots of critical current curves against the dose, as the one of Figure 26 → 29, can be constructed.

Finally, the sample holders are prepared and tested at CERN before each time sending them to the research institute that will perform the irradiation and critical current measurements. In this view, the study of the preparation procedure of the SIT sample holder has constitutes part of the experimental activity of the present work.

3.3 Search For the Irradiation Facilities

Starting from the conceptual design of the SIT irradiation tests, the irradiation facilities capable to host the radiation damage experiments have been searched from March 2009 to June 2009. A list of the candidate institute has been established and will be discussed in this section, together with the current status of the irradiation tests.

3.3.1 Irradiation Facilities at CERN

In Table 2, the characteristics of the CERN irradiation facility are reported.

The "CNGS - Cern Neutrinos To Gran Sasso" beam line has a *mixed* radiation field, that is the most proxy to the one expected around the LHC's - HLI magnets. Problems concerning the handling of activated Nb_3Sn samples and the activation of the test equipment have let fallen down this choice. Similar problems have been encountered when analyzing the characteristics of the "nTOF - neutron Time Of Flight" facility.

While some irradiation facilities work with a *quasi*[2] continuous particle beam, others do it with a pulsed one. The "Hi.Rad.Mat - High Radiation Materials" is of this kind, and produces a high intense proton beam, that is unfortunately too intense for the Nb_3Sn wire and would have consequently damaged the sample. On the other side, the "ISOLDE" and the "PS" beam lines were characterized by a too low proton flux, and this would have increased the cost of the irradiation tests.

3.3.2 Irradiation Facilities outside CERN

A fast neutron reactor, that has appositely built for the neutron irradiation of materials, has been first found in Valduc (France). This option has been discarded because the activation of the samples would have required too much time for the deactivation and handling and the time needed to prepare the samples did not match with the reactor's availability. Same arguments, together with

[2] In principle particle accelerator work with pulsed beams, but in some cases the frequency of these pulses is so high that the beam can be treated, in first approximation, as continuous.

Facility	**Irradiation Type**	**Energy**	**Ψ [part.*cm^{*-2}*sec^{-1}]**
CNGS	Mixed	Proxy to LHC	Installation's Zone Specific
ISOLDE	Protons/Neutrons	1.4 GeV/<1MeV	$3.2*10^8/3.2*10^6$
PS	Protons/Neutrons	24 GeV/c.a. 1MeV	Same as above
nTOF	Neutrons	1 - 100 MeV	31 - $3.1*10^8$
HI.RAD.MAT	Protons	450 GeV	$3.2*10^{13}$ per pulse, 2.7 μsec pulse duration

Table 2. Candidate Irradiation Facilities at CERN

a too high irradiation time, has led the SIT research team to abandon the choice for Mol's nuclear reactor in Belgium.

The TRIGA reactor of the L.E.N.A. research institute in Pavia (Italy) has been built for the irradiations of materials. The research team that manages this experimental apparatus has got a wide expertise in managing activated samples, and the maximum achievable neutron's Ψ was quite high. In this case, the solution has been discarded because of the too low (thermal) neutron energy.

The A.T.I. research institute in Vienna has irradiated and characterized in the past 20 years NbTi and Nb_3Snb sample for the I.T.E.R. project. A.T.I.'s research group performs irradiation tests in a nuclear reactor, and has also developed appositely sample holders and J_c measurement cryostats for high activated superconducting samples, so that the organization of the irradiation tests would have been less complicated for the SIT research team.

The Kurtshatov Institute for Nuclear Physics has constructed a Cyclotron, able to produce a 65 MeV proton beam, with a maximum $\Psi = 10^{14}$ $p^+*cm^{-2}*sec^{-1}$. Kurchatov's research team currently performs irradiation tests on structural materials for the I.T.E.R "first wall" problems (via (p, n) reactor with Be targets, or with a own fast nuclear reactor) and on medical drugs. Would the SIT research time decide to perform the proton irradiation test at Kurchatov's, then a totally new irradiation test station should be designed and tested, according to the guidelines introduced in section 3.2.

Finally, the SIT research team has investigated proton irradiations possibilities at the P.S.I. Institute in Villingen (Switzerland) and at the B.N.L. (USA). The staff of the these research institutes are currently trying to enhance the power of their particle accelerator (cyclotrons), and the exact features of their proton beam line can be, at present, not outlined. Also in these two cases, there are problems concerning the installation of the vessel + cooling system proxy to the beam line.
Table 4 reports the characteristics of the irradiation facilities outside CERN.

3.3.3 Current Status of the SIT Experimental Activity

In Mai 2010, a research agreement has been signed between CERN and ATI, to irradiate Nb_3Sn samples with fast neutrons, because of the already proved research capabilities of the ATI group. Proton irradiation tests have not yet been assigned to any of the mentioned institutes; in this sense, a final decision is expected in the next months, even though Kurchatov seems, at present, the best candidate to host this irradiation experiments.

Facility	**Institute / Location**	**Irradiation Type**	**Energy**	**Ψ [part.*cm^{*-2}*sec^{-1}]**
Valduc	French Army's Research Institute Valduc (France)	Neutrons	1 MeV	$3.2*10^{11}$
Mol	Belgian Nuclear Research Institute Mol (Belgium)	Neutrons	> 1 MeV	$3.1*10^{5}$
TRIGA Reactor	L.E.N.A. / Pavia (Italy)	Neutrons	< 1 MeV	c.a. 10^{13}
TRIGA Reactor	A.T.I. / Vienna (Austria)	Neutrons	1 MeV	$1*10^{13}$
Cyclotron	P.S.I. Villingen (Switzerland)	Protons	70-590 MeV	Data *not yet* available
Cyclotron	B.N.L. (USA)	Heavy Ions/Protons	200 MeV	Data *not yet* available
Cyclotron/Reactor	Kurtshatov Institute of Nuclear Physics Moscow (Russia)	Protons/Neutrons	35 MeV/ > 1MeV	$1*10^{14}$ / data not yet available

Table 3. Characteristics of the Candidate Irradiation Facilities outside CERN. Some features of the candidate irradiation facilities have not been obtained, for technical reasons related to the current power enhancement of these facilities or due to other technical reasons.

3.4 Design of the SIT Sample Holder

The design of the SIT sample holder has been done starting the conceptual design of the irradiation experiments, that has been *generally* introduced in section 3.2.

The detailed features of the various stages of the irradiation experiments will be now *more accurately* presented, to introduce the *technological requirements* that the SIT sample holder has to satisfy, and after that, the project of the sample holder will be described.

3.4.1 The Sample Holder Preparation and the Irradiation Stage

The sample holder will be first prepared and *pre - tested* at CERN, and successively sent to the foreign research institute that will host the irradiation experiments and J_C measurements. Once the device will arrive to the test laboratory, it will be mounted on a *mechanical support* (i.e. a shaft).

This support is then inserted into the irradiation vessel from its top; in this sense, the upper part of the shaft will work also work as *locking system* for the irradiation vessel. Considering the present status of the irradiation experiments, the irradiation vessel has to be designed for the *proton* irradiation tests in the future by the SIT research team. The mechanical support can to vertically move in the irradiation area, this to center the beam with the sample holder. A single superconducting *wire* will be mounted on the sample holder, and that the choice of the impacted area determines the height at which the device should stay into the irradiation vessel.

Once the irradiation chamber is locked, the coolant is pumped into it to fill the vessel up to a given level. After that, the irradiation can be started. Figure 33 shows a sketch of the general system for the irradiation stage.

The desired fluence will be given to the sample. The irradiation is then stopped, and the residual coolant is extracted from the vessel. Now, the shaft is extracted from the vessel thanks to a crane. The sample holder is then removed from the shaft and stocked into a radiation confinement area, to wait for its deactivation and for its best successive handling.

The *total cost* of the irradiation stage depends on these aspects: the beam intensity (because the exploiting of the radiation source is usually expressed in currency/hour), the total deposited power on the sample holder (because this power will determine the coolant mass flow that has to be pumped into the irradiation vessel, and thus, the cost of the coolant) and the necessity to buy already constructed equipment or to design, construct and test them before any irradiation experiments could be done. From this point of view, Kurchatov is, at present, the institute that has done the best offer to the SIT research team.

With respect to the irradiation stage, the *design of the sample holder* has taken into account: the centering of the beam with the sample (because the beam could have a spread over the device, due to its interaction - nuclear scattering phenomena - with the coolant), the study of the fixing solution of the wire to the sample holder (for reason that will be explained soon, the wire has to be perfectly fixed to the sample holder during the J_C measurements, and a soldering layer could absorb all the particle dose, leaving the underlying wire in the *non - irradiated* state), the estimation of the deposited power on the sample holder and the calculation of the sample holder's deactivation time after the irradiation stages.

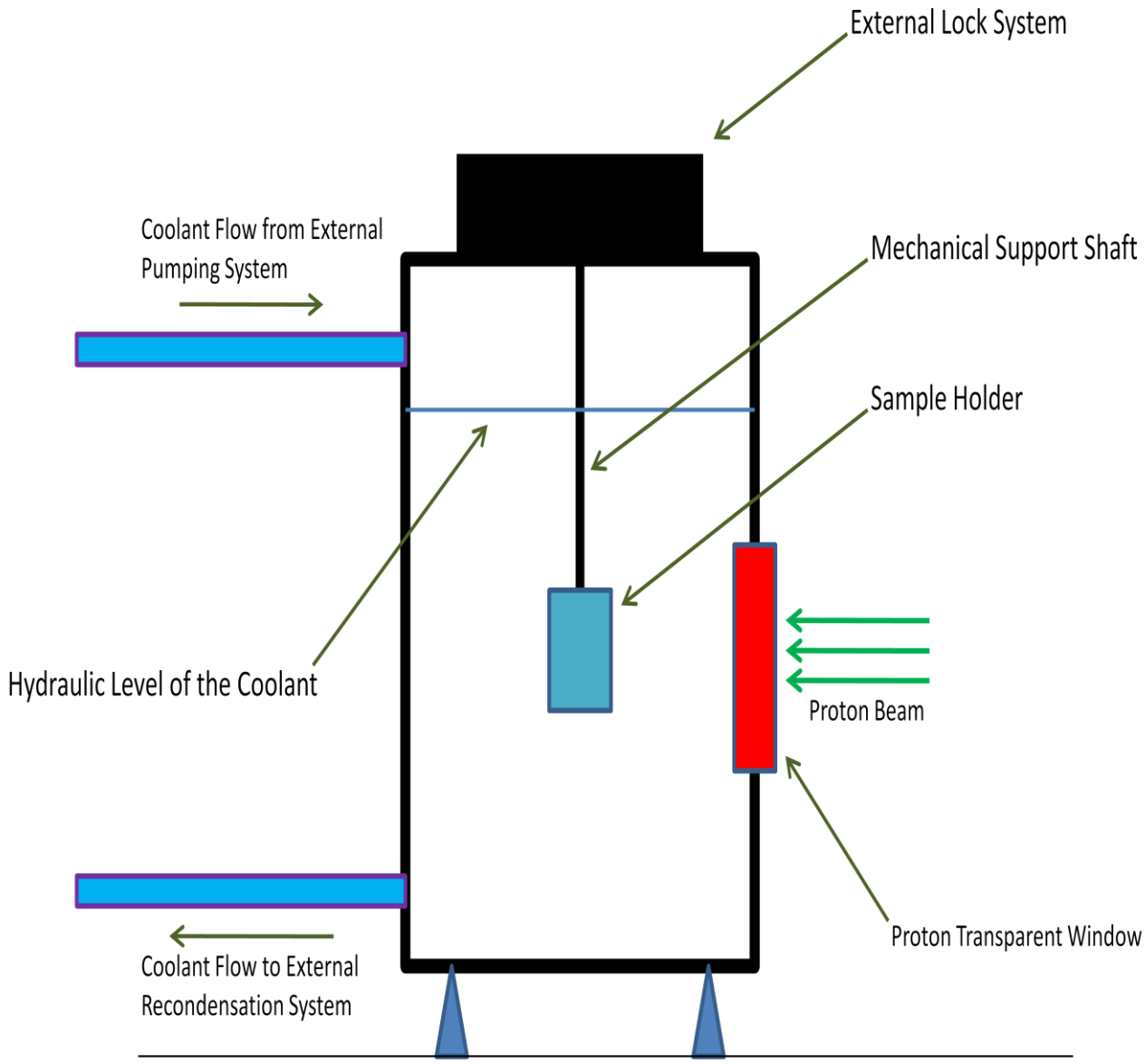

Figure 33. The proton irradiation stage of the sample holder. The sample is first put into the irradiation vessel, at the height of the window and thanks to a mechanical support. The vessel is then locked and the coolant is pumped from the upper part of the vessel thanks to a pipe system, and kept under forced flow. Once the irradiation chamber has been filled up to a certain hydraulic level, the irradiation is started. At the end of the irradiation session, the coolant is removed from the bottom and the sample holder is extracted from the chamber.

3.4.2 Critical Current Measurement Stage

The sample holder is taken from the radiation confinement area (intermediate stage of the irradiation tests) and mounted on a special shaft, that will then fit into the J_C measurement cryostat.

As introduction to the functions of the shaft and of the cryostat, the standard procedure and equipment for the measurement of the critical current on superconducting samples will be first presented, and followed by the description of the CERN *standard* critical current measurement cryostat.

3.4.3 CERN Equipment for the Critical Current Tests

The superconducting wire is mounted on a sample holder, that usually has a cylindrical shape. This standard sample holder is called "*LHC Standard*", and are currently used at CERN for the tests on Nb_3Sn wires. They have been developed from the "*VAMAS*" standard cylindrical sample holders, essentially varying the dimensions of the cylinder and the position of the voltage taps. As a general example of sample holder's geometry, Figure 34 shows a VAMAS *standard* apparatus [20].

A solenoidal groove is machined on its lateral surface, to host the superconducting wire. During the J_C measurements, a steadily increasing DC current I is given to the wire, and the voltage drop V is monitored thanks to a voltage taps system that is placed at the extremities of the wire.
When the material is in the superconducting state, $V = 0$; once the superconducting transition is reached, $V > 0$ at $I_C = J_C * A$, where A is the total cross section of the wire, according to the choice to measure the *engineering* critical current.

The sample holder is mounted on a shaft, and this shaft:

- brings the sample holder in the part of the cryostat, where the sample is immerged in liquid He at 4.2 K and surrounded by a couple of superconducting magnets, that impose the applied magnetic field B to the sample, in an experimental configuration where *B has to be perpendicular* to the direction of the current density vector $\vec{J}$ in any point of the wire.

- gives mechanical support to the wire (together with the sample holder), avoiding its movements under the action of a magnetic field B into the cryostat. In fact, wire's movements under Lorentz action can considerably alter the detected V - I curve, and introduce noise in the measurement if the wire is partially free to move into the cryostat.

- hosts the *current leads* that connect the wire to the external power supply and the *voltage taps system* that is connected with a data acquisition system put in proximity to the cryostat.

- works as *lock system* of the cryostat, in order to maintain the liquid He under pressure and at a fixed temperature.

The cryostat is connected with the external power supply, and a He external recirculation system. The upper part is divided, via the lambda plate, from the lowest part, where the shaft brings the sample between two superconducting magnets for the critical current test.

The CERN cryostats are designed to work in two ways: (1) the upper reservoir is filled with He at 4.2 K, and the lower with He at 1.9 K or (2) both the reservoirs are filled with He an 4.2 K. Nb_3Sn wires are currently tested at CERN following solution (2).

A high *Lorentz action* is transmitted from the cylindrical sample holder to the shaft; in order to contrast it and avoid movements, the whole cryostat is vertically inserted into a cave in the ground.

Different values of critical current are measured at different applied fields. An I_C *against* B graph is then plotted, and represents the *characteristic* of the material, that has to be analyzed and related to the study and optimization of its manufacturing processes.

Figure 35 shows a sketch of the layout of the critical current measurement station used at CERN, and illustrate how they work during the critical current tests.

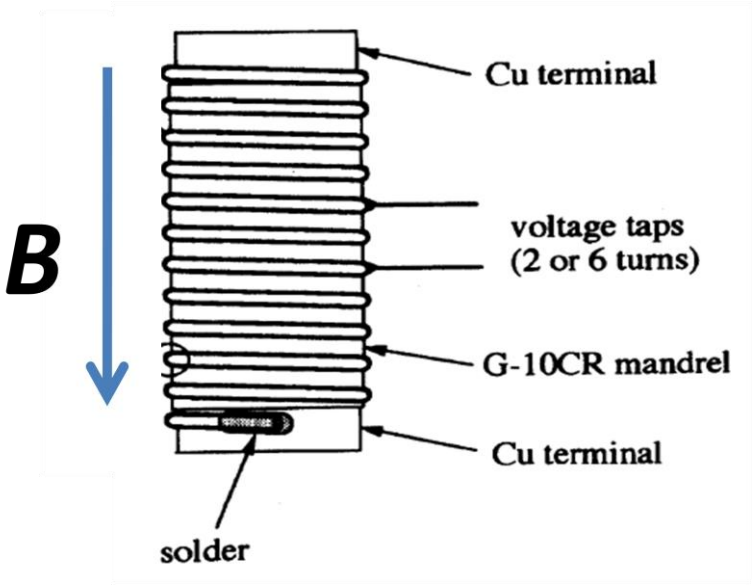

Figure 34. A "VAMAS" standard sample holder for critical current measurements, where the applied magnetic field B is parallel to the cylinder's axis [31]. The *LHC Standard* sample holders have been realized from this configuration, applying ***9*** turns of the wire and putting the voltage taps at the extremities of the cylinder.

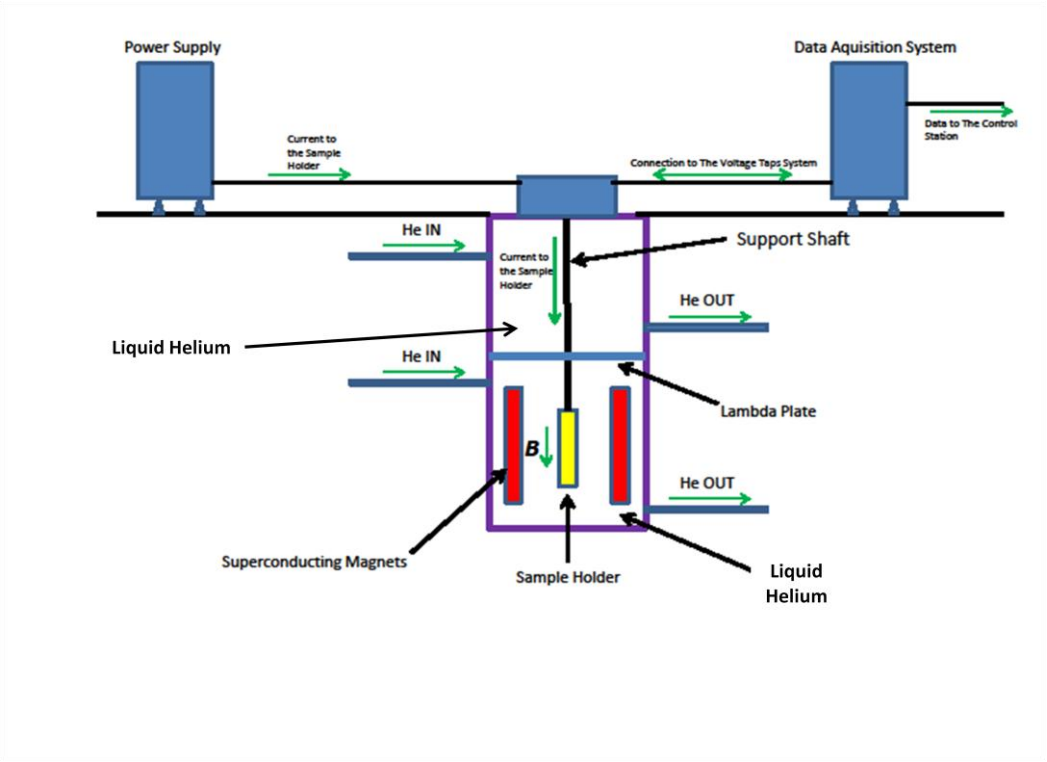

Figure 35. Sketch of the critical current test station used at CERN. An external power supply produces the electrical current, that is sent into the cryostat to the sample holder; at the same time, a data acquisition system detects the V - I curves in connection with the voltage taps system places on the sample holder. The cryostat is divided in two reservoirs thanks to the lambda plate. The reservoirs are connected, thanks to two pipe systems, to an He pumping and recirculation apparatus

3.4.4 Functional Requirements of the SIT Sample Holder

The SIT research team is *currently* evaluating if the cryostat, that will be used for the J_C measurements will have the same structure as the one used at CERN, or if it should be modified. In fact, this cryostat has to be integrated into the already existent experimental apparatus of the research institute to which the proton irradiation tests will be assigned. At present, this institute has not yet been chosen.

Nevertheless, it can be imagined that the modifications of this cryostat respect to the one used at CERN will not be significant. The general layout of the CERN cryostat has been thus kept as a reference for the design of the SIT sample holder, also in connection with the structure of the irradiation vessel and the *geometry* of the LHC Standard devices.

More precisely, the following functional requirements of the SIT sample holder have been identified:

- This sample holder should *uniformly expose* a piece Nb_3Sn sample to the proton beam, and this piece of wire should be considered as the *irradiated* sample.
- The voltage taps system should be put at the extremities of this piece of wire, and the sample holder *shape* should allow to measure the critical current under *perpendicular* magnetic field.
- The maximum diameter of the sample holder should be less than the bore size of the irradiation vessel and of the cryostat for the critical current measurements.
- It should be able to *easily* center the device respect to the proton beam in the irradiation vessel.
- Before the critical current measurement stage, the irradiated wire should be perfectly fixed to the sample holder, to not introduce any sort of noise in the J_C measurements.
- The irradiation will modify the mechanical properties of the sample holder's material, so that the *geometry* should be designed to resist to the relevant Lorentz Action transmitted by the wire during the J_C measurements.
- The sample holder's material should have a value of thermal contraction coefficient α, that is the closest Nb_3Sn wire's one, because otherwise the immersion of the device in liquid He from room temperature could cause fracture of the *brittle* wire.
- The sample holder's geometry should lower power that the proton beam deposits on it, thus helping to easily reach an acceptable temperature distribution in the device and enhance the proton flux Ψ (also, reducing the irradiation time τ and the cost of the whole irradiation test).

The possible use of the LHC Standard sample holders has been attentively evaluated, but at the end discarded, because this sample holder could not have been irradiated with a *homogeneous* particle flux over the turns of the superconducting wires. In fact, cyclotron beams are characterized by a *gaussian* distribution of the flux Ψ over the spot.

A totally new device has consequently been designed for the SIT project.

3.4.5 Sample Holder Shape

The shape has been determined from the precise design of the irradiation and critical current measurement procedures that have been illustrated in the previous sections. The shape that can satisfy all the functional requirements is a "U", that has been sketched in Figure 36. The wire will be fixed along the U, and be irradiated in its lowest straight part.

In particular, this geometry allows to:

- Easily center the proton beam on the wire, if the sample holder is *vertically* put in the irradiation vessel (and eventually shifted along the vertical axis of the vessel).
- Irradiate a straight Nb_3Sn wire, to measure the critical current under perpendicular magnetic field *B*.
- Respect the limitations on the bore size diameter of the irradiation vessel and J_C cryostat, *simply* by varying the distance between the two vertical arms of the U.
- Give the lowest possible Lorentz action that the wire transmits to the sample holder, by inserting the sample holder *vertically* into the J_C measurement cryostat, in an experimental configuration where the applied magnetic field *B* is *perpendicular* to the lowest part of the U and *parallel* to its vertical arms.
- Easily mount the wire to the U before the irradiation- or, *if possible*, between the various stages of the irradiation experiment.
- Reduce the deposited energy on the sample holder, by a proper choose of the thickness of the irradiated part of the device, respect to the spot size (diameter) of the proton beam.

3.4.6 Sample Holder Preliminary Engineering Design

Despite its simple geometry, the design and test of this sample holder has been complicated by the fact that this device should be designed in order to test it at CERN and, at the same time, integrate it into the irradiation test station. Because the proton irradiation experiments have not yet been assigned, and the irradiation station has not yet been designed, the project of the sample holder has been done to *preliminary* study its working conditions in the irradiation- and successive critical current measurement stage, as follows:

- Choice of the Sample Holder's Material
- Mechanical Calculations
- Numerical simulations of the radiation environment around the sample solder in the irradiation stage
- Estimations of the Deactivation Times at the End of the Irradiation Stage

and these points will be now presented. Other aspect of the sample holder design are related to the study of its preparation procedure for its first tests at CERN; for this reason they will be presented in the next chapter.

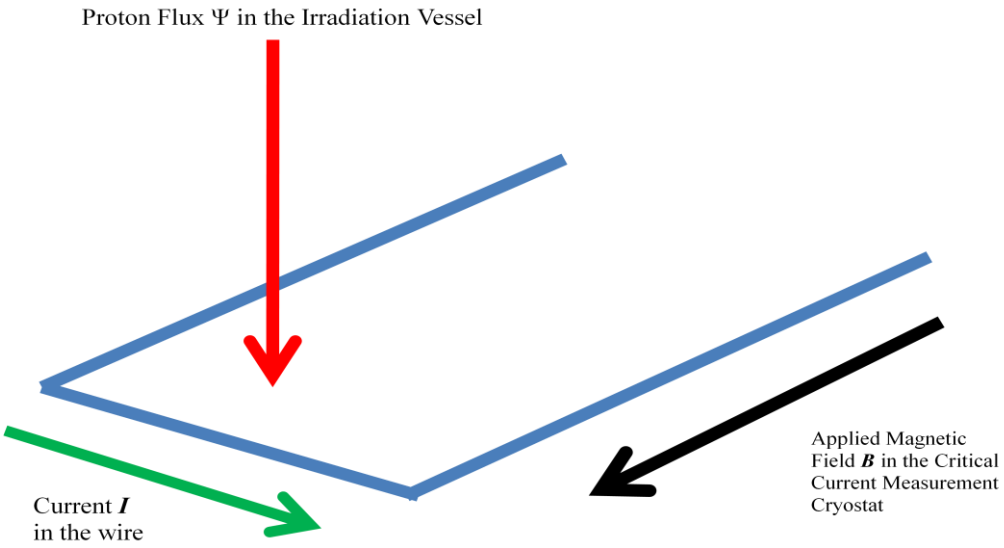

Figure 36. The position of the geometrical axis of the "U - shape" (in blue) respect to the proton flux Ψ and the applied magnetic field *B*. During the critical current tests, a single superconducting wire will run along the whole structure, thus transmitting a Lorentz action to the sample holder only in the zone where *I* is perpendicular to *B*.

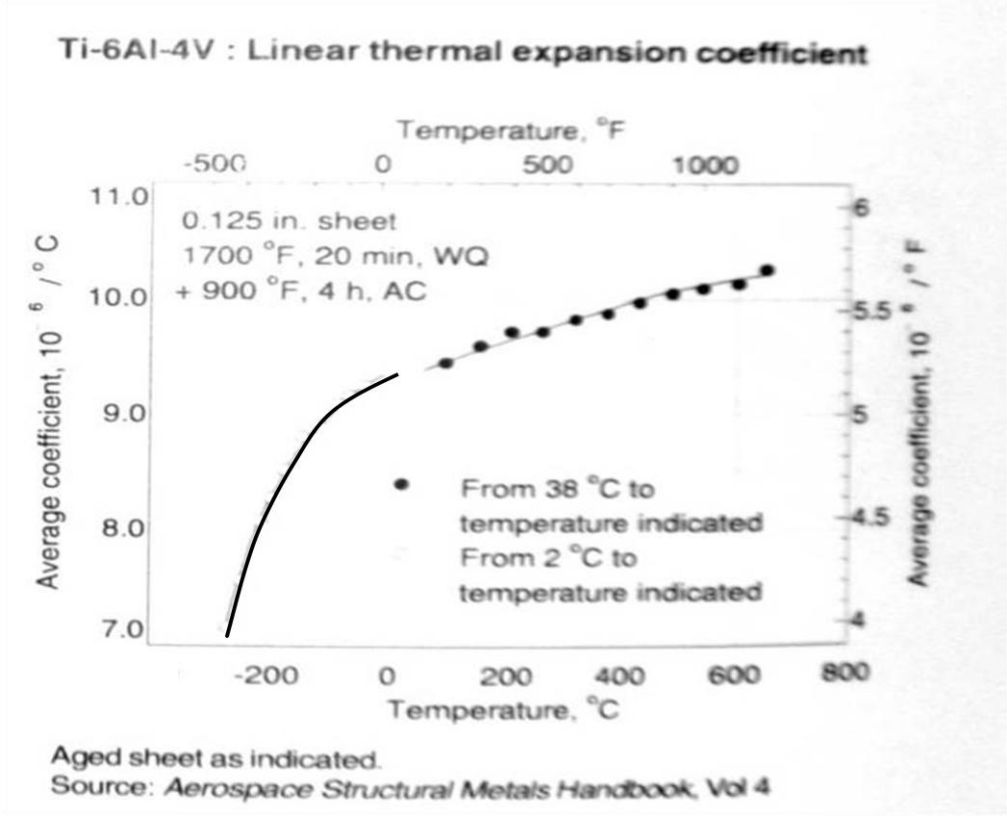

Figure 37. The variation of the linear thermal expansion coefficient of the commercial ("aged") Ti - Alloy against the temperature [21]. The plot valid from 0º C to -273.15 ºC has been remarked, due to the low quality of the scan and at the same time, due to its ***uniqueness***.

3.4.6.1 Material Choice

The Ti-Al6-V4 alloy is frequently used in cryogenic applications, and it has been found to have the *closest* value of the thermal expansion coefficient α to the one of the Nb_3Sn wire.

Specifically, the mean value of the idrostatic component of the deformation tensor $\boldsymbol{\epsilon}$, representing the thermal deformation in each point of the sample holder during its immersion in the J_C measurement cryostat, has been evaluated, starting from diagrams as the one of Figure 37 [21, 22].

Nevertheless, supposing then that the system "shaft + sample holder" can be able to freely contract himself into the critical current measurement cryostat, no thermal stresses have been included in the mechanical design of the apparatus.

3.4.6.2 Mechanical Design

The mechanical design of the "U" has been done considering that the proton beam could spread over the sample holder as a consequence of the nuclear scattering by proton - coolant interaction in the irradiation vessel. This observation has been combined to the necessity of having a the most *rigid* device, that has to resist to the bending action transmitted by the Nb_3Sn sample during the critical current measurement in the most general experimental layout where the sample holder is connected to the cryostat structures only at his two upper ends.

The irradiation of the structure can alter the *mechanical properties* of the Ti alloy, but no data on the variation of the mechanical properties of the Ti alloy after irradiation have been found in the literature. The mechanical design of the sample holder has been thus *conservatively* approached, as it will be now illustrated:

- A *distributed* Lorentz force will act at the basis of the sample holder during the critical current tests, and this force can be written as:

$$\frac{\vec{F}}{L} = I * \vec{n} \times \vec{B} \tag{16}$$

  where the current I assumes the form of a vector (by its multiplication per the unit vector $\vec{n}$, that is directed parallel to the basis of the U), that is multiplied via vector product per the applied magnetic field $\vec{B}$. L is the length of the basis of the U, and has been put equal to the local value of the diameter of the CERN shafts for I_C measurements. Also, it has been imagined that the applied field lies in the plane of the U, producing thus a bending action on the sample holder.

- Following the mechanical load model of Figure 36, the maximum bending stress in the cross section at the upper part of the U has been calculated, for a *square* cross section of inertia moment I as:

$$\sigma_{MAX} = \frac{F*L*d}{I} * \left(\frac{t}{2}\right) \tag{17}$$

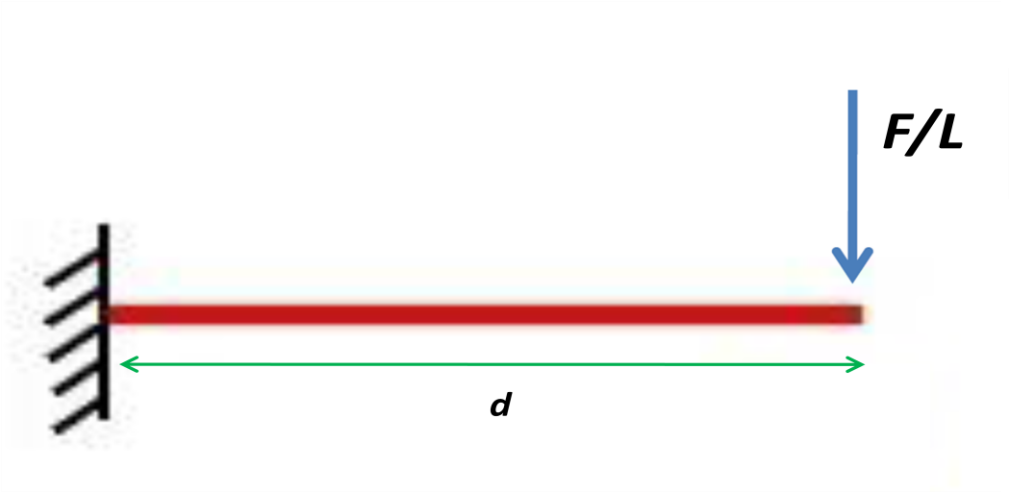

Figure 38. The mechanical model for the irradiated SIT sample holder under the action of the superconducting magnets in the critical current measurement cryostat. In the model, the maximum value of the mechanical stress in the beam is expected at its connection point with the wall.

where t is the cross section's thickness and d the length of the vertical arms of the U. Substituting then eq. (16) into eq. (17), and taking into account that, after irradiation, the critical current of the wire I_C will be enhanced by a factor α, equal to the maximum in $\frac{J_C}{J_{C0}}$ the final expression for the maximum value can be obtained. Considering the plot of Figure 31, it has been set $\alpha = 5$.

- Eq. (20) has been compared with the yield stress value of the Ti - Alloy σ_Y, enhanced by a safety factor μ.

- Imposing then:

$$\sigma_{MAX} = \sigma_Y * \mu \tag{21}$$

in eq. (17), the inertia moment I has been deduced and the thickness of the upper part of the sample holder has been calculated.

No data on the variation of the Ti-Al6-V4 alloy yield stress with fast neutron, as well with proton irradiation, have been found in the literature at the energies of interest. Also, the spread of the particle beam on the U, due to the proton - coolant interaction, had not yet been simulated. Correspondingly, the value of yield stress in the non - irradiated state of the material has been used ($\sigma_Y = 1030\ MPa$ [21, 22]), and the irradiation effects have been taken into account by a proper choice of the safety factor.

The A.S.M.E. Nuclear Boiler and Vessel Code [23] has been written for the mechanical calculations on the structural elements in nuclear power plants. According to this code, the choice of the safety factor for heavy irradiated structural elements is specific for the radiation *energy*, *type* and *fluence*. Nevertheless, it is usually comprised between *1.5* and *3*.

Substituting these values in eq. (21), two thicknesses t have been deduced, choosing $d = 10\ cm$ as a first possible height of the vertical part of the U, in relation to the characteristics of the CERN measurement shaft, as it will be illustrated in the next section.

The first value of thickness corresponds to μ = 1.5 and is *t = 5 mm*, while the second corresponds to μ = 3 and is *t = 10 mm.*

The transversal deflection of the U has been estimated using the "Elastic Line Method" and with particular attention to the "bore size restrictions*"* in the design of the sample holder and the necessity to avoid the contact of the sample holder with the superconducting magnets in the cryostat.
Following to this scheme, the transversal deflection ν of a beam representing the *geometric axis* of the sample holder has been calculated using the differential equation:

$$\frac{d^2\nu}{dx^2} = \pm\frac{M(x)}{EI} \tag{22}$$

In eq. (22) *E* is the Young Modulus of the material, *x* the axial coordinate of the beam and *M(x)* the distribution of the bending moment along *x*. Also, the sign $\pm$ is chosen according to *curvature* of the beam (to the up or to the down) respect to the *orientation* of the coordinate system *(0, x, v)* that has been fixed on the beam.

For the Ti - Alloy, E = 115000 MPa has been choosen, corresponding to the non - irradiated state of the material [21, 22], because: (1) at cryogenic temperatures the Ti works elastically, (2) at the same time, irradiation usually *enhances* the yield stress and (3) E should consecutively not be changed after irradiation.

A *linear* distribution of the bending moment has been determined, that is 0 in the point of application of the Lorentz action, and increases along *x* up to his maximum value:

$$M = \left(\frac{\alpha I_{C0} B}{L}\right) * L * d \tag{23}$$

at the connection of the beam with the wall. In eq. (23), the *distributed* Lorentz action has been transformed to a *localized* load by its multiplication per *L*. Figure 37 shows the plot *M(x)*. As boundary conditions for the integration of eq. (22) it has been assumed *v(d) = v'(d) = 0*, where the reference of origin *0* of the reference system *(0,x)* has been put, in the model, in the point of application of *F/L*.

The transversal deflection has been estimated at B = 11 T (the highest applied that is currently used at CERN for the test of Nb_3Sn wires), and a enhancement factor α = 5 on the critical current I_{C0} value at this applied field. The resultant plots is shown in Figure 40 and 41. Respect to the bore size limitations, a maximum transversal deflection of 1 mm is accepted, that apparently only the 10 mm thick sample holder can guarantee.

3.4.6.3 Final Design for the Pre - Test at CERN

Following the mechanical design of the previous section, two prototypes of sample holder have been constructed for their ***preliminary test*** at CERN:

- A *thinner* one, of cross section equal to "*5x5 mm*^{2}", obtained imposing $\mu = 1.5$ in eq. (21). This prototype has been called "SIT *5x5 mm*^{2} Basis Sample Holder".

- A *thicker* one, of cross section equal to "*10x10 mm*^{2}", obtained imposing $\mu = 3$ in eq. (21). This prototype has been called "SIT - *10x10 mm*^{2} Basis Sample Holder".

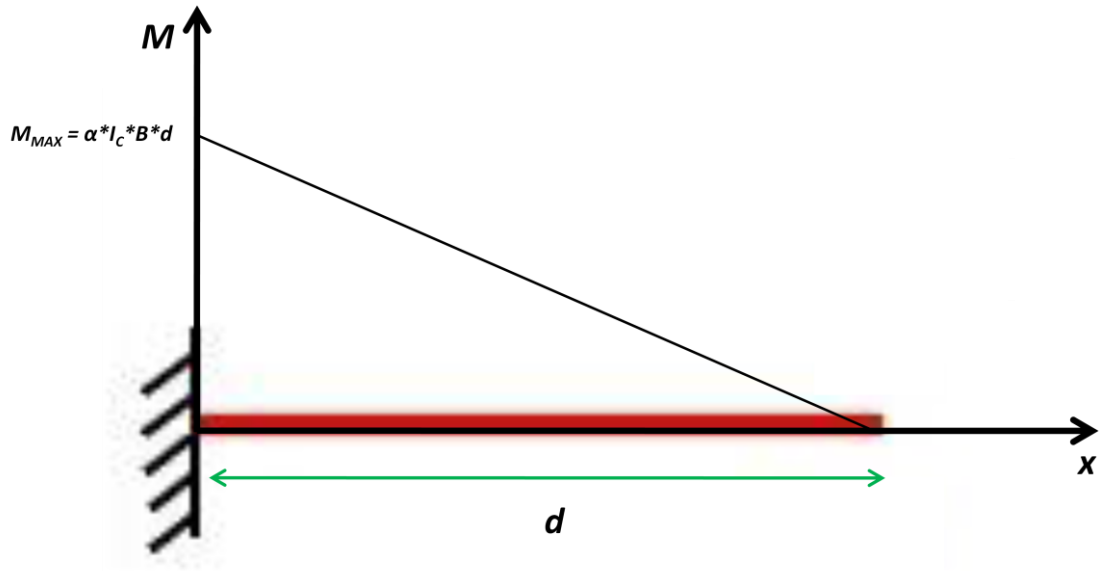

Figure 39. The expected distribution of the bending moment *M(x)* along the SIT sample holder during the critical current tests on irradiated superconducting wires. As a convention for the plot, the positive values of the bending moment have been reported on the side of the positively elongated fibers of the beam.

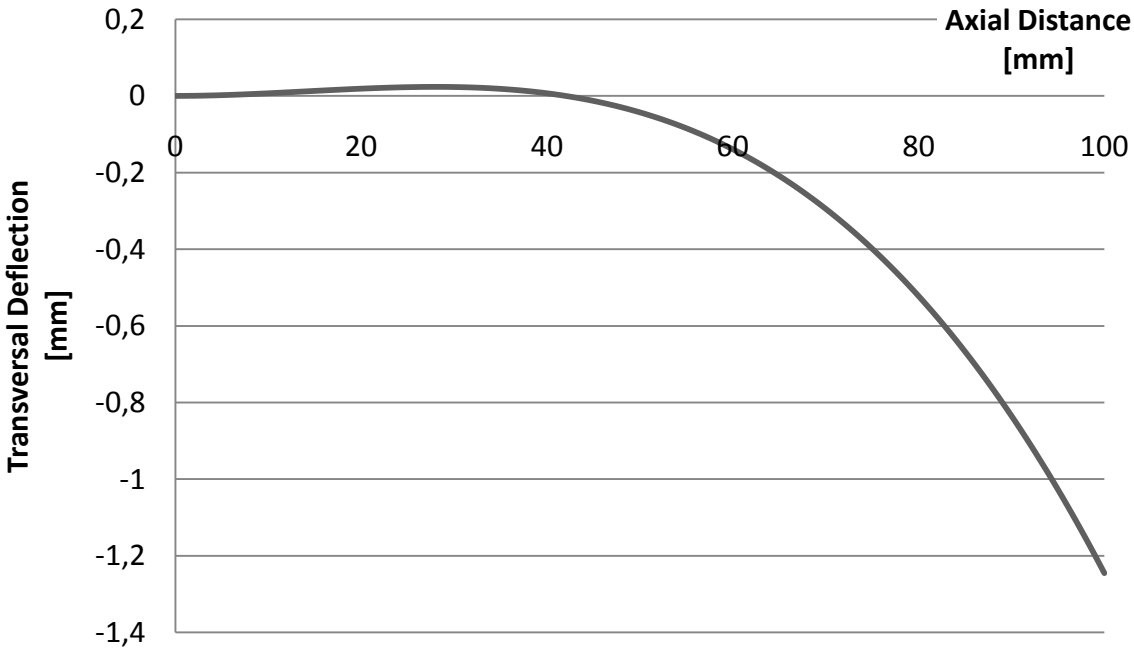

Figure 40. Expected transversal deflection of the 10 mm thick U thick sample holder, calculated for its maximum length *d = 10 cm*, and assuming its worse operating conditions during the critical current measurements. To interpret the diagram, it has to be imagined that the sample holder is fixed at x = 0 to the cryostat inner structure, and tend to bend himself towards the superconducting magnets.

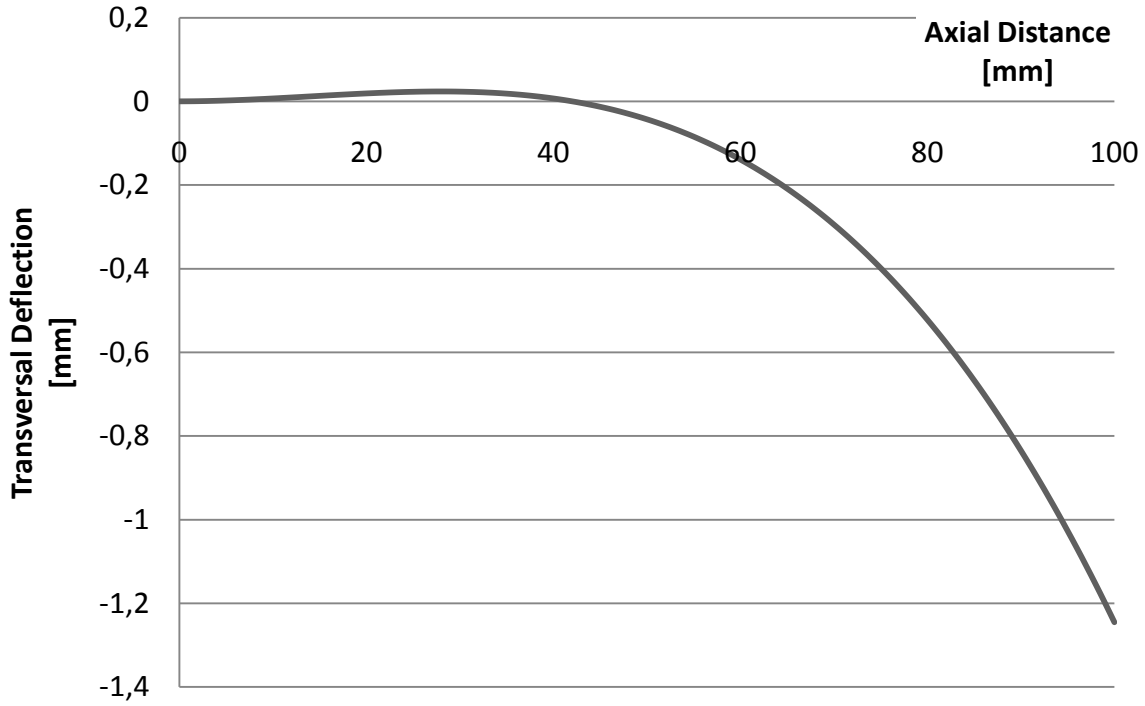

Figure 41. Expected transversal deflection of the 5 mm thick sample holder, calculated for its maximum length *d = 10 cm*, and assuming its worse operating conditions during the critical current measurements. To interpret the diagram, it has to be imagined that the sample holder is fixed at x = 0 to the cryostat inner structure, and tend to bend himself towards the superconducting magnets.

Respect to the first mechanical design, that has been presented in the previous section, the shape of the sample holder has been modified for its adaptation on the CERN shafts, and a mechanical support system (composed by a "*G10 - polymeric*" base and two metallic fixing plates) has been designed and constructed, to fit the two prototypes to one of the CERN shafts for their first experimental validation.

The mechanical support system guarantees the a complete connection of the U's to the shaft, and for this reason, the bending of the U has not been considered. The axial length *d* has been thus put equal to 12 cm. It should be pointed out that this mechanical support has only been designed for the preliminary test of the sample holder at CERN, and will thus not be used to mount the sample holder in the irradiation vessel, as well in the I_C measurement cryostat at the end of the irradiation stages. The preliminary mechanical design of the previous section is still the reference for the sample holder behavior during the irradiation tests.

During the sample holder preparation stage, the superconducting wire has to be mounted on the U thanks to a lateral groove excavated on the sides of the both sample holders, and fixed there either with a soldering layer either with a polymeric glue, because these fixing solutions are the *classically* used in Cryogenics. Figure 42, 43 and 44 show, respectively, the technical drafts of the two prototypes, and their application on the CERN shafts.

Particular attention has been put on the choice of the bending radius that connects the vertical with the lowest parts of the U, in order to lower the deformation that the sample will receive during its

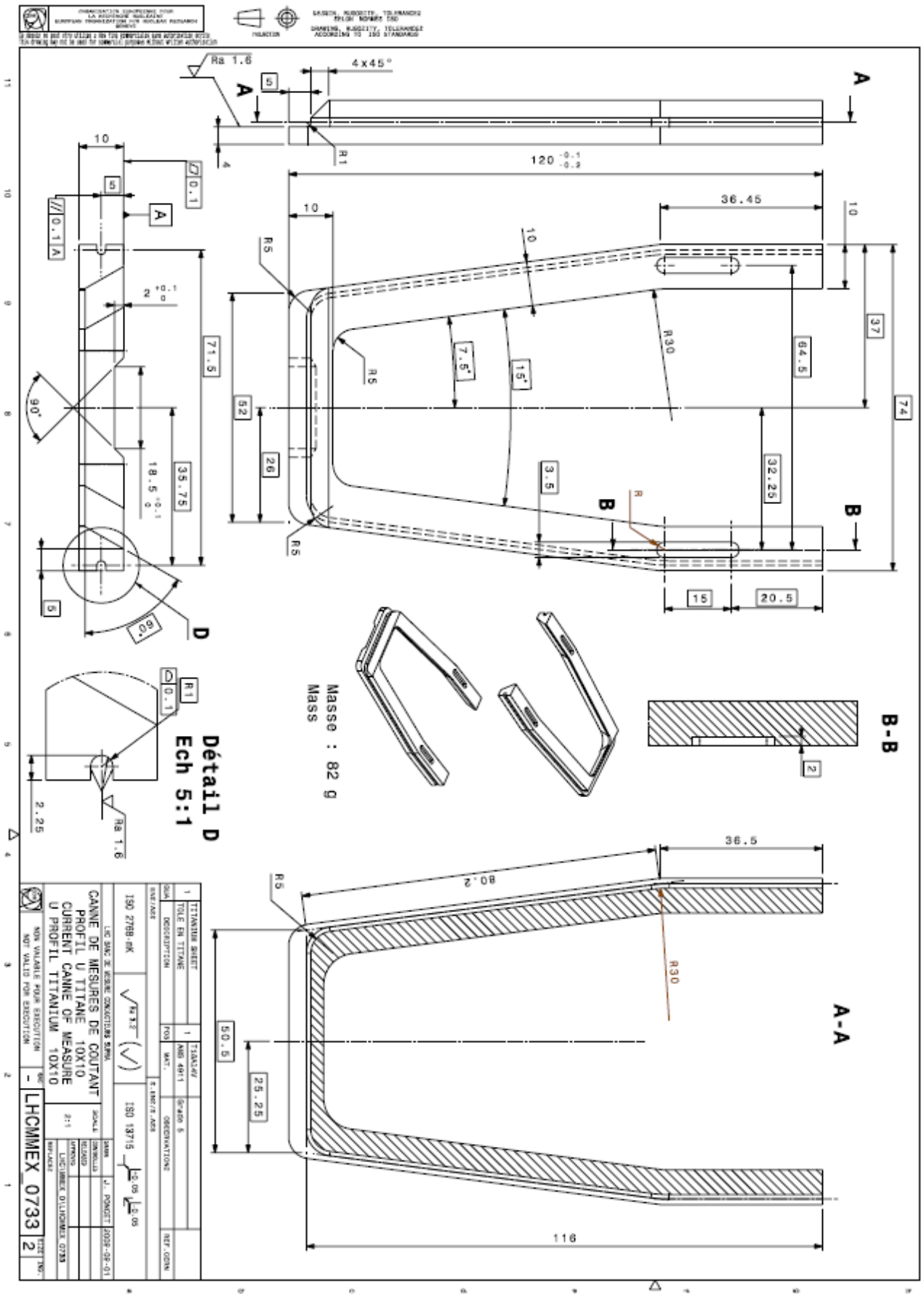

Figure 42. Technical draft of the "10x10 mm^2" basis sample holder prototype. Acknowledgements : Jean Poncet (CERN - EN - MME group).

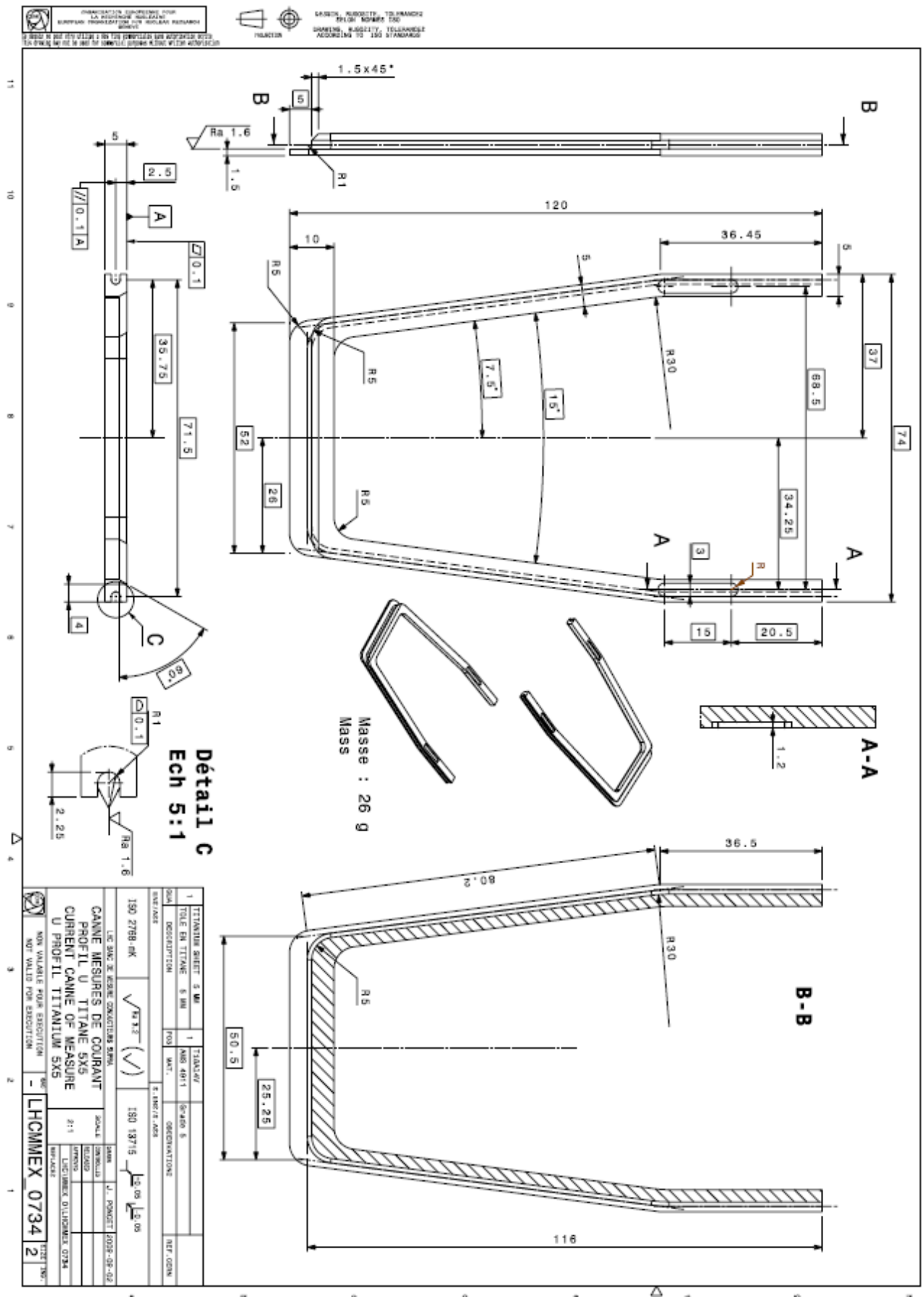

Figure 43. Technical draft of the "5x5 mm^2" basis sample holder prototype. Acknowledgements: Jean Poncet (CERN EN - MME group).

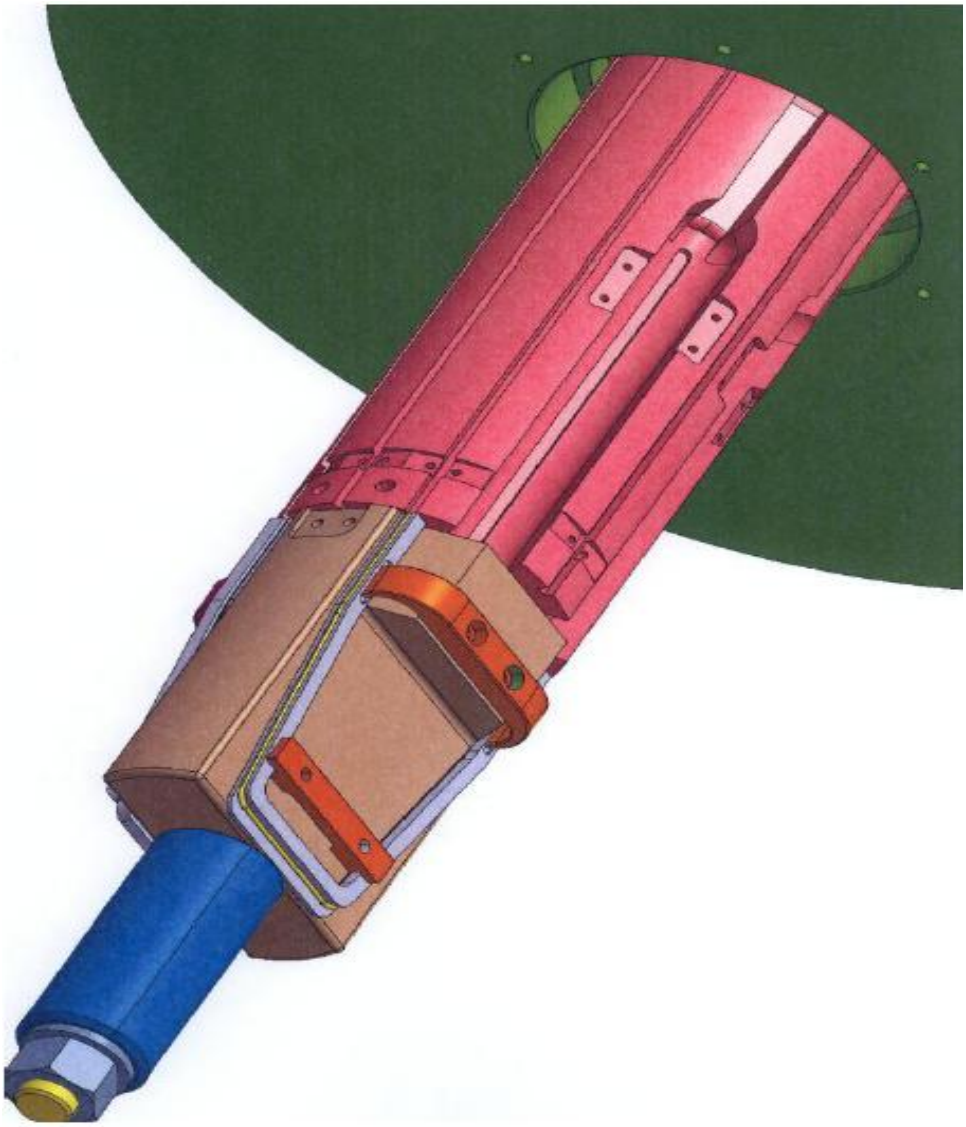

Figure 44. The two SIT sample holder prototypes, as mounted on the CERN measurements shafts and successively inserted into the CERN cryostat for their ***preliminary test*** at CERN. The sample holders are mounted on a polymeric mechanical support (brown in the Figure), and fixed to the shaft thanks to two metallic plates (orange in the Figure). The upper green disc is the Lambda Plate of these cryostats. Acknowledgements: Jean Poncet (CERN - EN - MME group).

preparation. Considering the mechanical properties of Nb_3Sn wires [22] and the CERN cryostat bore size values, a radius of 5 mm has been given to both prototypes.

On the basis of both prototypes, the cross section has been designed as a *step*, in order to correctly expose the Nb_3Sn wire to the proton beam, and easily connect the voltage taps at the extremities of the irradiated zone to detect the voltage drop on the irradiated part of the wire (the effective sample) during the critical current measurement stage.

The design of the prototypes has also comprised the study of the preparation procedure for the pre - tests at CERN, and a preliminary study of the *electrical* behavior of the apparatus. Being these aspects related to the *experimental* part of this work, they will be discussed in the next chapter.

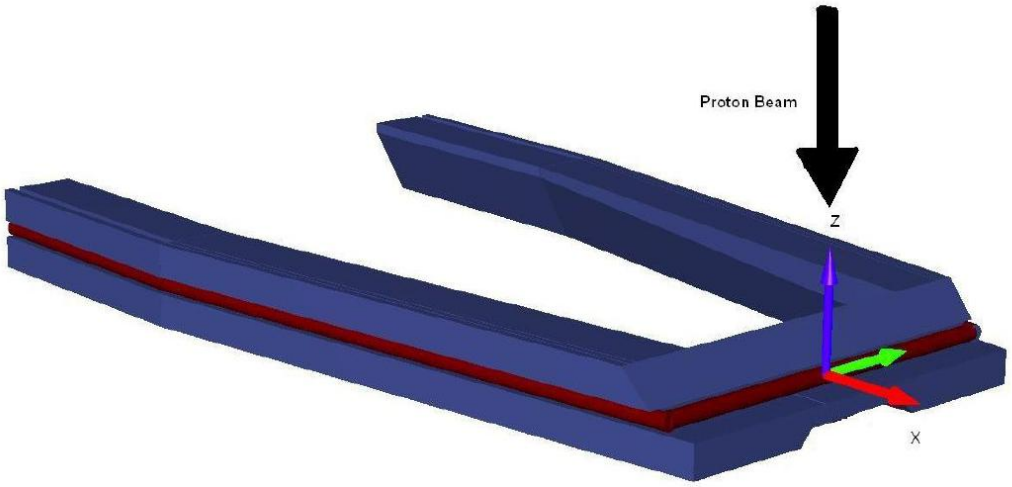

Figure 45. The geometry of the input file for the first FLUKA simulations of the SIT sample holder proton irradiation. The apparatus should be ideally put into the three candidate coolant baths. In the image, the Nb_3Sn wire (brown in the Figure) is fixed along the sample holder. Ref. [24]

3.4.7 Preliminary Simulations of the Radiation Environment in the Irradiation Stage

Broggi [24] has studied the radiation environment in the irradiation vessel, that is expected as a consequence of the beam - coolant interaction. He has used the Monte Carlo code FLUKA, in order to analyze:

- the spread of the nuclear particle on the SIT sample holder, for its immersion in three possible coolants: He (at 1.9 K), N_2 (at 77 K) and H_2O (at 298 K), in connection with the centering of the beam with the lowest part of the U
- the deposited energy in the sample holder and coolant environment
- the sample holder's deactivation time

The input file for the simulations has been first written, starting from the technical draft of the "*10x10 mm*^{2}" basis sample holder, and from the characteristics of the proton beam of the Kurchatov Institute (recall that this facility is, at present, the best candidate for the proton irradiation tests). In Figure 45, the geometry of the simulation is presented as it has been drawn for the input file.

A 30 MeV proton beam, of circular spot (diameter = 20 mm) hits the lowest part of the sample holder with a beam current of 20 μA, corresponding to $\Psi = 10^{14}$ protons*cm^{-2}*sec^{-1}. As a first approximation, the beam intensity has been assumed to be homogeneous on the spot, neglecting thus its true gaussian distribution over the spot diameter for reasons that have been already introduced.

In the first simulation campaign, the layer of fixing material has not been put on the sample holder. This particular choice has been done, starting from the following observations:

- One of the goals of these simulation is to study a fixing solution such that the fixing system won't shield the Nb_3Sn wire from the proton irradiation.

- Before the simulation, the particle spread on the U was not known, and it should be conservatively assumed that the proton would invest the whole sample holder

The SIT research team wanted consequently to have a first estimation of the proton - coolant interaction, and, starting from these observation, correctly design the fixing technique.

Figure 46 shows the maps of the deposited energy on the sample holder and on the closest coolant layer. In this map, the energy values are expressed in [$GeV*cm^{-3*}p.p.^{-1}$], where p.p. stands for the *primary proton* of the incident beam. The *specific deposited power* (power value per cm^{-3}) in each point of the geometry can be thus obtained multiplying these values per Ψ. Also, these values take into account all the possible nuclear reaction between the beam and the coolant layer and consequent *attenuation effects* of the beam intensity on the wire caused by the beam - coolant interaction.

The main results of this first simulation are:

1. The deposited energy has a maximum at the basis of the U, and rapidly decays along the vertical arms of the apparatus

2. The proton beam spreads over a large area of the U, when passing from He to H_20; this effect can be attributed to the increasing weight of the coolant's atoms

3. The proton - coolant interaction lowers the effective power that is deposited at the basis of the U, as summarized in Table 4

4. The lower part of the sample holder receives a homogeneous power over an approximate length of 2 cm

Result (1.) and (4.) confirm that the experimental geometry efficiently focalizes the beam on the lowest part of the sample holder. Independently of the final sample holder preparation procedure, the voltage taps can be put on the base of the U, over a distance equal to the beam diameter. Under the hypothesis that the temperature distribution in the sample holder will be determined only by the energy flux that *effectively* hits the U, result (3.) is *one* of the *possible* starting points for the final choice of the coolant and the design of the cooling system.
Also, result (1.) says that the highest part of the sample holder, where the bending stress during the critical current measurements is supposed to be the highest of the whole structure, does not receive a considerably high particle dose, and a *significant* variation of *local* the mechanical properties of the Ti-Al6-V4 alloy (in particular, of its Young Modulus *E* and Yield Stress σ_Y) are not expected after irradiation. For these reasons, the mechanical design of the sample holder, that has been presented in section 3.3.4.2 has not been repeated, under the *assumption* that the *"10x10 mm^2"* basis prototype is, between the two prototypes, the best *candidate* for the final shape of the device, due to its *bigger* (resistant) cross section.

A second simulation campaign has been then performed, starting from the results of the ***first***, to study the effect of the sample's soldering *before* the irradiation. The input file has been modified in such a way that an eutectic Ag - Sn soldering strip has been put only *at the basis* of the sample holder.
The FLUKA simulation results are usually highly influence by the geometry of the problem, and an exact estimation of the geometry of the soldering layer was not possible. For simplicity, this layer has been designed in a way it transformed the cross section of the sample holder from a step to a square, as sketched in Figure 47.

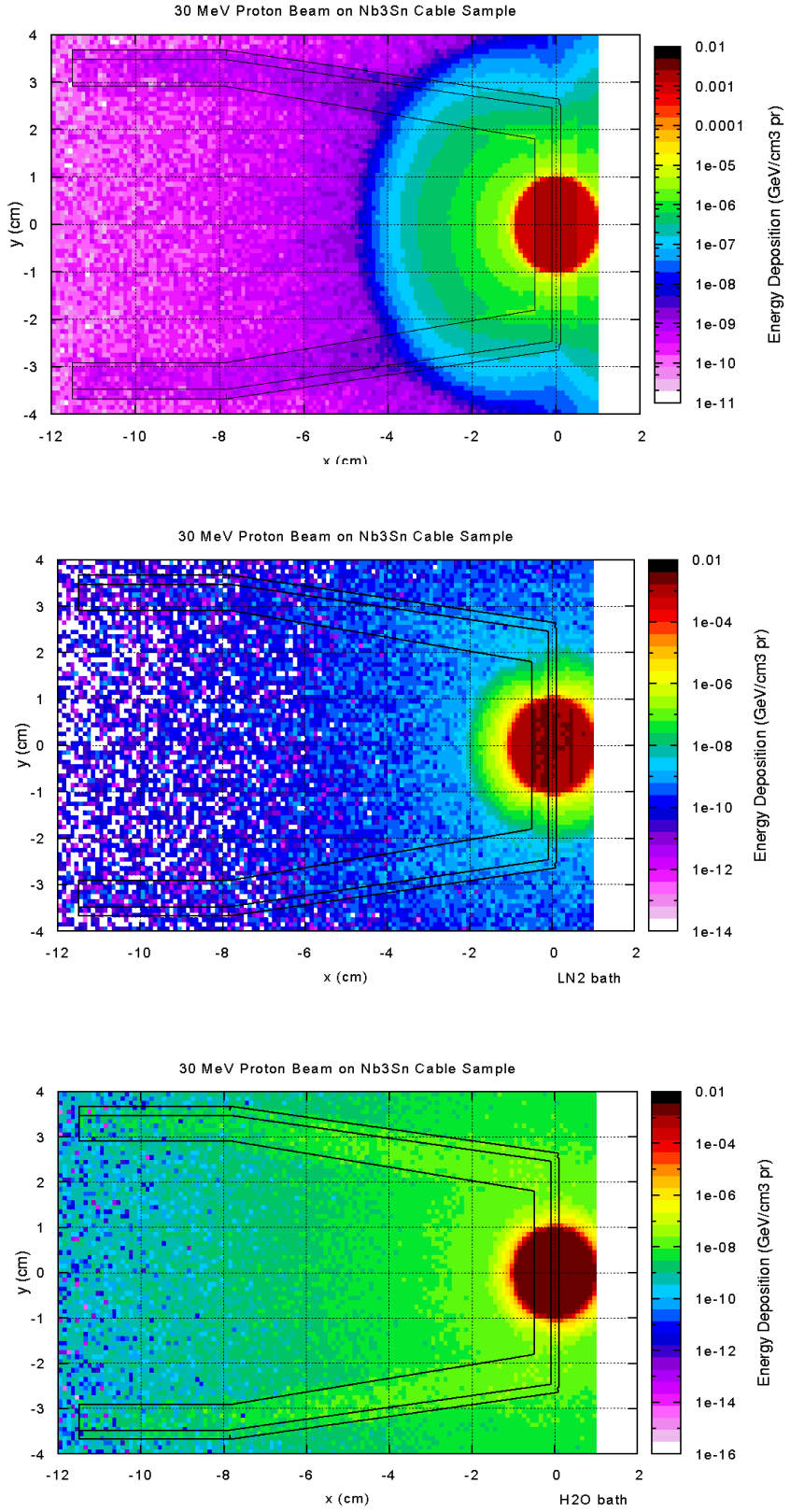

Figure 46. Map of the deposited energy on the SIT sample holder, that have been obtained in the three possible coolant solutions (He, N_2 and H_2O, respectively, from the top to the bottom) and without the fixing material on the device. Ref. [24].

	Ti5 Sample Holder	**Nb_3Sn Cable**	**Coolant**
LHe	$1.16 \times 10^{-2} \pm 0.01\%$	$2.65 \times 10^{-3} \pm 0.03\%$	$1.56 \times 10^{-2} \pm 0.008\%$
LN_2	$1.18 \times 10^{-2} \pm 0.01\%$	$2.64 \times 10^{-2} \pm 0.02\%$	$1.54 \times 10^{-2} \pm 0.007\%$
H_2O	$9.40 \times 10^{-3} \pm 0.01\%$	$2.35 \times 10^{-2} \pm 0.02\%$	$1.82 \times 10^{-2} \pm 0.003\%$

Table 4. Energy deposition in the sample holder, Nb_3Sn cable and coolant, in the point close to the basis of the sample holder. The values are expressed in [GeV*cm^{-3}*p.p.$^{-1}$], and the errors in the calculation are referred to the statistical process of the FLUKA calculation algorithm. Converting these values in Ψ, it is easily seen that the proton - coolant interaction reduces the flux (and thus the *specific deposited power*) at the basis of the sample holder and respect to the *nominal* value ($\Psi = 10^{14}$ protons*cm^{-2}*sec^{-1}) by 2 orders of magnitude for the He and N_2 bath and by 3 order of magnitude for the H_2O bath. Ref. [24].

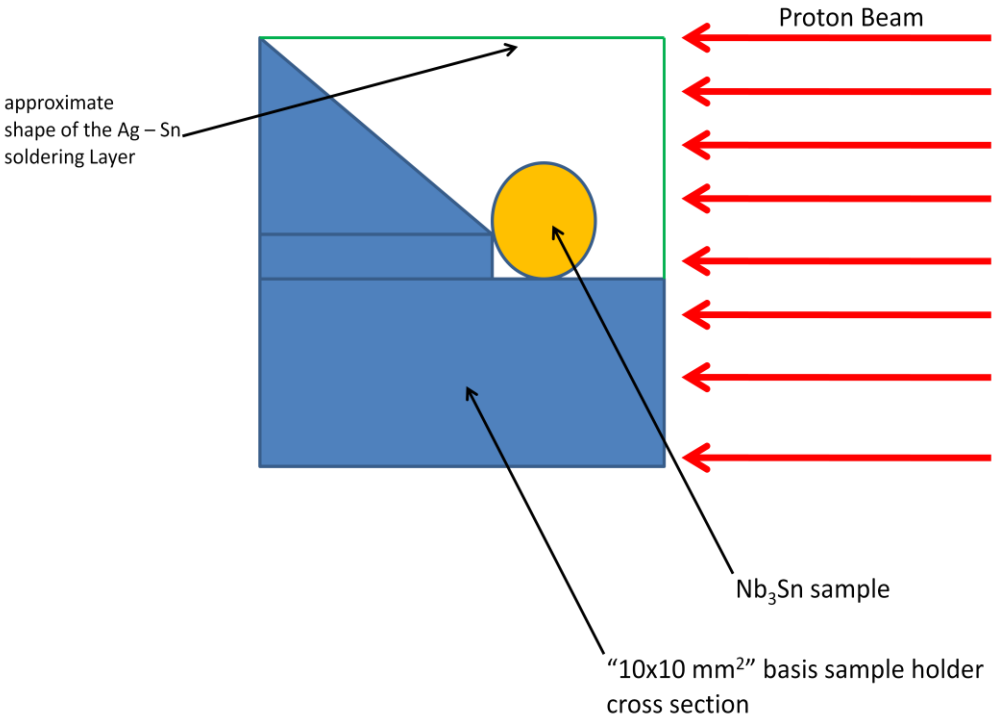

Figure 47. Sketch of the modification of the FLUKA input file for the second simulation campaign, for a preliminary study of the soldering of the superconducting wire to the sample holder with an eutectic Ag - Sn soldering layer.

The results of the second simulation campaign are summarized in Figure 48, for the lower basis of the sample holder, and tell us that the highest proton dose will be absorbed by the soldering layer, thus leaving the underlying Nb_3Sn sample in the non - irradiated state. Other soldering solution are currently under investigation, by the SIT research team, because soldering the Nb_3Sn wire to the sample holder before the irradiation stage would facilitate the sample holder's preparation procedure, with particular respect to the deactivation stage that has been taught in the conceptual design of the whole experiment.

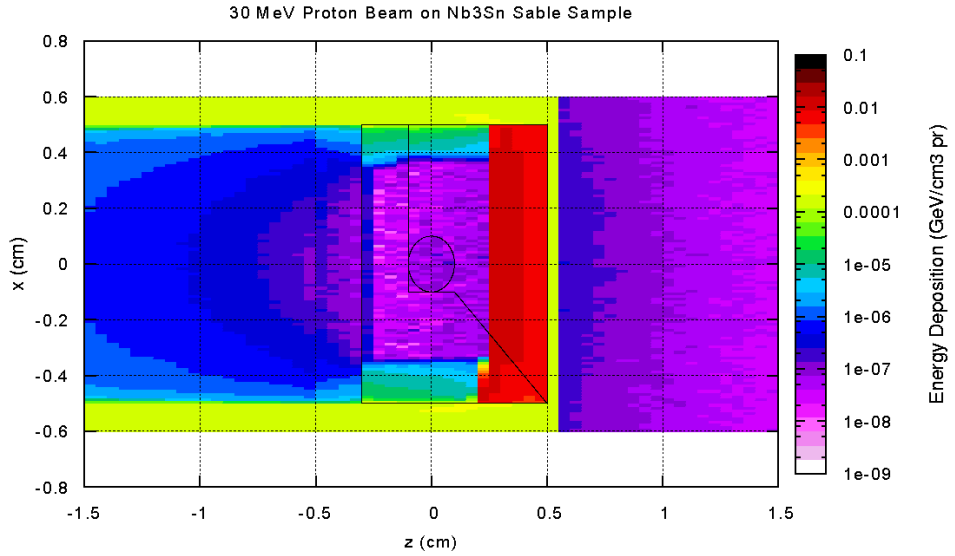

Figure 48. The map of the deposited energy at the basis of the SIT sample holder, that has been covered with an Ag - Sn soldering strip. The values of the map are calculated for the case of the irradiation in a liquid He environment, but similar values [24] are expected also for the other cooling solutions. Ref. [24].

Finally, the activity of the sample holder has been *preliminary* estimated as a function of the time from the results of the first simulation campaign , and the correspondent plots are reported in Figure 49.
If the soldering layer is not put on the sample holder before the irradiation, the activity of the device *rapidly* decays in time. Nevertheless, the *exact duration* of the sample holder deactivation stage has to be decided in connection with the radioprotection norms of the research institute that will host the irradiation experiments. The calculations of the deactivation curves for the immersion of a *soldered* sample holder in the three coolant baths are *currently in progress*.

3.5 Future Engineering Activities

At present, the future tasks of the SIT research team are:

- The final choice of the research institute that will host the proton irradiation tests
- The determination of the working flux of the proton beam line, in relation with the design of the cooling system attached to the irradiation vessel
- The adaptation of the SIT sample holder to other superconductors, that will be used in the LHC upgrade and, like Nb_3Sn, will be subjected to an intense radiation fields

In the last year the list of the candidate institute for the proton irradiation tests has been completed, and the final choice is now purely related to the economical offers that these institutes can do the CERN administration. The second and third aspect will be now briefly illustrated.

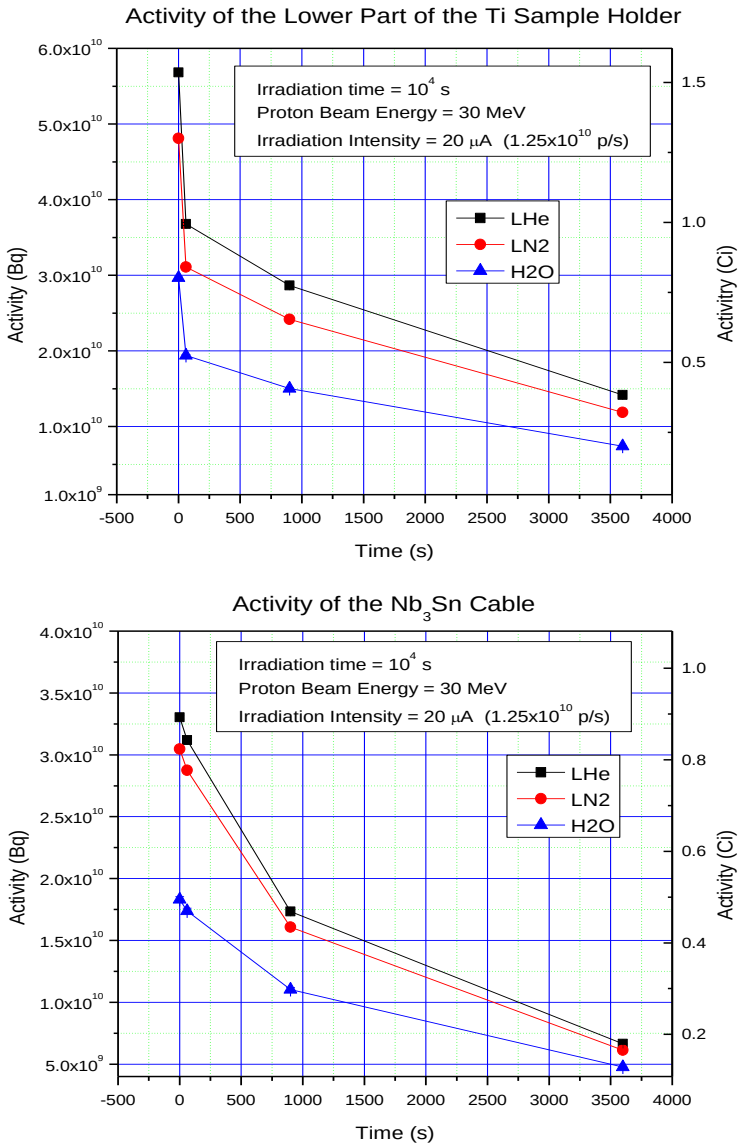

Figure 49. The activity of the Ti - sample holder (on the top) and of the Nb_3Sn cable (on the bottom) against the tim . In the model, the irradiation of the sample holder is performed *without* the fixing material and in the three possible coolant baths. Ref. [24].

3.5.1 Working Flux of the Proton Beam Line and Cooling of the SIT Sample Holder

The best way to introduce this problem is to first imagine that the irradiation tests will be, for some reason, performed at room temperature without any cooling system attached to the sample holder. Power will be then deposited on the device, that will be heated at a rate $\frac{\Delta T}{\Delta t}$. To be coherent with the previous sections, let's *suppose* to use the "10x10 mm^2" prototype, and ideally put it into the Kurchatov beam line in a situation the heat deposition rate is so high that the Ti - Alloy has not enough time to dissipate this heat per conduction. Under these assumptions, the heat rate of the lowest part of the device can be written as:

$$\Psi * E * A_{HITTED} = M * c_p * \frac{\Delta T}{\Delta t} \tag{24}$$

where A_{HIT} is the cross section of the sample holder that is effectively invested by the beam, C_P the material's specific heat and M the mass of the invested volume of the sample holder[3]. At 298 K temperature, the heat capacity of the Ti-Al6-V4 alloy is equal to 0.47 $J*g^{-1}*K^{-1}$; the "10x10 mm^2" basis sample holder will be exposed for an area of 2 cm^2 and, considering that the position of the penetration depth of 30 MeV proton in the material is around 3 mm, a mass M = 2.658 g can estimated. If then the Kurtchatov beam line would work at maximum power, a flux of 10^{14} protons$*cm^{-2}sec^{-1}$ would give $\frac{\Delta T}{\Delta t} = 741\ \mathrm{K} * \mathrm{sec}^{-1}$. Under the hypothesis that the conduction process of the deposited heat is slow compared to the power deposition rate, this would produce significant temperature gradients in the apparatus.

The simplest solution for the cooling is to immerge the device into a coolant bath. Irradiation performed in liquid He or N_2 would have the advantage to recreate environmental condition the closest to the true working condition of the superconductor in the LHC magnets. Conversely, water is frequently used as coolant of the systems attached to the modern particle accelerators, and also this coolant can be taken in consideration. Possible activation of the coolant by the proton beam are also a serious problem, but this will, for the present illustration, not be discussed here.

He or N_2 will interact with the proton beam, and the flux that will effectively invest the basis of the SIT sample holder is of two orders of magnitude lower than the nominal flux of the Kurtchatov cyclotron. This flux will correspond to a heat flux q = 4.8 $W*cm^{-2}$.

Let's imagine that the coolant bath of these two cryogens would be static and at ambient pressure during the irradiation. Considering the geometry of the problem, the conditions for "flat plate and large diameters" should be then selected from the plots of Figure 50 and 51 to estimate the convective temperature difference ΔT between the surface of the sample holder and the bulk coolant. It is seen that this difference would be of some thousands of degree, corresponding to a complete film boiling regime.

Correspondingly, the flux Ψ of the cyclotron should be lowered, and the cryogen put under forced flow. But at this stage, problems concerning the higher τ of the irradiation of a single sample (the cost of exploitation of the beam line can be even more than 1000 USD/hour!) and the relevant bigness of the external cryogenic cooling system that is attached to the irradiation vessel (and has to fit, in the SIT experimental design, near the proton beam line) are problems that, also for the choice of water, have to be considered. These could be only solved, when the proton irradiation tests will have been finally assigned.

3.5.2 Other materials

MgB_2 and YBCO are presently candidate materials power enhancement of the current leads that connect the LHC tunnel to the electric line in surface. These current leads are planned to be used in the form of wires (MgB_2) and tapes (YBCO), as the one shown in Figure 52 and 53.

Some sectors of these superconducting lines will be close to the LHC detectors, and thus be subjected to an intense radiation field, that is not too different from the one expected in the HLI insertions. For this reason, these superconductors will be tested, together with Nb_3Sn, in the SIT project and the SIT research team is currently modifying the design of the sample holder to adapt it to MgB_2 and YBCO samples. The new sample holder prototype is shown in Figure 54.

[3] Charged nuclear particle penetrate into a metal for a specific *penetration depth*, that is a function of the particle's energy. In the case of the SIT sample holder, an *invested volume* of mass *M* can be thus defined.

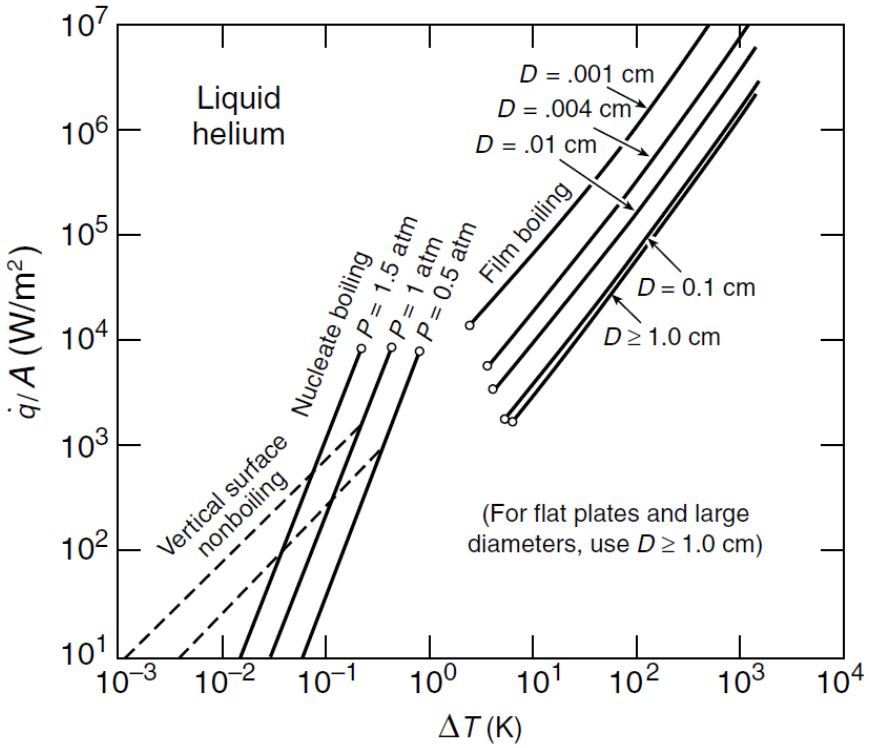

Figure 50. The heat flux q against the convective temperature difference ΔT for liquid He. Recall that also for cryogens, $q = h^* \Delta T$, where h is the convective heat exchange coefficient. Ref. [38]

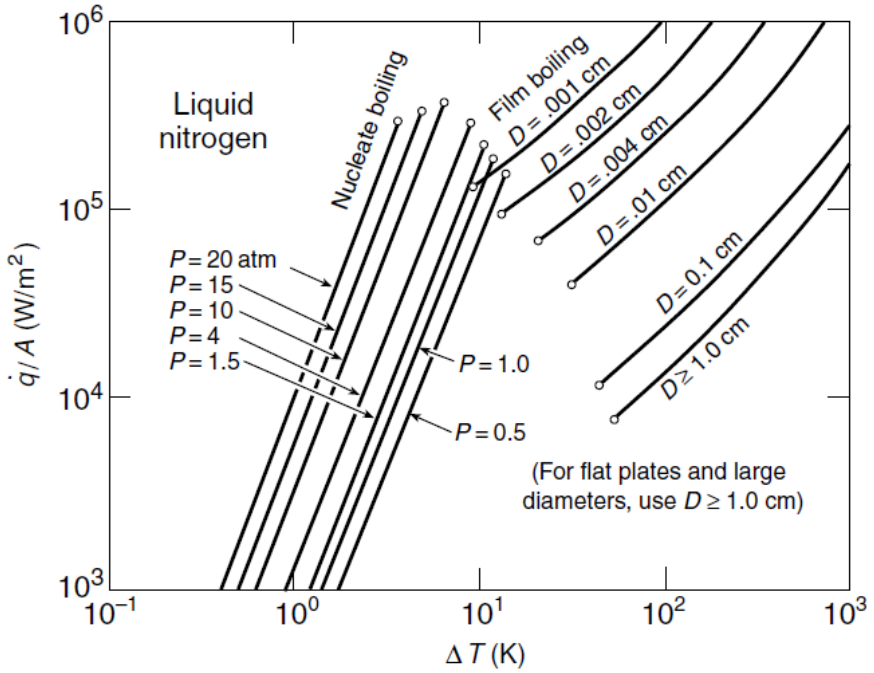

Figure 51. The heat flux q against the convective temperature difference ΔT for liquid He. Recall that also for cryogens, q = h* ΔT, where h is the convective heat exchange coefficient. Ref. [38]

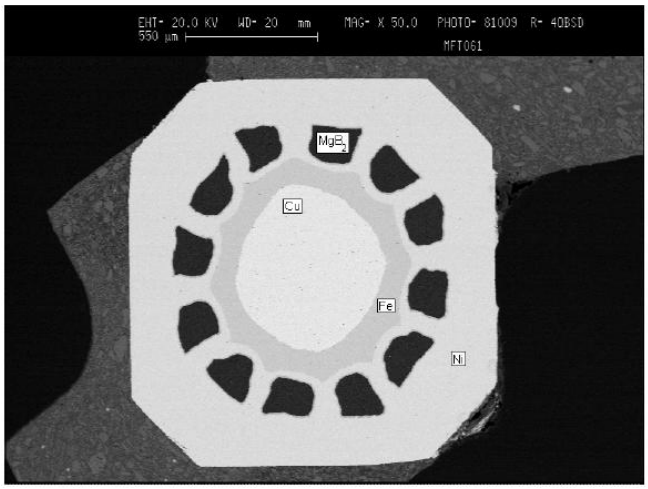

MgB_2 (Vol %)	14.6
Fe (Vol %)	10.8
Cu (Vol %)	13.8
Ni (Vol %)	60.8
Total cross section (mm^2)	2.3
Single MgB_2 filament average section (mm^2)	0.036

Figure 52. Composition and internal structure of a MgB_2 composite wire. Acknowledgements: Amalia Ballarino (CERN - TE - MSC group)

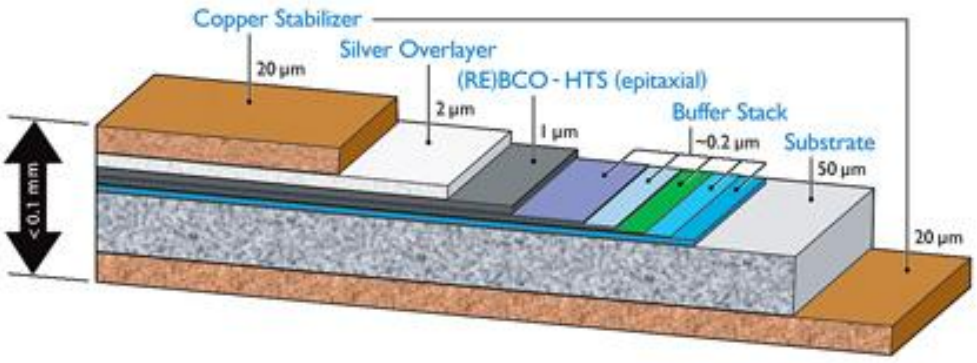

Figure 53. Internal structure of an YBCO superconducting tape. Acknowledgement: Amalia Ballarino (CERN - TE - MSC group)

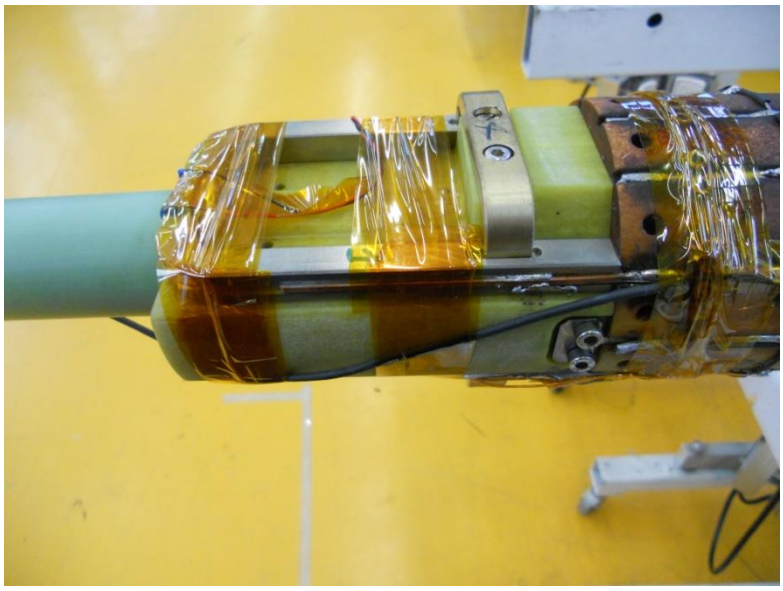

Figure 54. A new prototype of SIT sample holder for the irradiation of MgB_2 wires, during its preliminary tests. Acknowledgement : Amalia Ballarino (CERN - TE - MSC group)

Chapter 4

First Experimental Activities of the SIT Project

4.1 Introduction

The experimental activities of the SIT project of the year 2009/2010 will be now presented.

The experimental validation of the sample holder prototypes for the proton irradiation tests have started in November 2009 at CERN. First critical current tests have been done mounting NbTi wires on the *"10x10 mm^2"* and *"5x5 mm^2"* basis sample holders prototypes. The experimental results that have been obtained from these tests have been analyzed and compared with the one of the LHC - Standard sample holders.

The experimental validation of the SIT prototypes with Nb_3Sn wires has started in May 2010, and is currently in progress.

In May 2010, the research agreement with the A.T.I. Institute in Vienna has been signed, and the *first* critical current tests on fast neutron irradiated Nb_3Sn wires have been done.

4.2 Preliminary Experimental Validation of the SIT Sample Holder Prototypes

Two sets of sample holder prototypes for the proton irradiation of Nb_3Sn have been constructed in October 2009, and these prototypes have been used up to date for their preliminary experimental validation. The results of these preliminary tests will be presented in the next sections.

4.2.1 Study and Test of the Sample Holder Preparation Procedure

The SIT sample holder have been first tested for its possible use in the proton beam line of the Kurchatov Institute. In fact, the characteristics of this beam line, as well as the technical equipment of the russian research center, are the closest to the needs of the SIT research team. The most important features of this test session, will be now illustrated.

The distance between the voltage taps has been chosen in relation with the diameter of the proton beam that will invest the lowest part of the sample holder *after its interaction* with the coolant bath. At the time when the tests have been started, the results of the FLUKA simulation had not yet been published. For this reason, the voltage taps have been put over two distance L:

- The first, *L = 20 mm*, has been chosen under the hypothesis that the proton - coolant interaction will be negligible, and that the length of the irradiated part of the sample holder would correspond to the diameter of the proton spot.

- The second, *L = 40 mm*, has been chosen to take into account the proton - coolant interaction.

This experimental configuration has been kept constant during the whole test session, even after the results of the preliminary FLUKA simulations. Figure 55 shows a detail of one of the SIT sample holder prototypes, where the two voltage taps distances have been indicated.

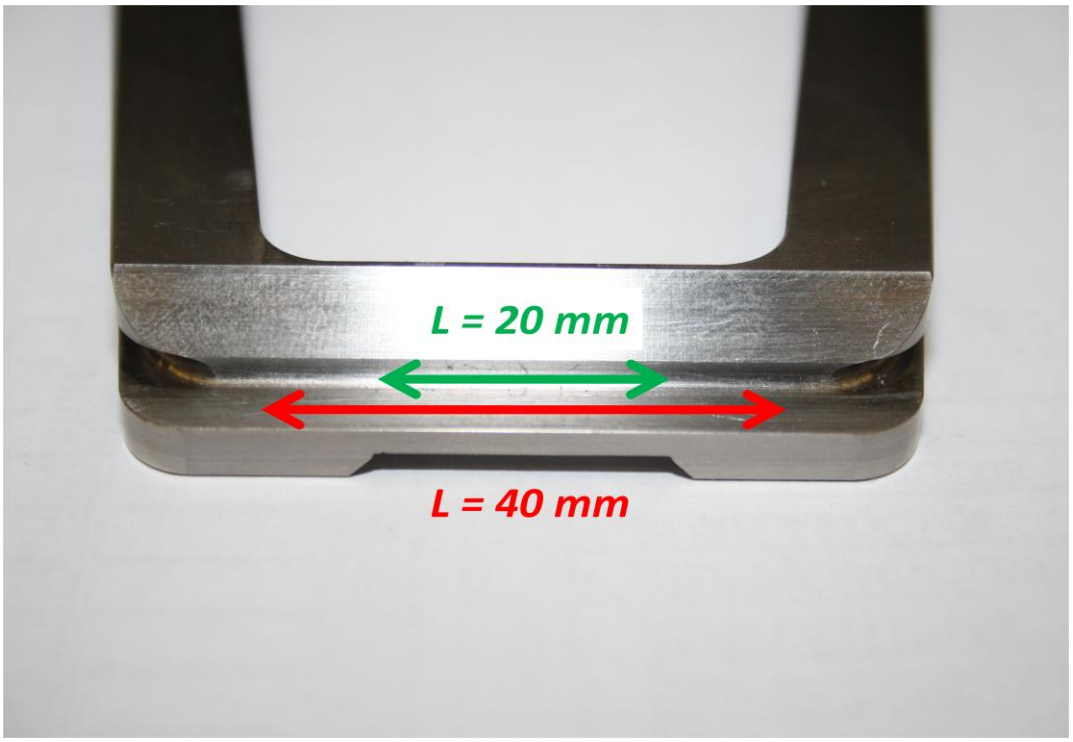

Figure 55. The basis of the SIT "10x10 mm^2" basis sample holder prototype, and the exact distances of the two set of voltage taps that have been put there for the first tests of the apparatus.

According to the VAMAS Standards in the critical current measurements [20], the sample has to be perfectly fixed to the sample holder, because the applied magnetic field *B* can, in principle, cause micrometric movements of the wire, and these movements can introduce noise in the V - I curves.

For these reasons, a first set of critical current measurement has been done, fixing *step by step* the NbTi wire to the SIT prototypes thanks to *Stycast*, a polymeric glue for cryogenic applications. Once the *best* V - I curves have been obtained, the *effective* tests on the sample holder prototypes have been started. In this configuration, the wire has been *totally* fixed to the sample holder, including his electric connection with the *current lead* of the shaft, as it has been reported in Figure 56, 57, 58. Figure 59 shows one of the best V - I curves that have been obtained at the end of the tests of the fixing procedure.
The study of the electric connection between the NbTi wire and the current leads in the shaft will be now illustrated.

The current leads are immerged in the liquid He bath of the cryostat and, in order to avoid the boiling of the coolant, these electric lines have been made of NbTi. In order to connect them to the sample, it has been decided to use a "bridge" connection: a piece of NbTi, over the two NbTi electric lines (wire on the sample holder and current leads of the shaft).
The whole connection system has then been soldered on with an eutectic Ag - Sn alloy strip, over a length that has been estimated imposing that the dissipated power *P* of the joint should be less than 1 W. Applying the Ampère's law ($P = R*I^2$, where, in this case, *I* is the current flowing in the electric system and *R* is the *total* joint resistance), it has been estimated that this should correspond to a maximum joint resistance of $1*10^{-8}$ Ω, being the optimal soldering length greater than 80 mm, as represented in Figure 60 and 61.
From qualitative estimations, the NbTi bridge has been finally soldered on the joint over a length of 100 mm.

Figure 56. Installation of the two SIT sample holder prototypes on the CERN measurement shafts, thanks to the new mechanical support, that has been designed to test both prototypes using a single shaft.

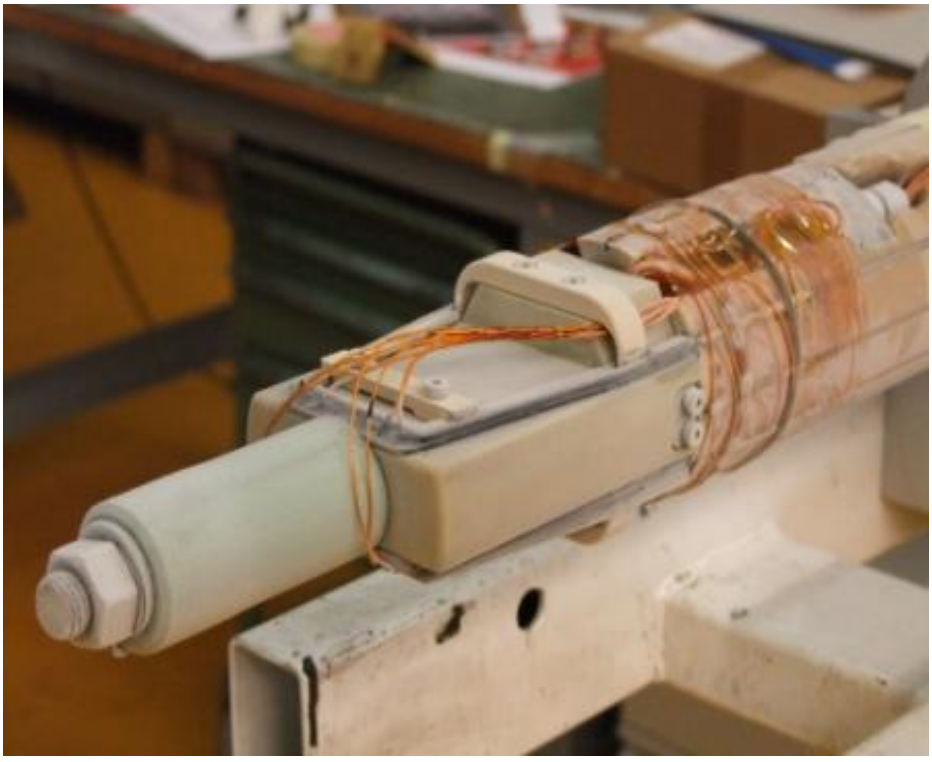

Figure 57. The (frozen) shaft after its extraction from the cryostat during the first tests of the SIT sample holder. The black strip along the U is the layer of polymeric glue that has been put to *totally* fix the wire. This figure also shows the two sets of voltage taps (copper filaments) connected to the basis of the sample holders.

Figure 58. The soldering strip on the electric connection between the current leads during the sample holder preparation.

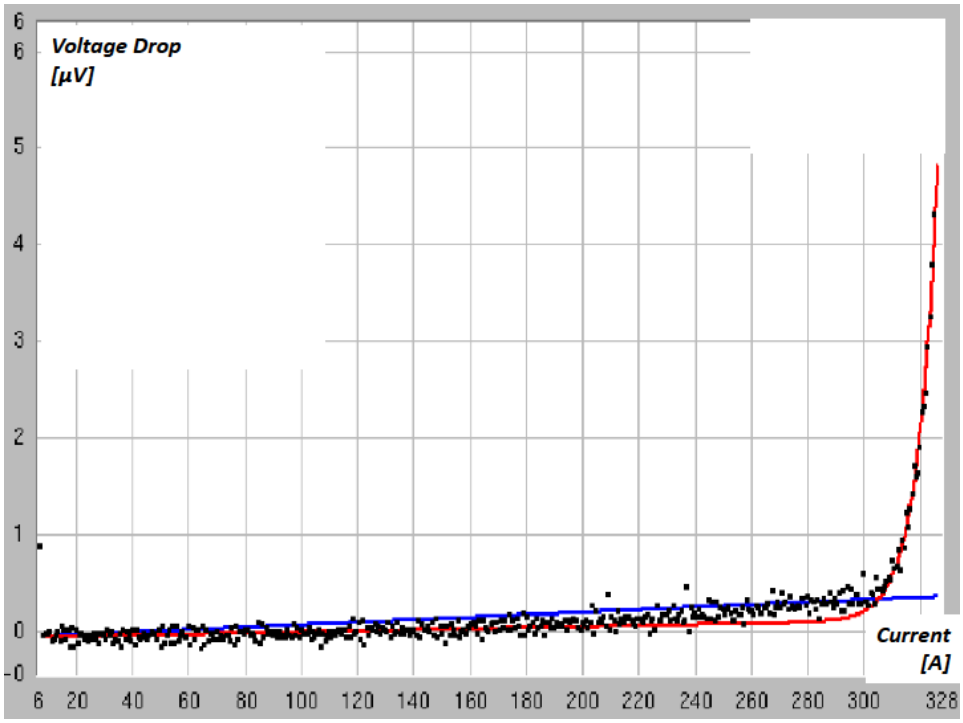

Figure 59. An example of the best V - I curve obtained during the tests of the fixing solutions. The red curve is the fit of the experimental points, while the blue curve is connected to one of the criteria that have been used in the critical current measurements. The apparent slope, that corresponds to the superconductive state, is an electronic artifact, and is corrected introducing in the data analysis a vertical offset *Q*.

$$L(I,P) = C * \left(\frac{I^2}{P}\right)$$

Length L of the Soldering Strip

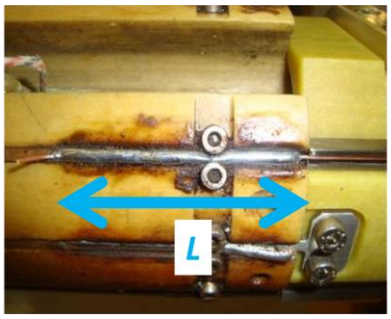

$$C = \frac{2\rho_{Cu}A + \rho_{AgSn}B}{H}$$

C = Electrical Joint Total Resistance R

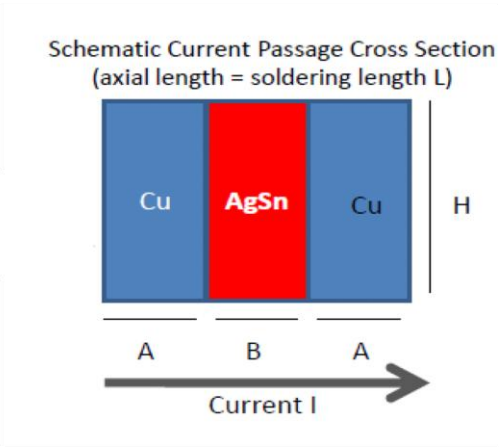

Figure 60. The analytical model for the calculation of the soldering length over the electrical joint between the wire on the sample holder and the current leads of the measurement shaft. The two *Cu* blue layer are the external electric shunt of the NbTi wires, and are divided by an Ag - Sn soldering layer. The current I passes from the wire to the electric bridge (or equivalently, from the current lead to the bridge), across the Ag - Sn layer. *L has not* to be confused with the distance between the voltage taps.

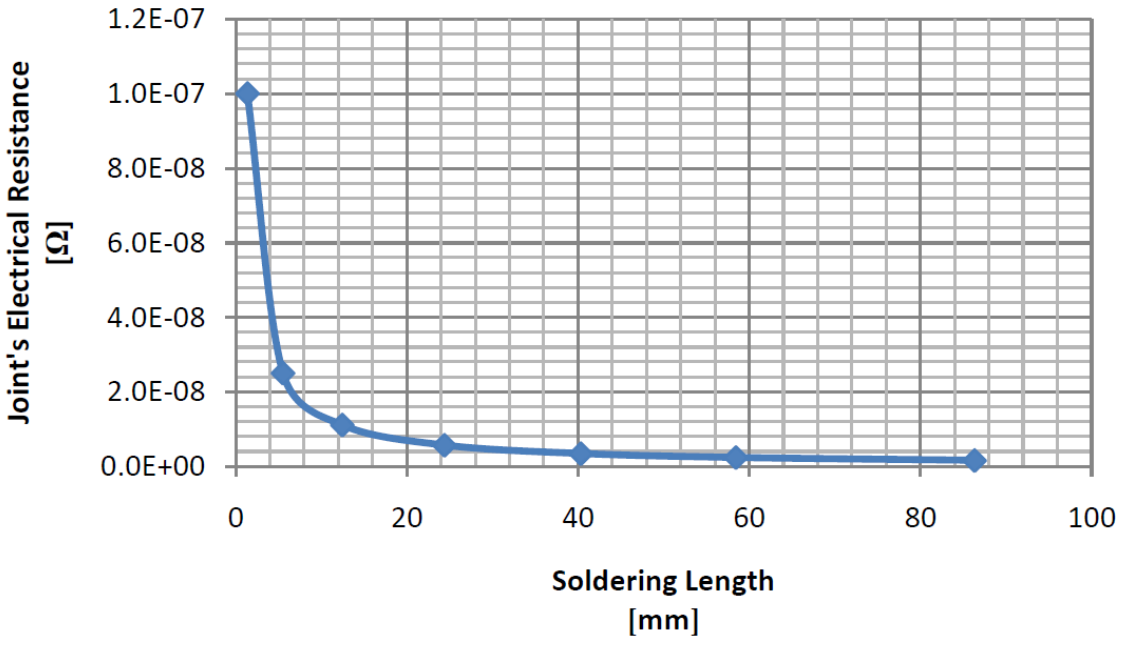

Figure 61. The total resistance of the joint versus the soldering length, calculated according to the model of Figure 52.

Wire	**Diameter [mm]**	**Copper/Superconductor Phase Ratio**
NbTi – 02R	0.825	1.25
NbTi – 01E	1.250	1.65

Table 5. Characteristics of the superconducting NbTi wires that have been used for the first tests of the SIT "5x5" and "10x10 mm^2" basis sample holders. The wire's name are the CERN reference classifications.

4.3 Preliminary Tests with NbTi Wires

The SIT prototypes have been finally tested, after the end of the first stage of preparation. The results are presented in this section, and compared with the one obtained from the LHC Standard sample holders.

4.3.1 Adopted Criteria for the Testing and for the Data Analysis

The Data Analysis has been started considering the characteristic features of the NbTi wires that have been used. 02R and 01E reference wires were mounted on the SIT prototypes. Table 5 presents the characteristics of these wires.

In each experiment, ramp rates varying between 5 to 12 $A*sec^{-1}$ have been imposed to the two wires, this to find a compromise between the time of each measurement and the avoiding of early quenches of the wires (that are known to happen if the current ramp rate is too high).

The critical current have been measured at applied fields of 6, 7 and 8 T, in order to compare the results of the critical current measurements to with the *available* data that had been obtained mounting the same NbTi wires on the LHC Standard sample holders.

The acquired V - I curves have been first selected, to choose the best defined. This selection has reduced the statistics in the measurement, up to a point where per each applied field only one curve was available. Conversely, this particular choice has allowed to characterize the superconductor in a way that is completely independent of the electronic noise of the V - I curve. Also, the error in the measurement have been thus related to the measurement errors that are characteristics of the data acquisition system.

The computer station that controls the cryostat during the critical current measurements produces a file in LabView format. This files has been converted into a .txt one, and all the acquired data have been inserted in a common Xcel electronic sheet, to perform the curve manipulations. The superconducting transition of the V - I curves has been isolated, and put into another Xcel file for the definitive data analysis.

The superconducting transition of a wire can be well fitted by the Power Law formula [39]:

$$\left(\frac{V}{V_0}\right) = \left(\frac{I}{I_0}\right)^n \tag{25}$$

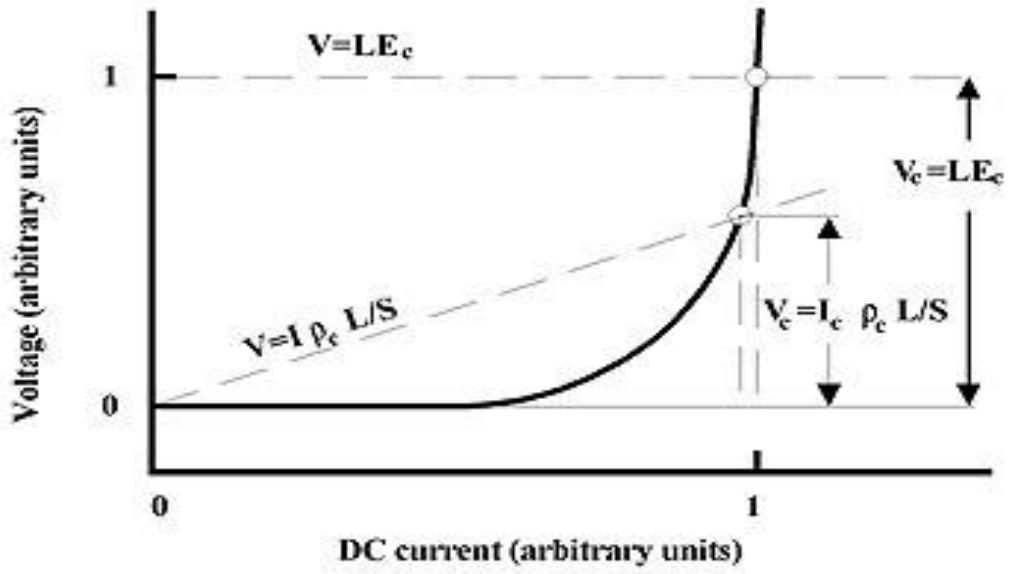

Figure 62. Sketch of the electric field and resistivity criterion for the determination of the critical current from a V - I curve.

where V_0 and I_0 are reference values for the voltage drop and the current, and n a material dependent coefficient, simply called "*n - value*". The *n - value* is an important characteristics of the superconductor, because it indicates the abruptness of the superconductive transition, and it is a function of the applied magnetic field *B*. It can ranges from 30 to 120 for all the type II superconductors.

Following equation (25), the isolated segments of the *V - I* curves have been continuously filtered from the electronic noise and interpolated with a power law of the kind $V = A*(I)^n$ up to the point where the *n - value* was the closest to the already known ones of the 02R and 01E wires.

The interpolated curves have been then intersected with the resistivity criterion line, because this is the standard criteria that has been used for the characterization of the NbTi superconducting wires. The resistivity criterion line is described by the following formula:

$$V = \left(\frac{\rho_C * L}{S}\right) * I + Q \tag{26}$$

where ρ_C is the criterions resistivity (of value 10^{-14} Ω*m), *S* the wire's cross section and *Q* the vertical offset, that is introduce in the critical data analysis to compensate possible slopes (electronic artifacts) in the V - I curve before the transition to the normal state is reached (see also Fig. 62). At the point of intersection between the interpolation curve and the resistivity criterion line, the measured current I_M has been read.
For completeness, it is reported that the critical current of a superconducting material can also be measured applying the electric field criterion, according to which I_C can be read on the current axis of the V - I graph in the intersection point between the superconductive transition and an horizontal line, of equation $V = E_C*L$. The critical electric field E_C is equal to 100 μV*m.

The resistivity and electric field criteria are sketched in Figure 62, while Figure 63 and 64 show, respectively, some of the best obtained V - I curves and the plots that have been done during the data analysis.

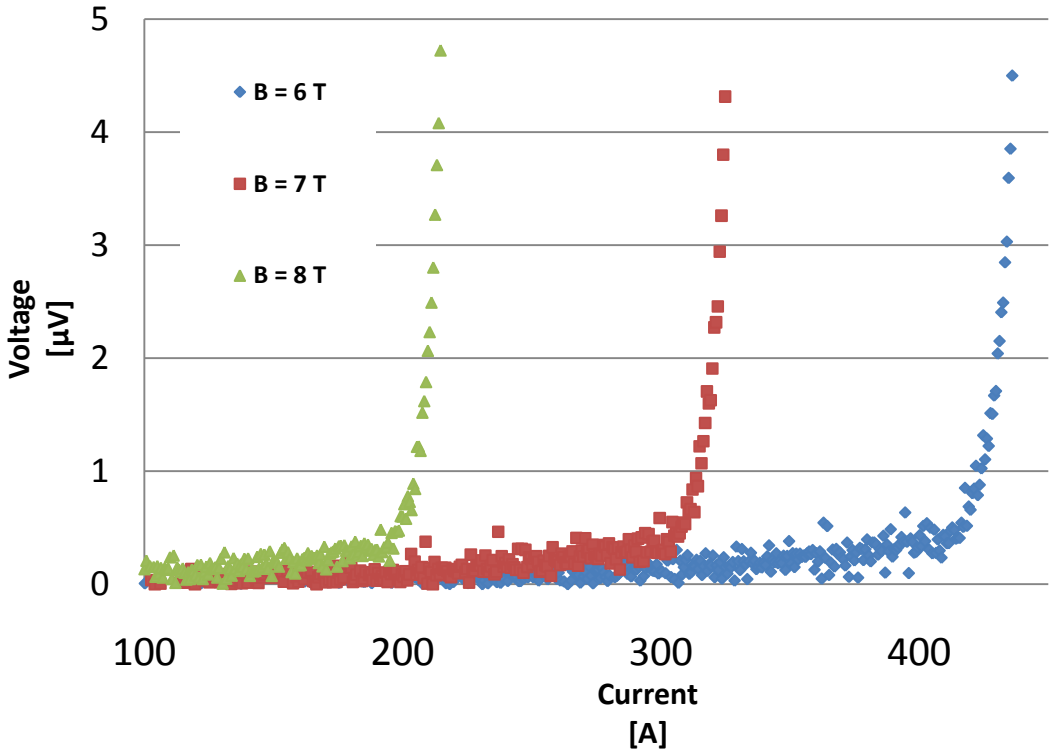

Figure 63. Superposition of some of the best obtained V – I curves (data taken from the test of the "5x5 mm^2 basis sample holder, choosing a distance between the voltage taps of 40 mm).

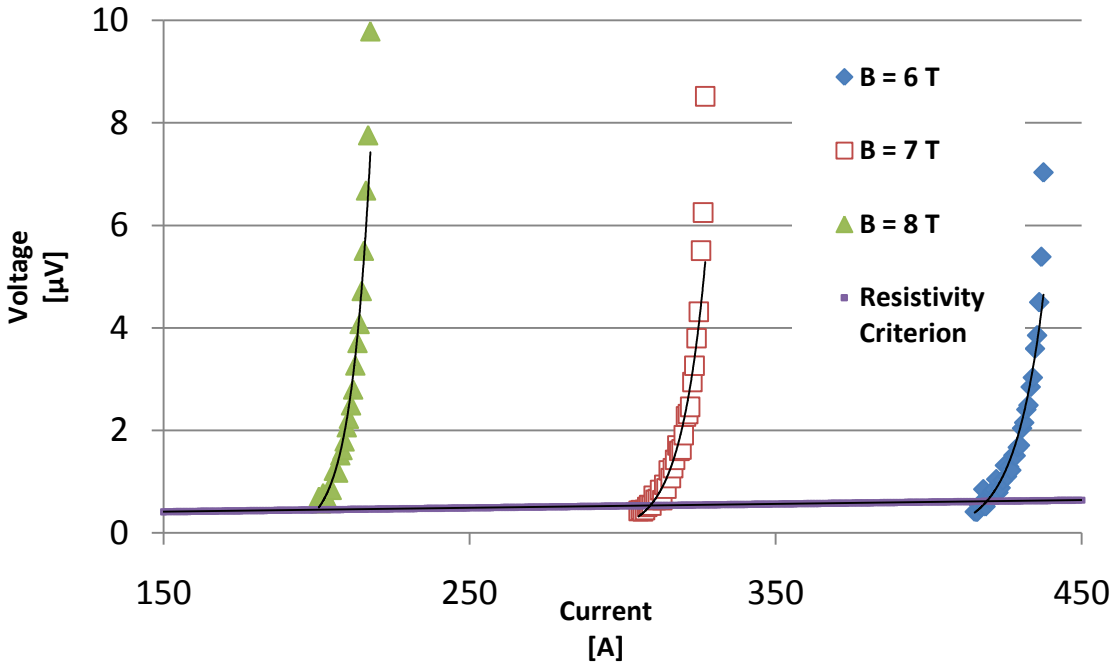

Figure 64. The determination of the measured current I_M: the superconductive transitions are isolated, fitted and intersected at the end with the resistivity criterion line. I_M is read on the current axis at this intersection point, taking thus into account the vertical offset Q.

For technical reason related to the cryogenic pumping systems that fills the cryostats, it has been extremely difficult to maintain the measurement temperature at 4.222 K, and all the measurements have been performed at 4.333 K. The critical current has been also recalculated, as a function of I_M thanks to the Lubell formula [25]:

$$\frac{I_C}{I_M} = \frac{T_C - 4.222\ K}{T_C - 4.333\ K} \tag{27}$$

where the critical temperature of the NbTi superconductor scales with the applied magnetic field as [25]:

$$\frac{T_C(B)}{T_{C0}} = \left[1 - \left(\frac{B}{B_{C2}}\right)\right]^{\frac{1}{1.7}} \tag{28}$$

being T_{C0} the critical temperature of the composite material at zero applied magnetic field.

4.3.2 The results of the "5x5 mm^2" basis sample holder test

The "5x5 mm^2" basis sample holder has been tested using a NbTi 02R reference wire. The device has produced a well defined *V* - *I* curve over L = 40 mm. The measurements acquired at L = 20 mm were so noisy, that the critical current determination has not been feasible.

In Table 6:

- The SIT and LHC Standard *n - values*
- The SIT and LHC Standard I_C *values*

are preliminary compared.

A first analysis of these values shows that the difference in the measured critical current between the SIT prototype and the LHC Standard sample holder lies between 10 and 12 A at all applied magnetic fields, that have been selected for the measurements. For all the measurements, this would give roughly less than 2% difference in the critical current measures when using the SIT "5x5 mm^2" basis sample holder instead of the LHC Standard. A more precise comparison will be done in section 4.3.3

4.3.3 Results of the "10x10 mm^2" basis sample holder test

This prototype has been tested using the NbTi 01E reference wire, with success for *both* distance between the voltage taps. Like the previous case, in Table 7 the SIT and the LHC Standard results are compared.

The tabulated values show this time, that the difference in the measured critical current lie between 19 and 26 A for L = 20 and for L = 40 mm, giving a percentage error in the experimental values of c.a. 4 % at all the applied magnetic fields. This observation will be better investigated in the next section.

$B_{APPLIED}$ [T]	n_{SIT}	$n_{LHC\ Std.}$	$I_c(\rho_c)$ SIT [A]	$I_c(\rho_c)$ LHC Standard [A]	Difference [A]
6	46.5	48	437 ± 0.5	424 ± 0.5	11
7	40.5	42	324 ± 0.5	312 ± 0.5	12
8	33.5	33	211 ± 0.5	201 ± 0.5	10

Table 6. The experimental results of the "5x5 mm^2" sample holder test, in comparison with the LHC Standard past critical current measurements. The uncertainties in the measurement can be related to the features of the test stations (data acquisition system connected to the cryostats)

Voltage Tabs Distance [mm]	$B_{APPLIED}$ [T]	n_{SIT}	$n_{LHC\ Std.}$	$I_c(\rho_c)$ SIT [A]	$I_c(\rho_c)$ LHC Standard [A]	Differences [A]
20	6	48.4	49	728 ± 0.5	702 ± 0.5	26
"	7	45.7	48	560 ± 0.5	538 ± 0.5	22
"	8	33.1	36	391 ± 0.5	372 ± 0.5	19
40	6	47.2	49	728 ± 0.5	702 ± 0.5	26
"	7	44.1	48	559 ± 0.5	538 ± 0.5	21
"	8	35.7	36	391 ± 0.5	372 ± 0.5	19

Table 7. The experimental results of the "10x10 mm^2" basis sample holder test, in comparison with the Modified VAMAS past critical current measurements. The uncertainties in the measurement can be related to the features of the test stations (data acquisition system connected to the cryostats).

4.3.4 Comparison between the SIT and LHC Standard sample holders experimental results

The experimental results of material test are, in principle, independent of the specific technique that is used during the test. For this reason, the I_C versus B curve of the SIT prototypes should coincide with the one of the LHC Standard. In Figure 65, 66 and 67 the values presented in Table 6 and 7 are plotted against the applied magnetic field.

The best way to compare the two sample holder's behavior is to plot the critical current values as a function of the total magnetic field. This can be written as the sum:

$$\overrightarrow{B_{TOT}} = \overrightarrow{B_{Backgr}} + \overrightarrow{B_{Self}} \tag{29}$$

where B_{Backgr} is the applied magnetic field, and is increased by a quantity given by the magnetic field that is induced by the superconducting wire B_{Self} .

For the SIT sample holder, the absolute value of the magnetic field induced by the wire has been estimated as:

$$\left|\overrightarrow{B_{Backgr\ -SIT}}\right| = \frac{\mu_0 * I_C}{2\pi * R} \tag{30}$$

where R is the wire's diameter.

The calculation of the medium magnetic field that is induced by the superconducting wire by its turns on the LHC Standard sample holder should, in principle, require a dedicated Finite Element Analysis to obtain precise values. To simplify the work, various *analytical* models have been applied to calculate the self field correction of the LHC Standard sample holder in the point of application of the voltage taps, but the one that has given the best[4] data analysis results will be now presented [27].

The LHC Standard self field has been seen as the resultant action of *a single circular filament*, in which a current value equal to I_C flows. The origin of a (r, z, φ) reference system has been ideally put at the basis of a cylinder, which radius r and height h are the same of the LHC Std. sample holder. The geometry is shown in Figure 56.

B_{Self} has been then calculated as:

$$\langle\overrightarrow{B_{self\ -LHC\ Std.}}\rangle = \mu_0\langle\vec{H}\rangle \tag{31}$$

where the value of $\vec{H}$ has been calculated as the mean arithmetic contribution of the 9 turns of the superconducting wires as [27]:

$$\langle\vec{H}\rangle = I_{C*}\frac{1}{9}\sum_{i=1}^{9}\left|\frac{(r)^2}{2((r)^2+(id)^2)^{\frac{3}{2}}}\right| * \overrightarrow{\iota_z} \tag{32}$$

[4] At first, the self field corrections for the LHC Standard sample holder could be calculated from the classic solenoid model, but in this case, the turns too distant on the cylinder surface to have, in first approximation, a continuous distribution of turns per unit of length.

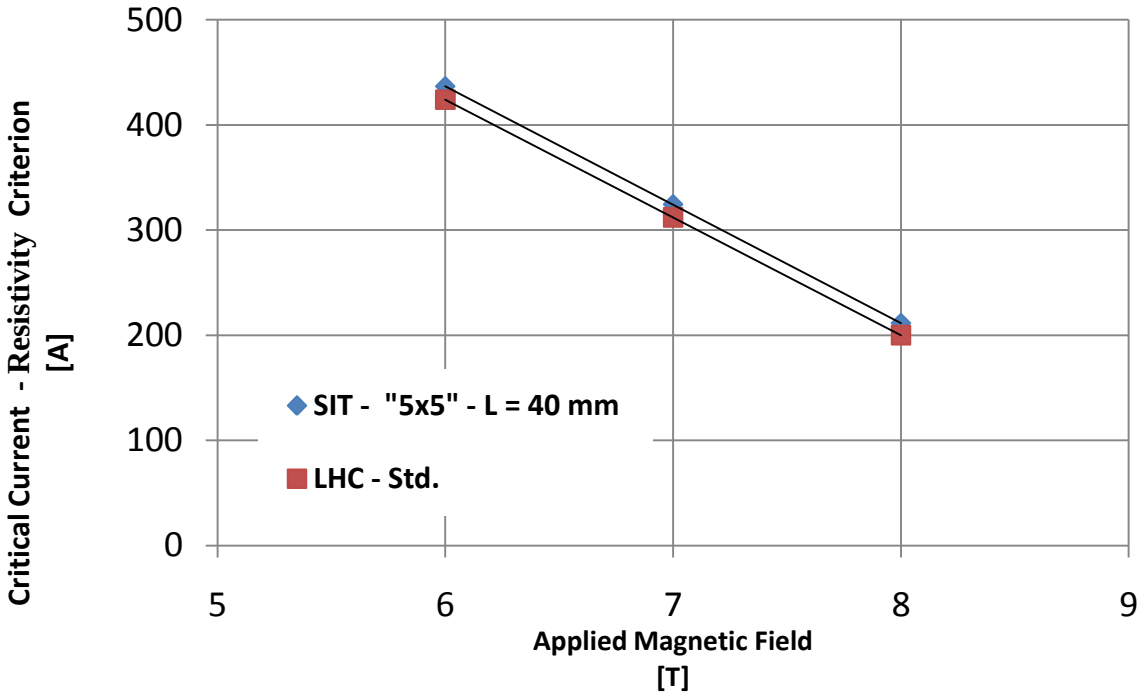

Figure 65. First Comparison between the SIT "5x5 mm^2" basis (Voltage taps distance = 40 mm) and the LHC Standard Sample Holder experimental results

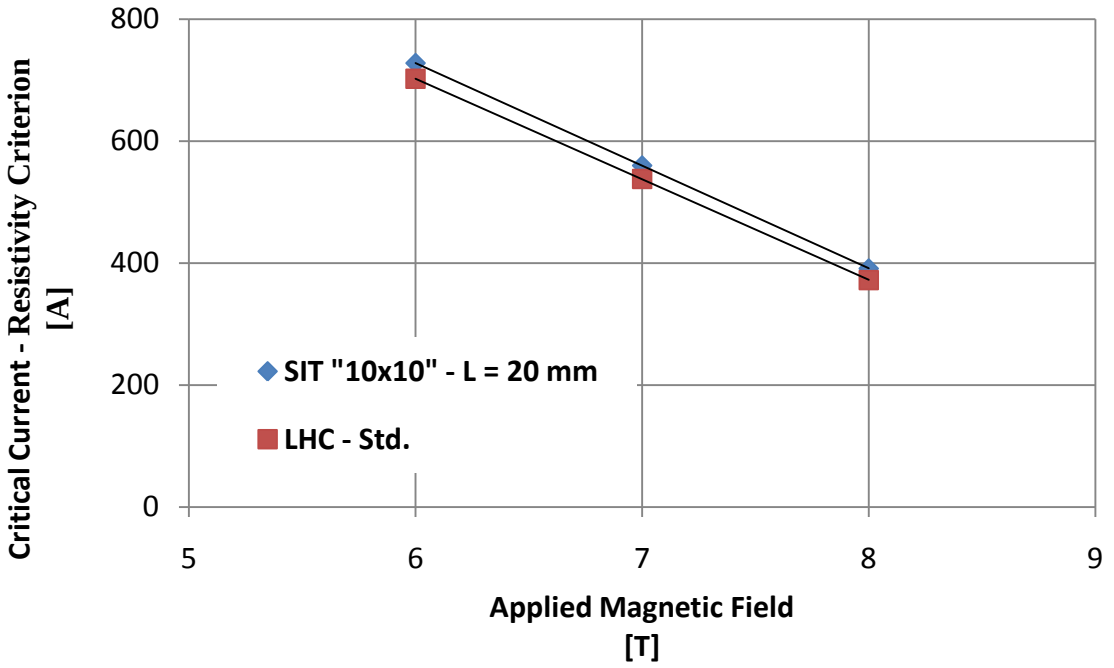

Figure 66. First Comparison between the SIT "10x10 mm^2" basis (Voltage taps distance = 20 mm) and the LHC Standard sample holder experimental results.

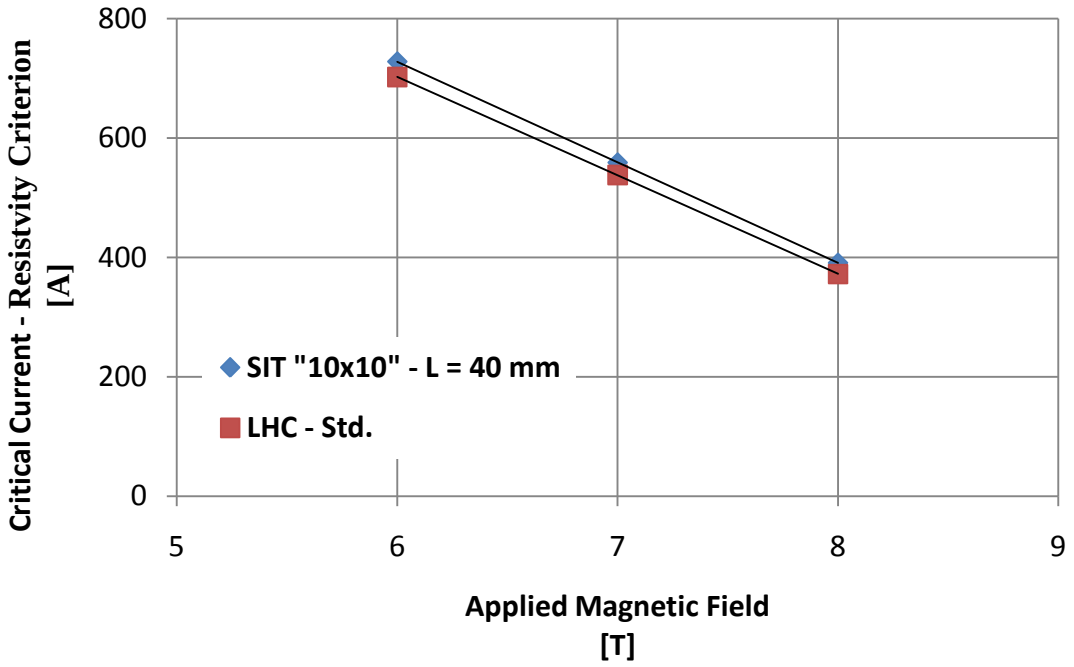

Figure 67. First comparison between the "10x10 mm^2" basis (Voltage taps distance = 40 mm) and the LHC Standard sample holder experimental results.

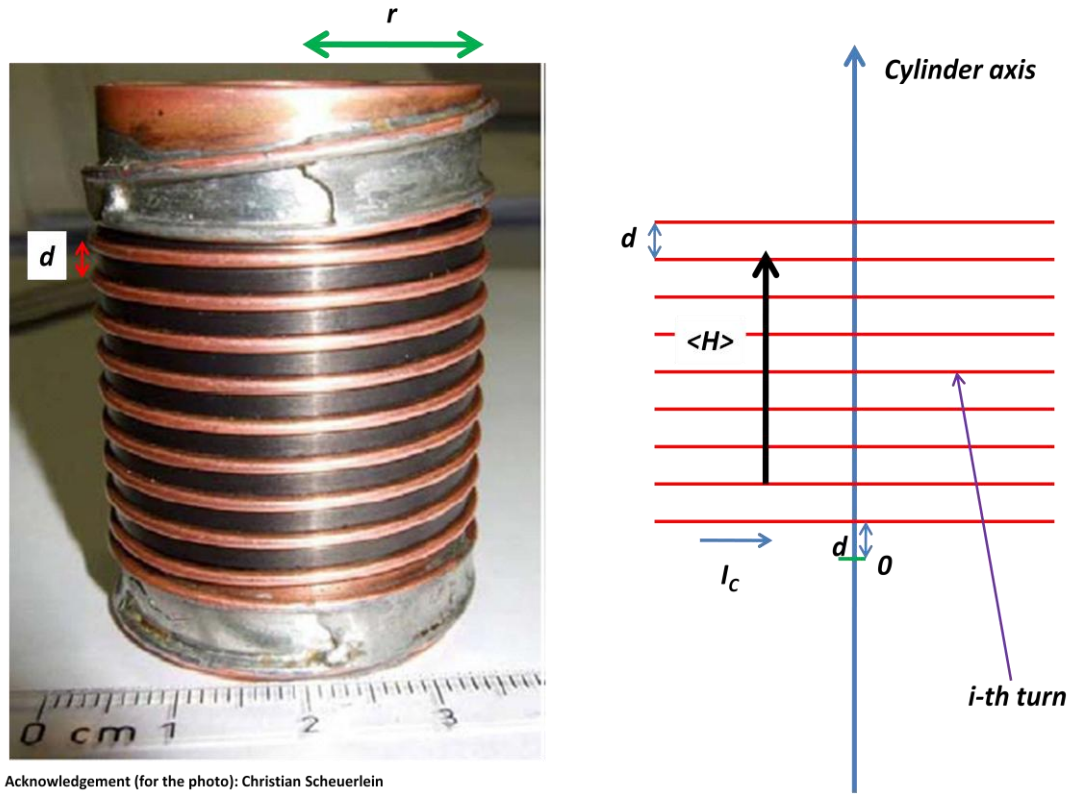

Figure 68. Sketch of the 9 circular filaments (of infinitesimal cross section), that represent the 9 turns of the LHC Sample Holder as in the model of eq. 31 to 33.. In *each* of these filaments flows a current equal to I_C. The mean value of $\boldsymbol{H}$ has been supposed homogeneous in the cylinder.

In eq. (32), the magnetic field induction vector has been calculated *on the axis z* of the cylinder, ideally starting from its bottom (z = 0) and considering the contribution of the *i-th* turn, that placed, on the axis of the cylinder, at a height equal to *id*. This schematization is illustrated in Figure 68.

The absolute values of the calculated self field correction for both sample holders have then been added to the applied magnetic field as:

$$|B_{TOT-SIT}| = |B_{Backgr}| + \frac{\mu_0 * I_C}{2\pi * R} \quad (37)$$

$$|B_{TOT-LHC.Std.}| = |B_{Backgr}| + \mu_0 * \langle \vec{H} \rangle \quad (38)$$

In eq. (37) and (38), the two magnetic fields have been linearly added because the two vectors, in the two model for the experimental configurations of the SIT and LHC Standard sample holders, are parallel. At this point, the critical current values of Table 6 and 7 have been plotted against the total magnetic fields for both sample holders. These plots are shown in Figure 69, 70 and 71.

It is seen that the LHC Standard plot always lies above the SIT one, in agreement with the fact that the expected correction respect to the applied field are of the first and second order, respectively for the SIT and the LHC Standard sample holder [28]. Nevertheless, the two plots do not coincide, and the SIT research team is *currently* performing Finite Element Analysis of the magnetic field in the LHC Standard sample holder, to compare its behavior with the one of the SIT prototypes. Possible variation of geometry of the SIT prototypes are also under investigations, in order to match the SIT I_C against B_{TOT} plots with the LHC Standard one.

4.4 Current Status of the Experimental Validation of the SIT Sample Holders

The first experimental studies of the preparation procedures and working conditions of the SIT sample holders with Nb_3Sn wires will be presented here, up to the actual stage of the testing session.

4.4.1 The Sample Holder's Preparation Procedures

The preparation procedure of the SIT sample holder for its use with Nb_3Sn wires completes the conceptual design of the sample holder's preparation stage at CERN, before its shipping to the research institute that will be in charge of the irradiation tests.

A first solution has been tested, and consisted in fixing a *non - reacted* Nb_3Sn wire on the two prototypes, and successively perform the heat treatment of the wire. In this way, the wire has assumed directly the shape of the sample holder.

More precisely it has been:

- Deposited a 100 μm thick Ni film on both prototypes. This step was intended to prepare the sample holder for the heat treatment, putting in contact the outer *Cu* surface of the non - reacted wire with a affine metallic layer from the thermo - chemical point of view.

- Fixed the wire to the sample holder thanks to copper filaments

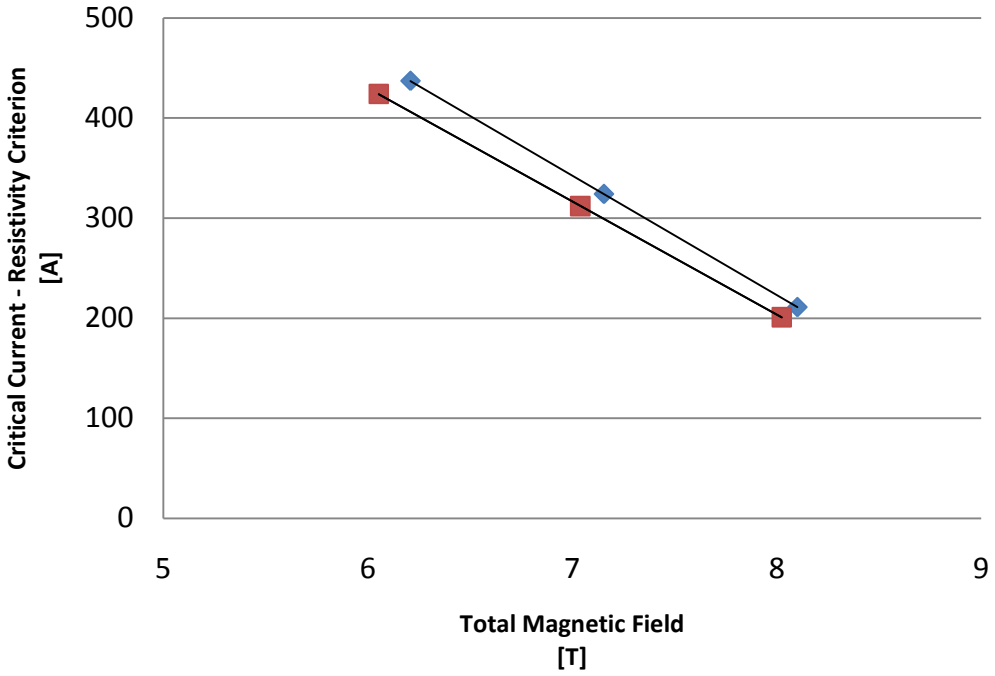

Figure 69. Plot of the SIT (blue dots - "5x5 mm^2" basis sample holder - L = 40 mm) and the LHC Standard (red dots) I_C experimental results against the total applied magnetic field.

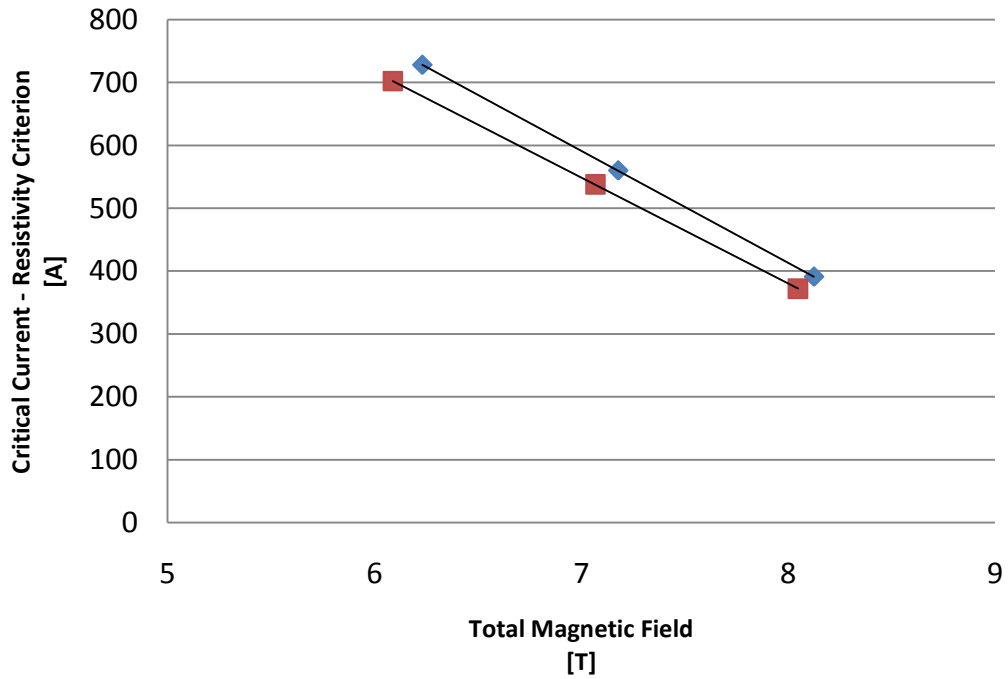

Figure 70. Plot of the SIT (blue dots - "10x10 mm^2" basis sample holder - L = 20 mm) and the LHC Standard (red dots) I_C experimental results against the total applied magnetic field.

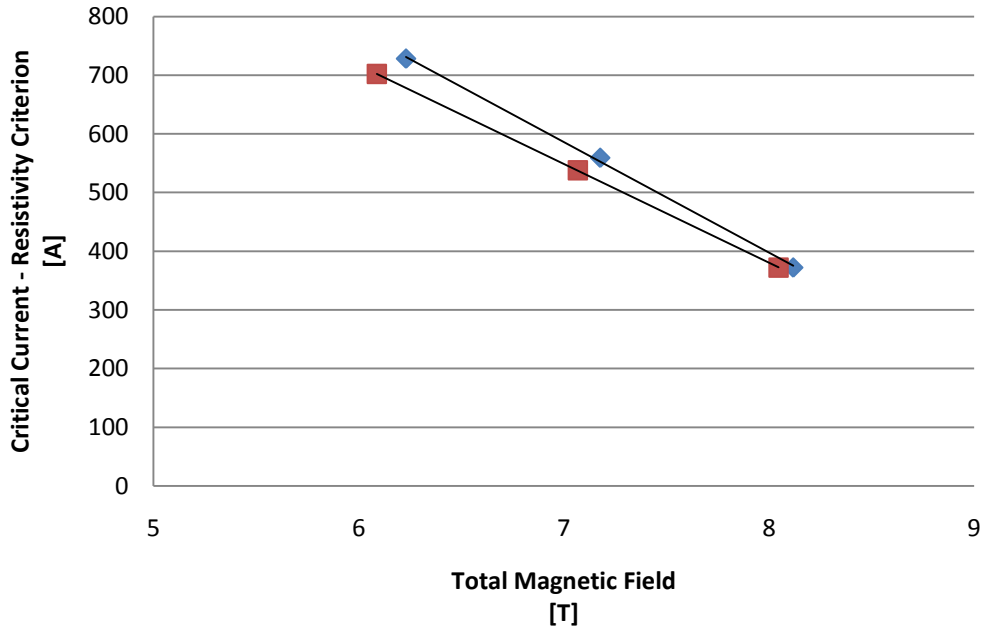

Figure 71. Plot of the SIT (blue dots - "10x10 mm^2" basis sample holder - L = 40 mm) and the LHC Standard (red dots) I_C experimental results against the total applied magnetic field.

- Put the U into the furnace, for a 10 day long heat treatment (that has generated the superconducting phase in the wire)

- Extracted the U from the furnace at the end of the heat treatment, and covered the wire with a Sn-Pb soldering alloy, to (1) prevent wire's movement during the successively critical current measurement, (2) easily solder it after the heat treatment and (3) also take into account the results of the FLUKA simulation[5].

This preparation has *failed*, because, during the soldering stage, the relevant heat that has been given to melt the Sn-Pb soldering alloy has deformed the excessively deformed the wire at the height of the bending radius *r*, while the wire was rigidly fixed to the sample holder, and thus, not able to freely expand. The zone where the Nb_3Sn wire has broken is shown in Figure 72.

A new preparation procedure has thus been tested. It consisted in:

- Plate the "10x10 mm^2", that was covered with the Ni film, with a new Ag layer, in order to facilitate the soldering procedures after the heat treatment.

- Fix the non reacted wire to the "5x5 mm^2" basis sample holder, allowing him to *expand* during the heat treatment along the lateral grooves of the sample holder and using this sample holder as *shape precursor*.

- At the end of the heat treatment, fix the wire, that has assumed the shape of the U, on the "10x10 mm^2" basis sample holder for the soldering, with the Sn-Pb-Cd alloy.

[5] Recall that an An-Sn soldering alloy would absorb all the deposited power during the irradiation tests, leaving the Nb_3Sn sample in the non-irradiated state

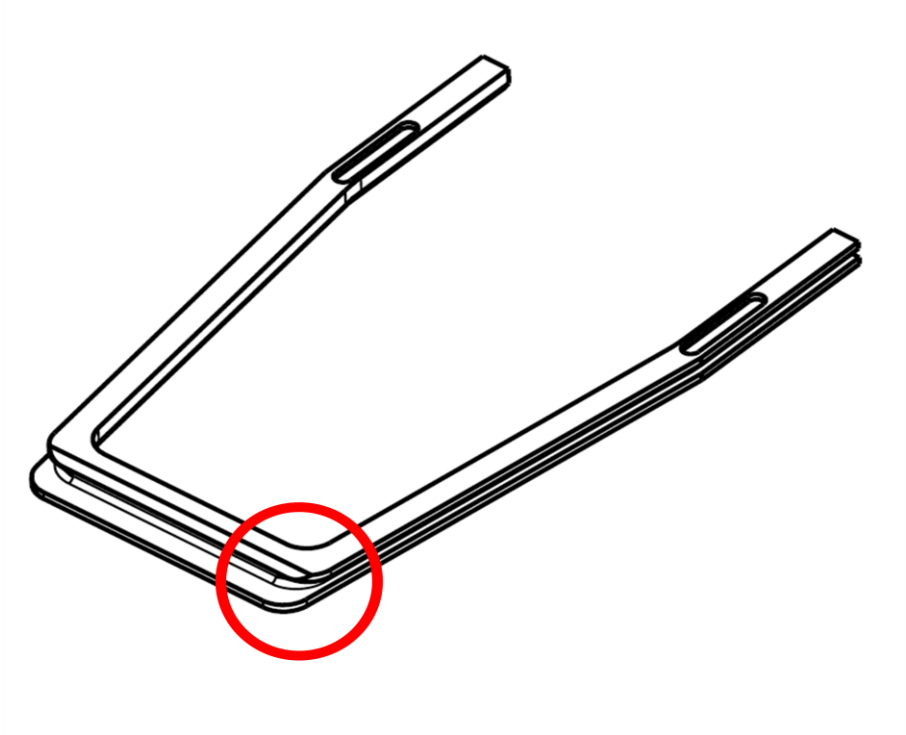

Figure 72. The SIT "5x5 mm^2" basis sample holder and the zone (red circle) where the Nb_3Sn wire has broken during the preparation of the apparatus.

This particular choice has been done because Sn-Pb-Cd has a lower melting point respect to the Sn-Pb, and thus enables to lower the heat power that the superconducting sample would have received in the point of highest bending radius *r*; this solution has to avoided the breaking of the sample during the sample holder's preparation, and the "10x10 mm^2" basis sample holder has been successively used for the I_C tests.

4.4.2 First Critical Current Measurements

The "10x10 mm^2" basis sample holder has been tested for applying magnetic fields of 8 to 11 T to the wire, and monitoring the voltage drop either over L = 20 mm either over L = 40 mm. The applied magnetic field have been chosen in the above range, to be coherent with the test sessions of Nb_3Sn wire that are currently in progress at CERN

Other problems have been encountered during the sample holder tests. Independently of the different choices of the electric current ramp rate that have been done for the tests, as well of the applied field value, the wire has always quenched well before the superconducting transition.

The reason for these early quenches are *currently* under investigation by the SIT research team, putting the voltage taps in different points of the sample holder, and detecting the voltage drop across these points, to check if the quench are due to current redistribution in the wires during the measurements, or if other causes may explain these failures.

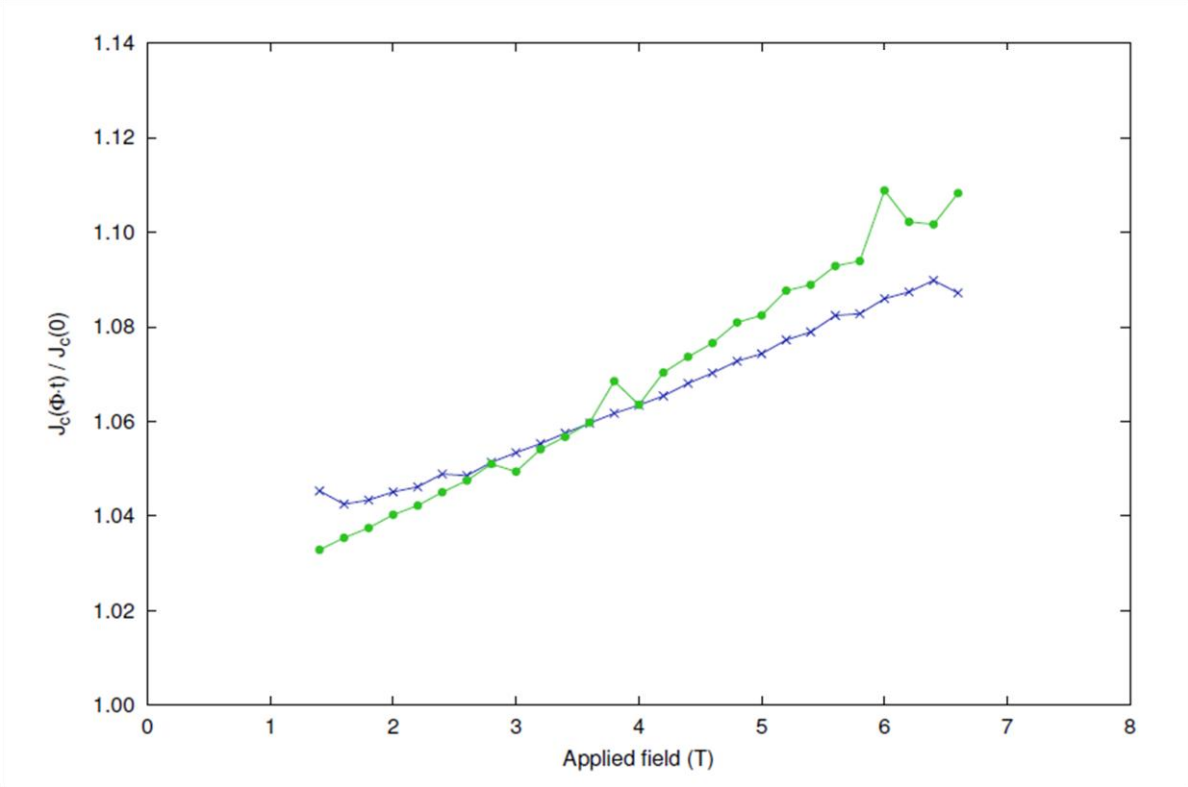

Figure 73. The first experimental data obtained under the CERN - A.T.I. collaboration on samples of alloyed Nb_3Sn samples, produced by the R.R.P. technique. Acknowledgements: T. Baumgartner (PhD Student, A.T.I. Institute)

4.5 First Experimental Results of the A.T.I. - CERN collaboration

In September 2010, the first data on the fast neutron irradiation effects (E > 0.1 MeV) have been produced in Vienna at the A.T.I. institute. Ti - alloyed Nb3Sn samples, produced with the R.R.P. technique, have been irradiated up to a fluence of 10^{17} neutrons*cm^{-2}, showing almost no changes in $\frac{J_C}{J_{C0}}$ at all applied magnetic fields.

Figure 73 shows these results. Even though they represent the *first* data that have been measured on alloyed Nb_3Sn superconductors, they have been obtained for fluence below the one where the maximum in the reduced critical current density of alloyed Nb_3Sn wires is expected.

Nevertheless, these data are among the first in history, and represent the *beginning* of a longer experimental activity, that will complete the plot of Figure 27 in time respect to the LHC - Phase II upgrade in 2016.

Conclusions

This work has dealt with the conceptual design of the "Nb_3Sn - Superconductors Irradiation Test" project and with the design, preparation a first tests of the sample holder that will be used for the *proton* irradiation experiments of the sample holder.

A first literature review has then identified the available, as well as the missing data that are of interests for the 2016 LHC Upgrade project. While the past *neutron irradiation* studies have extensively characterized the variation of the upper critical field B_{C2}, the critical temperature T_C and the normal state resistivity ρ_0, a big amount of data is particularly missing on the proton and (partially) on the neutron - induced variation of the critical current density of alloyed Nb_3Sn.

Starting from the characteristics neutron and proton particle spectra, that are expected in the LHC quadrupoles, irradiation facilities that were equipped or capable to host the SIT irradiation experiments have been searched. At the end, the ATI Institute in Vienna (Austria) has signed a R&D contract with CERN, to perform the neutron irradiation tests. Proton irradiation tests have, at present, not yet been assigned, even though the Kurchatov Institute for Nuclear Physics in Moscow (Russia) is, at present, the best candidate.

The conceptual design of an irradiation test station, capable to perform both king of irradiation tests, has been done, in absence of the final assignments of the irradiation test to any of the selected institutes. The ideal layout of the irradiation test station has been first defined, and their working conditions have been, where possible, precisely estimated in connection with the parallel design of the sample holder that will be used for the irradiation tests.

The design of an new sample holder, based on the conceptual design of the SIT experiments, has been done, and its working conditions in the irradiation area of the SIT test station have been studied. At the end, a first reasonable design of the apparatus has produced its first two prototypes: the "10x10 mm^2" and the "5x5 mm^2" basis sample holders. The first experimental validation of the this two prototypes has constituted the experimental activity of the SIT project of this year.

The first tests of the SIT sample holder prototypes with NbTi wires (that are ductile, and can be thus easy bent and fixed on the SIT prototypes) have produced reasonable experimental result, respect to the one of the LHC Standard sample holder, if the expected corrections to the applied magnetic field are compared with the one that have been obtained from an analytical model.

The preparation procedure of the SIT sample holder with Nb_3Sn wires has been successful when one of the prototypes has been used as *shape precursor* for the wire during the heat treatment, and when the wire has been the soldered on the other prototype with a low melting point soldering alloy.

Future Work

Respect to the conclusions of this work, the future activity of the SIT research team will be focused on:

- The final assignment of the proton irradiation tests to a specific institute, and the project and testing of the experimental station that will be used there for the proton irradiation tests of Nb_3Sn, as well of the other superconductors that will be tested for the LHC - Phase II upgrade.

- The precise estimations of the self - field correction in the case of the LHC Standard sample holder, to match its results with those of the SIT prototypes for the test of NbTi wires.

- The completion of the FLUKA simulation for the irradiation of a *soldered* SIT prototype

- The completion of the preparation procedure of the SIT sample holder for its tests with Nb_3Sn wires, in connection with the results of the future FLUKA simulations

while the collaboration with the A.T.I - CERN collaboration will produce the missing data on alloyed Nb_3Sn critical current variation after irradiation with fast neutrons.

References

More than 120 publications have been considered for this work; the *most significant* are listed here:

[1] Sweedler, Cox, Moeleke; Journal of Nuclear Materials 72 (1978) 50 - 69
[2] Flukiger, Uglietti, Senatore, Buta, Seeber; Cryogenics, Vol. 48, Issues 7 - 8, 293 -307
[3] Cerutti, Borguglietti, Broggi, Mauri, Mereghetti, Todesco, Wildner; Proceedings of the 2008 HHH Conference, Coppet (Switzerland)
[4] Cerutti, Mereghetti; Proceedings of the Workshop on Radiation Damage in Superconductors and Insulators; CERN, December 2009
[5] Flukiger; Proceedings of the WAMSDO Workshop, CERN, November 2008
[6] Gary S. Was; "Fundamentals of Material Radiation Damage - Metals and Alloys", Springer Verlag
[7] Pitcher *et. al.*; Proceedings of The Simposium on Materials for Spallation Neutron Sources, Orlando (Florida), 1997
[8] Putti, Rowell, Vaglio; Superconductors Science and Technology, Vol. 21, No. 4 (2008)
[9] Summers, Guinan, Miller, Hahn; IEEE Transaction on Magnetics, Vol. 27, Issue 2 (1991). The experimental results of Brown *et. al.* are extensively described in this paper.
[10] Brown, Blewitt, Scott, Wozniak; IEEE Transaction on Magnetics, Vol. 13 (1977)
[11] Weiss, Flukiger, Maurer; IEEE Transaction on Magnetics Vol. 23 (1987)
[12] Hahn, Hoch, Weber, Birtcher, Brown; Journal of Nuclear Materials 141-143 (1986)
[13] H. Weber; Seminar on Fusion Neutron Irradiation Effects in Superconductors for the I.T.E.R. Project, CERN, December 2009
[14] Voronova, Mihailov, Sotnikov, Zaikin; Journal of Nuclear Materials 72 (1978)
[15] Bode, Wohleben; Physical Review Letters 33 (1974)
[16] Snead; Journal of Nuclear Materials 72, Issues 1-2 (1978)
[17] Personal talk With Prof. René Flukiger (University of Geneva, DPMC)
[18] Blewitt, Coltman, Klabunde, Noggle; Journal of Applied Physics, Vol. 28, Issue 6, 1957
[19] Omar, Robinson, Thompson; Journal of Nuclear Materials, Vol. 84, Issues 1-2, 1979
[20] Hada, Walters, Goodrich, Tachikawa; Cryogenics, Vol. 34, No. 11 (1994)
[21] Harold Mindlin, "Aerospace Structural Handbook", Vol. 4, USAF Handbook Operation Publisher
[22] Material Properties Database at www.matweb.com
[23] Prof. Marco Beghi and Prof. Lelio Luzzi; Documents for the "Nuclear Materials Technology" Course, Milan's Polytechnic University, Academic Year 2009-2010
[24] Broggi; "First Simulations of a 30 MeV Proton Irradiation of a Nb_3Sn Sample on a Ti-Al5-V4 Sample Holder", CERN document server
[25] Bernard Seeber; "Handbook of Applied Superconductivity", IoP Publisher
[26] Richard G. More, John M. Tarr; "MHD and Fusion Magnets", John Wiley & Sons
[27] Personal talk with Dr. Luca Bottura (CERN - TE - MSC - SCD group)

Acknowledgements

I first dedicate this work to my late father. His memory has given me the necessary power to deal with the intense rhythm of work of the last two years.

I am very thankful to Prof. Marco Beghi (Milan's Polytechnic University - Energy Department), for his guidance and support.

Gratitude goes to Dr. Giovanni Volpini (L.A.S.A. Laboratory - Italian Institute For Nuclear Physics "INFN" - Milan's Division), who has first established the first contacts that have enabled to come to CERN for this invaluable experience, and to: Prof. Matteo Passoni (Milan's Polytechnic University - Energy Department), Prof. Carlo Bottani (Milan's Polytechnic University - Energy Department) and Prof. Ferdinando Amman (University of Pavia - Electronics Department), who have helped me orient my MSc's studies to the subject of Material's Radiation Damage.

I am also very grateful to Dr. Luca Bottura and Prof. Lucio Rossi, of CERN's TE - MSC - SCD research group, because I have learnt a lot working with them from the professional, as from the human point of view.

I would also like to express my sincere thank to all the people that have followed or helped me in different times during my thesis work at CERN, but principally: Dr. Ian Pong (TE - MSC - SCD group), Prof. René Flukiger (University of Geneva, DPMC), Dr. Luc Oberli (TE - MSC - SCD group), Dr. Christian Scheuerlein (TE - MSC - SCD group), Dr. Sandrine Naour (TE - MSC - SCD group), Dr. Amalia Ballarino (TE - MSC - SCD group), Dr. Alessandro Dallocchio (EN - MME group) and Dr. Marco Buzio (TE - MSC – MME group).

Special thanks goes to Dr. Francesco Broggi (L.A.S.A. Laboratory - Italian Institute For Nuclear Physics "INFN" - Milan's Division) for its precious support with the FLUKA simulations on the SIT Sample Holder, (and for the common passion for A.C. Milan.!)

I thank Carlo Petrone, Lucio Fiscarelli, Giuseppe Montenero, Giancarlo Golluccio, Giovanni Spezia, Tiziana Miani, Simon Heck, Emmanuele Ravaioli, Federico Carra, Andrea Manzi, Vitaliano Inglese for moments I have passed with them, during the work pause, as well during my free time in Geneva.

Lastly, I am particularly grateful to my university colleagues Fabio Moretto, Nicola Mariani, Alessandro Calabró, Roberto Calabró, Mattia Bellogini and Alessio Lorenzi for their precious friendship.